Past Indian Summer Monsoon Variability from the Southeastern Arabian Sea at Multi Centennial Scale Resolution

A Thesis

submitted to the Goa University for the Award of the Degree of

DOCTOR OF PHILOSOPHY

in

Marine Science

Goa University

by

Sidhesh Nagoji

Research Guide

Dr. Manish Tiwari

Scientist-E & Incharge (Paleoceanography)

National Center for Polar and Ocean Research

Vasco-da-Gama, Goa – 403804, India

2018

Declaration

I hereby declare that the thesis entitled "**Past Indian Summer Monsoon Variability from the Southeastern Arabian Sea at Multi Centennial Scale Resolution**" is an authentic record of research work carried out by me under the supervision and guidance of Dr. Manish Tiwari, Scientist-E, National Center for Polar and Ocean Research, in the partial fulfillment of the requirement of the Ph.D. degree in the Faculty of Marine Science and no part thereof has been presented for the award of any other degree in any University/Institute.

(Sidhesh Nagoji)

Certificate

I certify that the thesis entitled, **"Past Indian Summer Monsoon Variability from the Southeastern Arabian Sea at Multi Centennial Scale Resolution"** is an authentic record of research work carried out by Mr. Sidhesh Nagoji under my supervision and guidance at the National Center for Polar and Ocean Research in partial fulfillment of the requirements for the degree of Doctor of Philosophy and no part thereof has been presented for the award of any degree in any University/Institute.

(Dr. Manish Tiwari)

Scientist-E & Incharge (Paleoceanography)
National Centre for Polar & Ocean Research
Earth System Science Organisation (ESSO-NCAOR)
Ministry of Earth Sciences, Govt. of India
Headland Sada, Vasco-da-Gama – 403804, Goa, India

Acknowledgement

No words would express my deep sense of gratitude to Dr. Manish Tiwari, Scientist-E, at National Center for Polar and Ocean Research (NCPOR), Goa for the guidance and constant encouragement, which enabled me to complete the thesis. He not only introduced me to this fascinating subject of paleoclimate but also guided me efficiently throughout. I express my sincere gratitude for his valuable advice and motivation ever since I joined NCPOR.

I also express my sincere gratitude to Dr. M. Ravichandran, Director, NCPOR and Dr. Thamban Meloth, Group Director (Polar Science) for their support at several points during my journey.

I am thankful to Dr. P.D. Naidu, Senior Scientist at NIO, Goa and Prof. G. N. Nayak, Goa University for the valuable discussions and suggestions during various DRC meetings.

I gratefully acknowledge the research fellowship through a Ministry of Earth Sciences funded project - "Past Climate & Ocean Variability". This work was also partially funded by the project entitled "Interhemispheric teleconnection between the southern tropical Indian Ocean & Indian monsoon" by the Indian Space Research Organisation - Geosphere Biosphere Program.

I express my heartfelt gratitude to Mr. Prashant Redkar, Senior Scientific Assistant at NCPOR for providing technical help and support whenever required in the troubleshooting of the Isotope Ratio Mass Spectrometer coupled with Elemental Analyzer housed in Marine Stable Isotope Lab (MASTIL) at NCPOR.

If there is anyone I have forgotten, be comforted in the knowledge that I know this thesis could not have been completed by me alone and was only done with the love and support of you all. During the course of my Ph.D. there are too many of you to remember and name, and for that, I am blessed.

Finally, with all love and affection I wish to express my deep sense of gratitude to my parents and all my family members for their constant encouragement, prayers, and advice, without which I would not have been able to pursue my study. The special interest shown by my wife and her constant encouragement, love, and support are highly cherished.

My head bows before the God almighty, the cherisher and sustainer of the world, who gave me boundless blessings, rendered through various hands, which helped me in completing this work successfully.

To my parents,

for my education, constant love and endless hope in me.

To my wife,

for her infinite understanding, patience and support;

she has taught me an exceptional lesson about love.

&

To my daughter

Ahana

Contents

List of Figures

Figure 4. SST and salinity variability of the southeastern Arabian Sea since mid-Holocene. Bands depict the periods of higher salinity/reduced Indian Summer Monsoon precipitation; dashed lines depict the long-term trend determined through linear regression (least square method): (a) $\delta^{18}O$ values of *Globigerinoides ruber*, which is a function of temperature and salinity (closed triangles indicate the position of the Accelerator Mass Spectrometer (AMS) radiocarbon dates); (b) SST values derived from the Mg/Ca ratio of the G. ruber (closed squares depict the repeat values; see text for more details); (c) ISM precipitation intensity shown by salinity fluctuations in the southeastern Arabian Sea; note that the salinity scale is reversed; (d) solar activity indicated by TSI variability (Steinhilber et al., 2012); the capital alphabets depict the Maunder, Spörer, Oort, and Wolf minima. Dark gray lines in panel 'a' show the precision of the $\delta^{18}O_{ruber}$ measurement while those in panels 'b' and 'c' show the calibration uncertainty in the SST and the $\delta^{18}O_{seawater}$ reconstruction (see text for more details). LIA: Little Ice Age.

Figure 5. Spectral analysis including the Continuous Wavelet Transform (CWT) and the Squared Wavelet Coherence. Panels 'a' and 'b' show the CWT power spectrum for the salinity and the SST, respectively. Squared Wavelet Coherence between the salinity and SST is shown in panel 'c', while panel 'd' represents the Squared Wavelet Coherence between salinity and TSI. The 5% significance level against red noise is shown as a thick contour. Phase arrows pointing right means in-phase, left means anti-phase, down means salinity leading by 90°, and up means salinity lagging by 90°. The lighter shades depict the cone of influence.

Figure 6. Marine-versus terrestrial-based high-resolution studies and their relation to

the periods of TSI minima. The gray bands depict the major period of aridity observed by various studies. The gray bands in panel 'a' depict the periods of low solar activity. Panels 'b'–'f' show the marine-based studies, while panels 'g'–'i' show the terrestrial-based reconstruction of the ISM precipitation.

Figure 7. Modern salinity, dissolved oxygen, and temperature profiles (monthly average) near the core location. The months of August and December represent the summer and winter monsoon periods, respectively. The conditions prevailing inter-monsoon periods are represented by the months of May and October. This figure is based on the World Ocean Database 2009 (Boyer et al., 2009).

Figure 8. Location of the core (shown by the closed circle) and the bathymetry of the study area. Core SN-6 is from the upper continental slope of India. The inset shows the age-depth model based on five radiocarbon dates approximately at every 9 cm on selected species of planktic foraminifera; sedimentation rates are also shown (in cm/kyr).

Figure 9. Correlation of Al with selected major and trace elements. Correlation coefficient is given by r^2 value.

Figure 10. Correlation of $CaCO_3$ with selected major and trace elements. Correlation coefficient is given by r^2 value.

Figure 11. Downcore variation of geochemical proxies: (a) sedimentation rate; (b) $CaCO_3$ mass accumulation rate; (c) $\%CaCO_3$; (d) total organic carbon mass

accumulation rate; (e) % total organic carbon as a function of preservation; (f)–(h) V/Cr, V/Mo, and Ni/Co indicating redox condition; (i) Ti/Al indicating decline in detrital influx since mid-Holocene; and (j) sea surface salinity showing SASM precipitation strength.

Figure 12. The plot shows the provenance of the SOM. Atomic C/N and $\delta^{13}C_{org}$ values show a mixed productivity signal i.e. presence of both marine as well as terrestrial source of the SOM.

Figure 13. Correlation of TOC with TN. Correlation coefficient is given by r^2 value.

Figure 14. Comparing records of (b–e) Indian summer, (f and g) East Asian summer monsoons, and (h and i) African summer monsoon using diverse proxies from different regions and its response to precessional forcing. Figure 4a shows June insolation at 30°N.

Figure 15. Location of the core SK 274-4G with oxygen contours showing oxygen concentration at 300 m depth. White dashed line indicates nitrite maximum (>0.5 μM/l; Naqvi, 1991) coinciding with lowest oxygen concentration. The pink color indicates permanent OMZ (O_2 <20 μM/kg). Purple circle in the figure shows the location of the core SK 274-4G. Age-depth model (inset; shown in panel a) is based on 9 radiocarbon dates on selected species of planktic foraminifera; sedimentation rates are also shown (underlined; in cm/kyr). Present-day water column characteristics of the Indian Ocean are shown (inset; panel b and c). Oxygen concentration and nitrate deficit, N* data are from the World Ocean Circulation Experiment (WOCE)

stations I07N-819 (20°N 64°E; shown by red line), I01–910 (11°N–53°E; shown by light green line), I07N-716 (14°S–55°E; shown by blue line), I08N-346 (19°S–88°E; shown by purple line), I08S/I09N-23 (40°S–95°E; shown by black line) and a GEOSECS station (0–44.5°E; shown by dark green line) (http://cdiac.esd.ornl.gov/oceans/glodap/Glodap_home.htm).

Figure 16. Shows the depth profile of nitrogen isotope of NO_3^- in the Arabian Sea water column. Inset shows the station locations; the dotted curve depicts dissolved oxygen concentration.

Figure 17. Shows mixed source of the sedimentary organic matter at our core location.

Figure 18. Shows the scatter plots of $\delta^{15}N$ with (a) $\delta^{13}C_{org}$, (b) TOC, (c) TN and, (d) atomic C/N, respectively, along with their respective r (correlation coefficient) and n (number of data points) values.

Figure 19. Comparison of geochemical proxies (panel a, b and c) of the present study with the GISP2 $\delta^{18}O$ record (panel f) (Dansgaard et al., 1993); $\delta^{13}C$ of benthic foraminifera record (panel e) shows millennial-scale changes in SAMW-AAIW formation rate (Jung et. al., 2009), and the global mean sea level variability is shown in panel 'd' (Siddal et al., 2003).

Figure 20. Regional comparison of $\delta^{15}N$ signal from the different parts of the Arabian Sea compared with $\delta^{18}O$ of GISP2 record (panel e). Panel (a) shows the $\delta^{15}N$ profile

of the present study, panel (b) shows $\delta^{15}N$ profile from EAS; core MD04-2876, panel (c) shows $\delta^{15}N$ profile from WAS; core RC 27-23, and panel (d) shows $\delta^{15}N$ profile from WAS; core RC 14.

Figure 21. Spectral analysis including the Continuous Wavelet Transform (CWT) and the Squared Wavelet Coherence. Panels 'a' show the CWT power spectrum for the $\delta^{15}N$. Squared Wavelet Coherence between the $\delta^{15}N$ and $\delta^{18}O$ is shown in panel 'b', while between $\delta^{15}N$ and $\delta^{13}C$ is shown in panel 'c'. The 5% significance level against red noise is shown as a thick contour. Phase arrows pointing right means in-phase, left means anti-phase, down means $\delta^{15}N$ leading by 90°, and up means $\delta^{15}N$ lagging by 90°. The lighter shades depict the cone of influence.

Figure 22. Location of the core SK 274-1G

Figure 23. Downcore variation of geochemical proxies: (a) TN (%), (b) TOC (%), (c) $\delta^{15}N$, and (d) atomic C/N profile.

Figure 24. Correlation of $\delta^{13}C$ with $\delta^{15}N$ during MIS 1(a), MIS 2(b), and MIS 3(c). Correlation coefficient is given by r-value.

Figure 25. Correlation of TOC with $\delta^{15}N$, TN, and atomic C/N during MIS 1 (a, b, c), MIS 2 (d, e, f) and MIS 3 (g, h, i) respectively. Correlation coefficient is given by r value.

Figure 26. Nitrate deficit transact for the Arabian Sea from 23 ^{o}N to 8 ^{o}S at 0 to 2000

m water depth.

Figure 27. Regional averages of normalized and averaged $\delta^{15}N$ values from the northern (panel a), eastern (panel b), and western (panel c) Arabian Sea, compared with sea level reconstruction from the Red Sea (Siddall et al., 2003) (panel d), and $\delta^{18}O$ record from the GISP2 ice core (Grootes and Stuiver, 1997) (panel e).

Figure 28. CO_2 concentration in the Antarctic Taylor Dome ice core (Smith et al., 1999) (a) compared with the regional averages of normalized and averaged $\delta^{15}N$ values from the Eastern North Pacific (b), Eastern South Pacific (c), and the Arabian Sea (d). See text for more details.

Figure 29. Comparison of the atmospheric CO_2 concentration from the Taylor-Dome ice core (a) and atmospheric N_2O concentration from the GISP2 ice core (c) with the global denitrification index (b) calculated by averaging the individual normalized $\delta^{15}N$ values from the ETNP, ETSP, and the Arabian Sea.

List of Tables

List of Publications from the Thesis

1. **Siddhesh Nagoji** and Manish Tiwari (2017), Organic carbon preservation in Southeastern Arabian Sea sediments since mid-Holocene: Implications to South Asian Summer Monsoon variability. ***Geochemistry, Geophysics, Geosystems***, 18, DOI:10.1002/2017GC006804, (Impact Factor: 3.2).

2. Manish Tiwari, **Siddhesh S. Nagoji**, R. Ganeshram (2015), Multi-centennial scale SST and Indian summer monsoon precipitation variability since mid-Holocene and its nonlinear response to solar activity. ***The Holocene***, 25, 1415-1424, DOI: 10.1177/0959683615585840, (Impact Factor: 2.6).

3. **Sidhesh Nagoji** and Manish Tiwari (2018), Differential Response of Denitrification in the Southeastern Arabian Sea during Last Glacial Maxima and Holocene. ***Palaeogeography, Palaeoclimatology, Palaeoecology***, (Under review) (Impact Factor: 2.5).

4. **Sidhesh Nagoji** and Manish Tiwari (2018), Denitrification Variability in the Arabian Sea: Implications to Late Quaternary Nitrogen and Carbon Cycles. ***Paleoceanography***, (Under review) (Impact Factor: 3.2).

List of other Publications

5. Manish Tiwari, **Siddhesh Nagoji**, Vikash Kumar, Shubham Tripathi, Padmasini Behera (2018), Oxygen Isotope - Salinity Relation in an Arctic fjord (Kongsfjorden): Implications to Hydrographic Variability. ***Geoscience Frontiers***, DOI:10.1016/j.gsf.2017.12.007, (Impact Factor: 4.6).

6. Sivaji Patra et al., **Siddhesh Nagoji**, A.V. Raman & B. R. Subramanian (2017), Isotopic composition (C & N) of the suspended particles and N uptake by phytoplankton in a shallow tropical coastal lagoon. ***Chemistry and Ecology***, DOI:10.1080/02757540.2017.1356292, (Impact Factor: 1.5).

7. Vikash Kumar, Manish Tiwari, **Siddhesh Nagoji** and Shubham Tripathi (2016), Evidence of Anomalously Low $\delta^{13}C$ of Marine Organic Matter in an Arctic Fjord. ***Nature Scientific Reports***, DOI: 10.1038/srep36192, (Impact Factor: 5.3).

8. Manish Tiwari, **Siddhesh S. Nagoji**, Divya David T, N. Anilkumar, S. Rajan (2015), Oxygen isotope distribution at shallow to intermediate depths across different fronts of the Southern Ocean: Signatures of a warm-core eddy. ***Deep Sea Research Part II: Topical Studies in Oceanography***, 118, 170–176, DOI: 10.1016/j.dsr2.2015.04.022, (Impact Factor: 1.7).

9. Manish Tiwari, **Siddhesh S. Nagoji**, Thammisetti Kartik, G. Drishya, R.K. Parvathy, Sivaramakrishnan Rajan (2013), Oxygen Isotope - Salinity Relationships of discrete oceanic regions from India to Antarctica vis-à-vis Surface Hydrological Processes. ***Journal of Marine Systems***, 113–114, 88–93. DOI: 10.1016/j.jmarsys.2013.01.001, (Impact Factor: 2.4).

Abstract

Among the monsoon systems of the world, the largest one in extension and intensity is the South Asian Summer Monsoon (SASM). The economy of several countries and millions of lives are dependent on the SASM rainfall. Recent studies have shown that the presently experienced global warming can affect the SASM adversely. Therefore, it is of prime importance to understand the various external and internal forcing factors of the SASM and the underlying mechanisms on various timescales. The annual to decadal scale variability can be studied using the meteorological instrumental data, which is available just for the past ~150 years and that also only from the major cities. But to study longer timescales i.e., centennial to millennial, we need natural archives such as marine and lacustrine sediments, speleothems, corals, tree rings and so on. The approach followed in this work is based on the use of marine sediments from the southeastern Arabian Sea (SEAS) to reconstruct the past SASM variability on multi-centennial timescale spanning the Holocene and the last glacial period. Further, we have attempted to quantify the past climatic changes in terms of exact temperature and salinity changes that is required for modeling studies.

Three sediment cores from the SEAS - SN-6, SK274/1G, and SK274/4G - were retrieved: two from the continental slope off Mangalore, and one from the southern tip of the Indian continental slope. The isotopic (oxygen and carbon isotope ratio of foraminifer, carbon, and nitrogen isotope ratio of the sediments) and elemental (C, N, and trace elements of sediment and Mg/Ca ratio of planktic foraminifera) proxies are investigated to detect changes in paleomonsoon intensities, nature of terrestrial and marine organic matter exported to the deep ocean, productivity variations, and past water column oxygen conditions etc. The study of these three core led us to the following findings:

1. Earlier short time-series studies of Indian Summer Monsoon (ISM) shows a weak correlation with solar variability in the 20th century. However, such climatological observations on solar activity–monsoon relationship are very short and hence uncertain. A few paleomonsoon records also exhibit prominent correspondence with solar activity during early Holocene and beyond. But despite the strong recent solar minima (e.g. Maunder, Spörer, Oort, Wolf), their correlation with monsoon precipitation is weak and inconclusive. Additionally, many of the earlier studies have been from the western Arabian Sea that provides records of the ISM wind intensity instead of the ISM precipitation. Further, many earlier studies from the eastern Arabian Sea remain speculative primarily due to the lack of properly resolved SST and salinity component in monsoon reconstruction. In chapter 3, we present mid-Holocene to recent sea surface temperature (SST) reconstructed from Mg/Ca measurements of planktic foraminifera (*Globigerinoides ruber*; white, sensu stricto) on a centennial-scale resolution from the southeastern Arabian based on SN-6. These measurements are used to correct the oxygen isotope ratios of *G. ruber* to reconstruct salinity related to monsoon runoff in this region more precisely than hitherto. The long-term trend indicates that the ISM precipitation has declined since the mid-Holocene similar to the solar activity. On shorter multi-centennial timescale, we show that the ISM precipitation declined concurrently with the recent periods of strong solar minima, but lagged by a couple of hundred years beyond 1300 yr BP toward the mid-Holocene – confirmed statistically using wavelet analysis. This non-stationary phase relationship between the ISM and the solar activity indicates the possible influence of the tropical coupled ocean–atmosphere phenomenon.

2. The earlier studies show a contrasting long-term trend of the SASM after attaining the precessional forcing induced mid-Holocene maximum. The increasing total organic carbon (TOC) concentration of marine sediments in the SEAS has been interpreted to imply increasing productivity due to strengthening SASM since mid-Holocene by a few studies. However, TOC concentration is also influenced by redox conditions, sedimentation rate, and an influx of terrigenous matter depending on the regional settings. So, it needs to be ascertained whether the TOC concentration of the sediments in the SEAS is a signal of productivity related to the SASM strength or preservation. Therefore, in chapter 4 we studied multiple proxies (TOC, total nitrogen, atomic C/N, $\delta^{13}C_{org}$, $CaCO_3$, and major and trace elements concentration) for determining the productivity, redox conditions, detrital supply, and provenance in a sediment core from the upper continental slope of the SEAS spanning the past ~4700 years at centennial scale resolution. The present study shows that the observed increase in the TOC values since the mid-Holocene is a result of better preservation caused by increased sedimentation rate and enhanced reducing conditions. We further show that the SASM has been declining since mid-Holocene after attaining a precession-forced maximum, which corroborates the earlier model ensemble studies. This study will have major implication towards the interpretation of TOC variability in future studies using sediments from the Southeastern Arabian Sea, which would help to understand the past SASM variability more accurately.

3. The proposed oxygen minima zone expansion in the Arabian Sea in recent years will enhance the production of nitrous oxide through denitrification. Past

denitrification intensity is also used to infer past South Asian Monsoon strength on millennial and longer timescales. Therefore, it is important to understand the mechanisms controlling the denitrification intensity, not only with respect to the modern day settings but also on glacial-interglacial timescales to explore any temporal perturbations. Therefore in chapter 5 we studied multiple geochemical and isotopic proxies ($\delta^{15}N$, $\delta^{13}C_{org}$, total organic carbon, atomic C/N, *G. bulloides*) at centennial scale resolution in a sediment core from the SEAS spanning the past ~43 kyrs. We find that, during the last glacial period (~23 - 43 kyr BP), both the ventilation of the Sub Antarctic Mode Water – Antarctic Intermediate Water into the Arabian Sea and the SASM induced productivity played a crucial role in modulating denitrification. But, since 8 kyr BP and during the LGM, denitrification increased despite reduced monsoon-induced productivity. We show that since 8 kyr BP, increase in denitrification is caused by enhanced inflow of oxygen-depleted Red Sea Water and Persian Gulf Water into the intermediate depths of the SEAS due to rising sea level. During LGM, weakened thermohaline circulation resulted in reduced ventilation of the intermediate waters of the SEAS causing increased denitrification. Our study would help to more accurately interpret the $\delta^{15}N$ variability from the Southeastern Arabian Sea.

4. Changes in marine nitrogen cycle have been proposed to be a major cause of the climate variability on glacial-interglacial timescale. Marine denitrification – an important component of the nitrogen cycle – not only governs the bioavailable nitrogen required for oceanic productivity that sequesters atmospheric CO_2 but also produces N_2O, which is a powerful greenhouse gas.

There are three regions, globally, where perennial denitrification takes place presently: Eastern Tropical South Pacific (ETSP), Eastern Tropical North Pacific (ETNP), and the Arabian Sea. To get averaged-out, representative variability of denitrification in the Arabian Sea, ETNP, and ETSP we calculated normalized $\delta^{15}N$ for the last 50 kyrs in chapter 6. Normalization was achieved by averaging $\delta^{15}N$ data from 61 sediment cores from Arabian Sea, ETNP, and ETSP. An analysis of these normalized $\delta^{15}N$ records exhibit reduced denitrification during MIS 2 as compared to MIS 3 and an increase during the deglaciation across all the basins. However, during the Holocene, increasing denitrification occurs in the Arabian Sea in contrast to the ETNP and ETSP due to postglacial reorganization of intermediate water circulation following sea level rise. The atmospheric CO_2 concentration closely follows the Arabian Sea-denitrification pattern during the Holocene period. However, when the global (i.e., ETNP, ETSP and Arabian Sea) denitrification is considered, it results in a better match with the millennial-scale CO_2 and N_2O evolution during the last 50 kyr BP. It suggests the important role played by denitrification in governing the global nitrogen and carbon cycles, and the global climate during that period.

Chapter 1

General Introduction

1. Introduction

1.1. General Monsoon Circulation

The climate over India is heavily influenced by seasonal variations of surface winds. During summer monsoon, southwesterly winds prevail over southern Asia transporting huge amounts of moisture over the Indian subcontinent, leading to high rainfall rates. In contrast, during winter monsoon wind blows from the northeast, advecting drier and colder air into India, causing a little rainfall over most of the country (Kripalani and Kumar, 2004). India receives about 80 % of its annual rainfall during the summer months between June and September (Basu, 2007). As explained, the marked change in precipitation over India is caused by changes in the prevailing wind direction between summer and wintertime, which is called monsoon. The word monsoon itself originated from the Arabic word for the season called *mausim* (Rao, 2008). With respect to India, it can be distinguished between the southwest summer and northeast winter monsoon season.

Besides the Indian or South Asian monsoon, regions characterized by a reversal of the mean wind direction are found over parts of Africa and America, eastern Asia and northern Australia. All these monsoon systems have the same physical origin, which is the seasonal movement of the peak solar insolation, which in turn modifies the position of the Hadley Cell. During winter, increased solar radiation over the southern latitudes and reduced incoming solar radiation rates over the northern latitudes lead to a horizontal north-south temperature gradient, which leads to a cross-equatorial flow from the northern to the southern latitudes. This cross-equatorial flow reverses during summer due to higher incoming solar radiation over the northern compared to the southern latitudes. This general monsoonal flow on hemispherical scales, which is

largely associated with changes in the position of the Inter-Tropical Convergence Zone (ITCZ), is modified by land-sea distribution or high orography on regional scales. For the Indian subcontinent, an important factor modifying the general monsoonal flow is the Himalayan and the Tibetan Plateau (Hahn and Manabe, 1975). However, it is still discussed in how far the "thermal effect" due to the high elevation of the Tibetan Plateau or the "barrier effect", which prevents warm moist air to penetrate further north is more important (Chen et al., 2014). Besides the Tibetan Plateau, the Western Ghats mountain range at the western coast of India is an influencing factor for the spatial distribution of rainfall over the Indian subcontinent (Sijikumar et al., 2013).

Overall, the general monsoon circulation over India during summer is driven by differences in incoming solar radiation over the higher latitudes compared to the tropical latitudes. This, in combination with the differential heating of the Indian land-masses as well as the Tibetan Plateau, compared to the tropical oceans, lead to the formation of a surface low-pressure system over northwestern India and a near surface high-pressure system over the southern tropical Indian Ocean (Mascarene High) during summer. This is accompanied by near-surface southeasterlies, which are converts to southwesterlies due to the Coriolis force leading to the southwesterly monsoon flow. The lifting of air over the Indian continent is accompanied by high rainfall and a divergent upper-level anti-cyclonic flow. In the upper-troposphere, the main wind direction reverses to northerlies and a convergent cyclonic upper-level flow is found over the tropical oceans. Besides topography, the presence of the Arabian Sea and the Bay of Bengal heavily influence the Indian Summer Monsoon (ISM) (Ghosh et al., 1978; Levine and Turner, 2012; Polanski et al., 2014).

1.2. Indian Summer Monsoon and its Manifestations

Large populations in the south Asian countries thrive on agriculture, which depends on monsoon. Extreme variability in monsoonal rainfall has resulted in draughts and in catastrophic floods during the past. ISM winds not only deliver heavy rainfall on land but also lead to large seasonal physical/chemical/biological changes in the entire Arabian sea. (Nair et al., 1989). Since long, studies concerning past variability of monsoon and its manifestation have been of immense interest among climatologist/modelers and earth scientists. Numerous paleoclimatic and paleoceanographic studies have been conducted in the western Arabian Sea, where ISM is manifested with intense upwelling along the entire west coast of India and thereby high surface biological productivity. Oceanographers exploited this natural phenomenon to reconstruct a paleomonsoonal history of the late Quaternary. Thereafter, the paleoclimatic focus turned to northwestern Arabian Sea sediments, and voluminous literature is available from the work done in this region. Initially, most of these studies dealt with long-term glacial-interglacial changes using deep-sea sediment cores. Century-scale abrupt changes in monsoonal climate were first observed by Sirocko et al. (1993). He initiated high-resolution paleoclimatic and paleoceanographic studies using continental margin (slope and shelf) sediments of the Arabian sea. As these marginal sediments have faster deposition rates and ability to preserve some of the proxy records better compared to the open ocean sediments. These studies contribute to paleomonsoon and paleoceanographic proxy data from the western and northwestern Arabian Sea, where monsoon-induced upwelling and consequent surface biological productivity is the predominant feature.

However, average annual rainfall over regions along western and northwestern Arabian Sea is low ranging from 25-100 mm/yr. On the other hand, the coastal regions along the eastern Arabian Sea (EAS) receive high rainfall ranging from 1000-4000 mm/yr due to the orographic effect of the Western Ghats. From regions off Saurashtra to off Cochin, there is a steep increasing gradient in rainfall (350 mm/degree). Highest rainfall region is off Mangalore (Sarkar et al., 2000). High precipitation on land quickly drains to the coastal region of the EAS through several rivers and streams. Therefore, in addition to wind-induced upwelling and consequent surface biological productivity during summer months, the continental margin area of the EAS also receives large freshwater input due to river/stream runoff all along its coast. This makes this region most suited for studying monsoon variability, its various manifestation and complex inter-relationship among them. In addition, paleoclimate and oceanographic database from this region is rather sparse compared to the western and northwestern Arabian Sea. Continental margin sediments from the SEAS preserve high-resolution records of past variability in monsoon and its associated processes in the form of several proxies, systematic analysis of these will provide valuable information of past variations in monsoon intensity.

As mentioned earlier, past monsoon variability can be tracked through its imprints of associated oceanographic properties in the underlying sediments, the most predominant feature of which is large seasonal variation in surface biological productivity. Fig.1 shows seasonal changes in the surface productivity during ISM and northeast monsoon season. Primary production during 1994-95 measured as a part of the Indian JGOFS programme in the EAS showed surface productivity of ~0.6

g C m^{-2} day^{-1} during summer, ~0.3 g C m^{-2} day^{-1} during winter and ~0.2 g C m^{-2} day^{-1} during the inter-monsoon season (Bhattathiri et al., 1996).

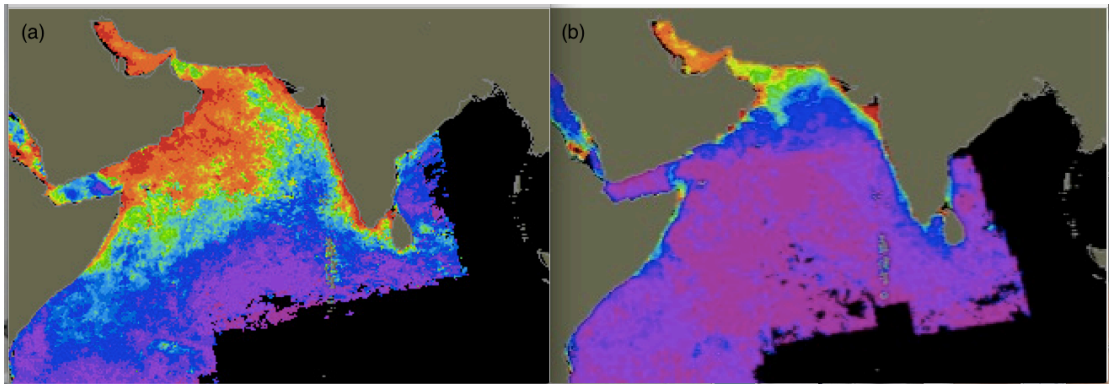

Figure 1. Satellite pictures of the Arabian Sea revealing seasonal contrast of surface biological productivity during (a) ISM (left) and (b) northeast monsoon season (right). Red & green colors indicate regions of high surface productivity, while blue and purple colors represent low productivity conditions (http://daac.gsfc.nasa.gov)

The monsoon signals are highly amplified within the southeastern Arabian Sea (SEAS) as major changes in salinity occur because of orographic precipitation runoff along the southwestern coast of India. Here, sea surface salinity reduces by 0.5 during the summer monsoon period because of surface runoff and overhead precipitation. Also, the salinity decreases by up to 0.8 during the post-monsoon period because of the transport of lower salinity waters from the northern Bay of Bengal (fresher due to input from the Ganges–Brahmaputra–Irrawaddy River system mainly fed by summer monsoon precipitation) via the wind-driven North East Monsoon Current. Additionally, the moderate upwelling causes SST to fall to a minimum of 27.5°C during the summer monsoon period from a high of 30.5°C during the pre-monsoon. These relatively large salinity and temperature changes in the study site make it uniquely suitable for reconstructing paleomonsoon precipitation.

The other significant oceanographic phenomenon in the Arabian Sea is subsurface denitrification. The Arabian Sea is one of the active denitrification-regions in the world oceans (Deuser et al., 1978; Naqvi, 1987, Altabet et al., 1995, 1999). Sub surface denitrification is generally thought to be maintained by a high export flux of organic matter, consuming almost all the dissolved O_2 leading to nitrate (NO_3^-) reduction in the intermediate depth waters. However, the intriguing peculiarity of subsurface denitrification in the Arabian Sea is that intense denitrification centers are geographically well separated from the most productive regions such as off Arabia and Somalia (Naqvi, 1991, 1994). Recently the EAS has received more attention after the realization that it is a potential source of atmospheric N_2O, a future threat to global climate (Patra et al., 1999, Naqvi et al., 2000). Since it is a semi-enclosed basin (Wyrtki, 1971), only source for ventilation of intermediate waters is from the south (Olson et al., 1993). A combination of high surface productivity and poor ventilation of subsurface waters causes O_2 depletion in the water column (dissolved oxygen concentration less than 0.5 ml/l) between 250 - 1250 m, known as Oxygen Minima Zone (OMZ), (Wyrtki, 1971, Naqvi, 1987). High export flux of organic matter from the mixed layer and unavailability of sufficient O_2, cause denitrification to meet the demand of heterotrophic bacteria for organic matter degradation. Analogous to the intensity of subsurface denitrification, bottom water redox conditions are also influenced by the export flux of organic matter. Several trace elements such as Mn, Cr, V, Ni, Zn, and Cu are used to track past changes in the bottom water redox conditions under which they precipitate/migrate (Somayajulu et al., 1994; Tribovillard et al., 1996).

As the instrumental all India rainfall records are available only for the last two centuries, estimates of past ISM variability can, therefore, be drawn as indirect inferences from the "proxy" indicators. A variety of multi-proxy records have been used in recent years from marine sediments to expand our understanding of the fluctuations in the intensity of the ISM, climate, and environment during the past. Numerous proxies from marine and continental records have been used to study the changes of monsoon variability and to understand its forcing mechanisms covering a time span of thousands of years (Clemens et al., 1991; Prell et al., 1992; Sirocko et al., 1993; Naidu and Malmgren, 1996; Schulz et al., l998; Gupta et al., 2003). Proxy indicators by virtue of their physical, biological and chemical origins are indirectly related to paleoceanographic and paleoclimatic variables of interest. Therefore, no single proxy has a unique and direct association with monsoon strength. All proxies have the potential to be influenced by processes other than changes in the monsoon or climate (Clemens and Prell, 2003).

Paleomonsoon reconstructions over South Asia since the Last Glacial Maximum (LGM) have relied on sediment cores from the western Arabian Sea (Sirocko et al. 1996; Overpeck et al., 1996; Zonneveld et al., 1997; Gupta et al., 2003; Jung et al., 2004). Several studies on the past variability of the Indian monsoon have made use of marine sediments from eastern Arabian Sea (Sarkar et al., 2000; Anderson et al., 2002; Prabhu et al., 2004; Prabhu and Shankar, 2005). However, the high-resolution database spanning the late Quaternary period from continental margin sediment of the SEAS, which can provide insight into several monsoon-induced oceanographic processes, is sparse. Such areas with high sedimentation rates (that can provide high resolution) are now the focus of major coring efforts (IMAGES Planning Committee,

1994). Sediments from such areas can document changes on the centennial timescale or even at the decadal scale (e.g., Hughen et al., 1996).

1.3. Objectives of the present study

In view of the scope of the work described above, the following specific objectives are proposed:

1. To reconstruct the past Indian Summer Monsoon (ISM) variability at a high-resolution (centennial to multi-centennial) from the Southeastern Arabian Sea sediments.

2. To *quantify* the past hydrographic changes from the Southeastern Arabian Sea (SEAS) in terms of exact sea-surface temperatures using Mg/Ca ratios, in combination with oxygen isotopes, of planktic foraminifera.

3. To assess the past denitrification variability and the strength of the Oxygen Minima Zone (OMZ) in the SEAS during Late Quaternary

4. To decipher the source and nature (preservation vs. productivity) of organic matter in Late Quaternary sediments from the SEAS.

5. To explore the relation between ISM precipitation variability and its forcing factors like insolation and high latitude climate change.

1.4. A brief review of the earlier work using various proxies for deciphering ISM variations

The Indian monsoon is an important feature of the tropical climate and is a complex system. The nature and the timing of these climatic changes and their relationship with the intensity of monsoonal precipitation are the foci of paleoclimatological research worldwide. The quaternary was a period of major environmental changes and has been the most eventful among all other geologic periods. Previous studies have suggested that the strength of the ISM, upwelling, and productivity in the Arabian Sea are related together. Majority investigations were mainly concentrated in the western Arabian Sea, especially in the Oman margin. The SEAS has been in the focus since last decade, as it is an intriguing region with respect to its response to the past monsoon variations. However, it is necessary to explore this region in more detail in order to understand the effects of past climate on relative strength of the monsoons and associated responses such as sedimentation history, productivity, fluvial input of detritus etc. whether these parameters in the SEAS responded in concert with varying monsoon regime or were they showing difference for a given climate scenario.

ISM induced upwelling brings subsurface nutrients to the euphotic zone of the EAS and thereby induces the copious amount of surface biological productivity. Remains of bulk productivity carriers *viz.* TOC, TN, $CaCO_3$ are expected to be well preserved in sediments depositing beneath both perennial as well as seasonal OMZ due to faster sedimentation rates, better preservation under reducing conditions and minimal bioturbation. The sedimentary TOC and TN have thus been used quite successfully as proxies of ISM intensity in sediments of the northeastern and EAS (Schulz *et al.,* 1998; Agnihotri *et al.,* 2002, 2008a). Likewise, sedimentary $CaCO_3$ also has been

used as a productivity proxy in the SEAS (Bhushan *et al.,* 2001; Agnihotri *et al.,* 2003a, b; 2008a). Traditionally, source characterization of organic matter has been done using C isotopes ($\delta^{13}C_{org}$) and C/N wt. ratios. Fontugne and Duplessy (1986) reported typical $\delta^{13}C_{org}$ of terrestrial and marine type organic matter of the Arabian Sea as −26 and −20‰. Likewise, mean C/N wt. ratio ranges ~8.0± 2 for a typical marine organic matter in this region (Calvert *et al.,* 1995; Bhushan *et al.,* 2001). Several studies carried out in the eastern Arabian Sea even in very shallow marine environment revealed a majority of organic matter is typically 'marine' (Bhushan *et al.,* 2001; Agnihotri *et al.,* 2002, 2003, 2008a) despite heavy monsoonal precipitation runoff on the west coast of India. Sedimentary $\delta^{15}N$, the most reliable and probably only means to measure the extent of past subsurface denitrification in most of the world denitrification zones may not be working in this biogeochemically complex marine realm (Agnihotri *et al.,* 2008a). Contrary to these inferences, in the perennial OMZ region of the eastern Arabian Sea, subsurface denitrification intensity (as measured by sedimentary $\delta^{15}N$) appeared to be varying in concert with surface productivity and hence ISM intensity on millennial time scale during the Holocene (Agnihotri et al., 2003) and same was the case, reported during the Late Quaternary (Ganeshram *et al.,* 2000).

Carbon and Oxygen isotopes of surface and bottom-dwelling foraminifera ($\delta^{13}C$, $\delta^{18}O$) are used to reconstruct evolution of past surface and bottom water hydrographic conditions, respectively (Duplessy *et al.,* 1981; Berger *et al.,* 1985; Rostek *et al.,* 1997; Sarkar *et al.,* 1990; Sarkar *et al.,* 2000; Thamban *et al.,* 2001). The $\delta^{18}O$ of foraminiferal calcite is a function of temperature and salinity of the waters in which they grow. Therefore, either a logical way or independent proxy (alkenone derived

temperature, for instance) can be used to correct the effect of minor influence from the major one, from the total signal. For example, $\delta^{18}O$ showed a significant positive relationship with surface salinity in the eastern Arabian Sea and hence can be used as a proxy indicator to decipher past surface hydrographic conditions, if appropriate temperature corrections are used (Sarkar *et al.* 2000). On the contrary to $\delta^{18}O$, $\delta^{13}C$ of foraminifera reflects productivity and several other factors of surface waters. Bio-productivity, in general, consume ^{12}C preferentially compared to ^{13}C leaving its signature in form of enriched $\delta^{13}C$ in foraminiferal tests, thereby enabling them to act as a proxy for surface productivity.

Several paleo-studies carried out in the EAS have attempted a suite of major and trace elements for tracking monsoon related processes. For instance, a sedimentary abundance of characteristic major and minor elements such as Al, Mg, Ti and also Fe track changes in lithic fraction either by changes in terrestrial runoff/ aeolian inputs (supply) or by just dilution by other biogenic components or both. Fe, although is a redox-sensitive element, amount of Fe taking part in redox-changes in continental margin regions is very small compared to its total abundance. Redox conditions in bottom waters/ sedimentary column strongly influence the distribution of some of the trace elements such as Mn, Cr, V and U. In sediment pore waters, depending on their oxidation states, these elements have different solubilities. For example, Mn is found to be enriched in sediments from the oxic zone, whereas in reducing environment it gets mobilized to pore waters, therefore, gets depleted in the solid phase (Bonatti *et al.* 1971; Somayajulu *et al.* 1994; Yadav, 1996). In contrast, Cr, V, and U are found to be depleted in the oxic zone and enriched in the reducing strata (Dean *et al.* 1997). Thus, an anti-correlation is expected in the depth-profiles between Mn/Al and Cr/Al

or V/Al (wt. ratios) during diagenetic changes in sedimentary column. Sediment cores lying outside the OMZ of the eastern Arabian Sea were found to have much lower abundance of TOC and TN contents due to much lower sedimentation rates and thereby longer oxygen exposure time at the sediment-water interface, leading to a probable poor preservation of these traditional surface productivity proxies (Agnihotri *et al.,* 2003). However, elemental ratio of Ba/Al or biogenic Ba content of the sediment has demonstrated its potential to be a reliable indicator of surface productivity proxy (Dymond *et al.,* 1992) in these settings (Agnihotri, 2001; Agnihotri *et al.,* 2003).

1.5. Outline of the thesis

In addition to this chapter, this thesis contains six other chapters. **Chapter 2** contains the theoretical and experimental basis for this thesis. Then, the results of this study are presented in paper format throughout the consecutive four chapters. **Chapter 3** presents high-resolution quantification of past SST and salinity from the SEAS, which demonstrate the influence of solar variability on Indian Summer Monsoon intensity. "An edited version of this paper was published by SAGE publishing. Copyright (2015) SAGE publishing." The full citation and a link to the open abstract is as follows: Manish Tiwari, Siddhesh S. Nagoji, R. Ganeshram (2015), Multi-centennial scale SST and Indian summer monsoon precipitation variability since mid-Holocene and its nonlinear response to solar activity, The Holocene, 25, 1415-1424, doi: 10.1177/0959683615585840. **Chapter 4** presents high-resolution paleoclimatic/ paleoceanographic history of the SEAS since mid-Holocene. "An edited version of this paper was published by AGU. Copyright (2017) American Geophysical Union." The full citation and a link to the open abstract is as follows: Siddhesh Nagoji and

Manish Tiwari (2017), Organic carbon preservation in Southeastern Arabian Sea sediments since mid-Holocene: Implications to South Asian Summer Monsoon variability, Geochemistry, Geophysics, Geosystems, 18, doi:10.1002/2017GC006804. In **Chapter 5** we discuss the influence of ventilation on the denitrification variability in the SEAS at a high-resolution (centennial scale) for the past ~43 kyrs, and the underlying mechanisms**.** This paper has been submitted for publication in 'Palaeogeography, Palaeoclimatology, Palaeoecology'. **Chapter 6** contains Late Quaternary paleoclimate/paleoceanographic history of the Arabian Sea with special emphasis on spatial and temporal variations in denitrification variability and its implications to Late Quaternary nitrogen and carbon cycles. This paper has been submitted for publication in 'Palaeoceanography'. The main conclusions drawn from this study along with a suggestion for future work are presented in **Chapter 7.**

Chapter 2

Materials and Methods

2. Materials and methods

2.1. Core details

Three marine sediment cores (Table 1) were retrieved from the Southeastern Arabian Sea to achieve the thesis-objectives: (1) core SN6 from the mid-OMZ, (2) core SK 274-4G from the lower boundary of the OMZ, and (3) core SK 274-1G from below the present day OMZ. Immediately after collection, sediment cores were maintained at 4°C for transport and storage. Previous to analysis, sediment cores were sub-sampled at every 1 cm interval. In the laboratory, parts of the sample were dried at 40°C, finely powered using agate mortar and were used to determine the content of bulk total organic carbon (TOC), total inorganic carbon (TIC), total nitrogen (TN), and total organic carbon and total nitrogen stable isotopic composition ($\delta^{13}C$, TOC, $\delta^{15}N$, TN) in sediments. An aliquot of wet sediment was preserved to separate planktonic foraminifera for measurements of ^{14}C, $\delta^{18}O$, and Mg/Ca ratio.

Core Name	Latitude	Longitude	Core length	Water depth
SN 6	12˚29` N	74°07`E	0.36 m	589 m
SK 274-4G	13˚59` N	72°0`E	2.50 m	1290 m
SK 274-1G	08˚0` N	75° 59` E	1.50 m	1491 m

Table 1. Shows details of the cores used in this thesis.

2.2. Proxies used in this study

In order to deduce past climate variability, the reconstruction of physicochemical seawater conditions is the primary objective of paleoceanography. As direct measurements of past physicochemical seawater conditions are no longer possible,

secondary indicators which have a close relationship to anyone environmental parameter are used for this task. These measurable descriptors for desired (but unobservable) variables are called "proxies" (Wefer et al., 1999). Some of the proxies employed in this study are discussed below.

2.2.1. Planktonic foraminiferal Mg/Ca and $\delta^{18}O$ as a proxy for past oceanic temperature and salinity

Foraminifera - unicellular organisms - secrete multi-chambered calcareous shells and occur in all ocean basins and may dwell in surface waters (planktonic species) as well as on the seafloor (benthic species). Widespread as they occur, they have the potential to record ocean wide seawater properties. The morphologic and geometric features of their skeleton, i.e. the arrangement of their successive chambers, enable the micropaleontologist to identify the different species (e.g. Kemle-von Mücke and Hemleben, 1999). Each of these species favors different environmental conditions (e.g. Bijma et al., 1990; Darling et al., 1999; Rutherford et al., 1999) and the knowledge of these habitat preferences allows focusing the paleoreconstructions on specific locations and timescales. Planktonic foraminiferal Mg/Ca thermometry is a relatively recent addition to the expanding set of proxies used for reconstructing past changes in sea surface temperature (SST). Mg^{2+} is one of several divalent cations, which may substitute for Ca during the formation of biogenic calcium carbonate. The temperature of the surrounding seawater influences its incorporation into foraminiferal calcite during growth such that foraminiferal Mg/Ca ratios increase with increasing temperature. Mg/Ca thermometry has distinct advantages over other temperature proxies. The oceanic residence times for Ca and Mg are relatively long (10^6 and 10^7 years, respectively) therefore the Mg/Ca ratio of seawater may be

considered to be constant over glacial/interglacial timescales. This assertion removes considerable uncertainty when reconstructing paleotemperatures using foraminiferal Mg/Ca ratios. In contrast, foraminiferal $\delta^{18}O$; which is also sensitive to changes in temperature, is strongly influenced by changes in the oxygen isotopic composition of seawater (δ_w). Since δ_w varies both as a function of global ice volume and local salinity differences, the direct interpretation of foraminiferal $\delta^{18}O$ is not straightforward. However, these two proxies can be combined in order to reconstruct variations in δ_w over time (Mashiotta et al., 1999; Elderfield and Ganssen, 2000; Lea et al., 2002). A similar approach has been to combine foraminiferal $\delta^{18}O$ with other SST proxies such as alkenones and faunal counting (Rostek et al., 1993; Cayre et al., 1999; Arz et al., 2003). However, only Mg/Ca ratios coupled with $\delta^{18}O$ can guarantee a common source of the signal, averaging the same environmental conditions (season and spatial habitat). This is one of the greatest contributions of Mg/Ca paleothermometry since errors and uncertainties for δ_w reconstructions can be substantially minimized. Further, since temperature estimates based on Mg/Ca ratios are specific to the species employed they may be used to reconstruct temperatures from different depths in the water column depending on the species' habitat preferences. Measurement of foraminiferal Mg/Ca ratios is quite straightforward with modern techniques of elemental analysis and as a result, high-resolution records may be attained in a relatively short time.

2.2.2. Organic matter content as proxy for surface water productivity/ preservation state

Organic carbon is the basic parameter used to determine the abundance of organic matter in sediments; in most cases, organic matter is 50% organic carbon. Since total

organic carbon, and thus total organic matter is measured as a weight percent, other components of the sediment may influence concentration (Meyers and Teranes, 2001). The concentration of organic carbon is dependent on three factors: production, dilution, and preservation. Increased production via photosynthesis generally results in increased accumulation of organic matter in the sediment, which is reflected by increased percent Total Organic Carbon concentration (TOC).

Organic matter in the marine environment is subject to a variety of processes, which can lead to its alteration and consumption, ultimately determining the level of preservation. These processes occur throughout the sinking, burial and post-burial stages of organic matter sedimentation (Hodell and Schelske, 1998; Schelske and Hodell, 1991; Meyers and Ishiwatari, 1993). Oxidation of organic matter occurs throughout the water column and can be prolonged by resuspension. Once organic matter reaches the sediment-water interface, it becomes an important part of the benthic food chain, leading to further alteration. Anoxic conditions, when present, decrease the rate of decomposition of organic matter, thus increasing preservation potential (Hodell and Schelske, 1998). Although alteration of organic matter is variable, can be difficult to quantify, and only a small portion of the original organic matter is often preserved, careful analysis of geochemical signatures retained within the sediment can still be useful to reconstruct marine paleoenvironments (Meyers and Teranes, 2001). To reconstruct the past productivity variability the TOC is a widely used proxy that can be related to various climatic factors. But this organic matter can be from marine as well as terrestrial sources. Therefore, it is important to ascertain the source of the organic matter for precise interpretation.

2.2.3. Atomic C/N, and $\delta^{13}C$ as proxies for sedimentary organic matter sources

Atomic C/N ratios, determined by elemental analysis of sediment, calculated from % TOC and % total nitrogen (%TN), are used to differentiate between algal and plant-derived organic matter. Atomic C/N ratios are generally between 4-10 in algae (non-vascular plants), due to an abundance of nitrogen-rich proteins and little lignin-cellulosic material. Terrestrial (vascular) plants exhibit atomic C/N ratios greater than 20, as they are primarily made up of carbon-rich cellulose (Meyers, 1997; Meyers and Teranes, 2001). Degradation of organic matter can affect atomic C/N ratios. Selective degradation of carbon-rich components of vascular plants can occur post-burial, resulting in lower atomic C/N values. Algal organic matter, however, may exhibit increased atomic C/N ratios during water column degradation due to selective degradation of more labile N-rich proteins. Despite selective organic matter degradation, several studies have shown that the changes of elemental composition of organic matter are not significant enough to alter the original source signal (Ishiwatari et al., 1977; Ertel and Hedges, 1985; Jasper and Gagosian, 1989; and others). Lower atomic C/N values are often found with greater distance from shore, as terrestrial influence decreases. Grain size may also affect atomic C/N ratios, through hydrodynamic sorting. Coarse sediments generally contain terrestrial plant debris, with higher atomic C/N ratios. Finer sediments are frequently clay-sized and therefore tend to adsorb more ammonia, increased surface area, decreasing the atomic C/N ratio even further with greater distance from the shore (Meyers and Teranes, 2001).

The isotopic composition ($\delta^{13}C$) of sedimentary organic matter can also be used to determine its terrestrial or aquatic origin (Dupont et al., 2010; Jennerjahn et al., 2004).

The proportion of stable carbon isotopes in nature is approximately 98.89% ^{12}C to 1.11% ^{13}C. Changes in carbon isotopic composition of sediment are determined by different biochemical processes and can be the result of shifts in organic matter source, changes in the form of available carbon and variations in productivity within the system (Stuiver, 1975). It is important to determine the environmental controls on the isotopic composition of the various organic matter sources in order to interpret bulk sedimentary organic matter data. In different categories of plants, the carbon fixation reaction involves different enzymes following diverse pathways. Organic matter produced by marine algae from dissolved bicarbonate ($\delta^{13}C$ value of ~ 0 ‰) typically has $\delta^{13}C$ values ranging from −11 to −39‰ and the mean value is −21‰ (Farquhar et al., 1989). Whereas, organic matter produced by land plants from atmospheric CO_2 ($\delta^{13}C$ ~7 ‰) using the Calvin Cycle pathway range from −20‰ to −36‰ with a mean value of −27‰ (Farquhar et al., 1989). These plants are called C3 plants. The other important pathway is the Hatch–Slack Cycle that occurs in plants called as the C4 plants. This pathway utilizes water much more efficiently. Hence the C4 plants readily colonize the arid environments. The $\delta^{13}C$ values of the C4 plants range from −9‰ to −17‰ with a mean value of −13‰ (Farquhar et al., 1989). It is clear from this discussion that the δ13C value of the organic materials from different sources overlap. Therefore, it is advisable to use $\delta^{13}C$ in combination with C/N ratio.

2.2.4. Nitrogen isotopes of sedimentary organic matter as denitrification indicator

Nitrogen has two stable isotopes, ^{14}N and ^{15}N (atomic masses of 14 and 15, respectively). ^{14}N is the more abundant of the two, comprising 99.63% of the nitrogen found in nature. Physical, chemical, and biological processes discriminate between

the two isotopes, leading to subtle but measurable differences in the ratio of ^{15}N to ^{14}N among different forms of nitrogen found in the marine environment. Nitrogen is a central component of marine biomass and one of the major nutrients required by all phytoplankton. In this sense, biologically available (or "fixed") nitrogen is representative of the fundamental patterns of biogeochemical cycling in the ocean. However, nitrogen differs from other nutrients in that its oceanic sources and sinks are dominantly internal and biological, with marine N_2 fixation supplying much of the fixed nitrogen in the ocean and marine denitrification removing it. The nitrogen isotopes provide a means of studying both the input/output budget of oceanic fixed nitrogen and it's cycling within the ocean.

N_2 fixation is the major input of fixed nitrogen to the ocean. N_2 fixation is carried out by N_2 fixers - cyanobacteria and other microorganisms - catalyze the conversion of atmospheric N_2 into biomass. Subsequent remineralization of this biomass supplies new nitrogen to the dissolved fixed nitrogen pools in the surface and subsurface ocean. Other inputs of fixed nitrogen to the marine environment include terrestrial runoff and atmospheric precipitation. Denitrification, the bacterial reduction of nitrate to N_2, is the major mechanism of fixed nitrogen loss from the ocean, occurring both in the water column and in sediments when the oxygen concentration is low (<5 μM). Denitrification strongly discriminates against the heavier isotope, ^{15}N, thus enriching the residual nitrate in the heavier isotope, which gets upwelled to the sea surface and is taken by the organisms as a nutrient. The $\delta^{15}N$ of the organic matter is governed by the isotopic composition of the source NO_3^- that is upwelled from below and fractionation experienced by NO_3^-during its uptake by the phytoplanktons (Altabet and Francois, 1994). In the oxic waters of the euphotic zone, the $\delta^{15}N$ of the nitrate is

5–6‰ (Liu and Kaplan, 1989) whereas, in the regions receiving waters upwelled from the OMZ the $\delta^{15}N$ is in the excess of 18‰ (Cline and Kaplan, 1975) that explains the highly enriched $\delta^{15}N$ values observed in the particulate organic matter. This enriched $\delta^{15}N$ signature is preserved even when the organic matter settles down and gets preserved in sea sediments (Saino and Hattori, 1987). Thus, a high $\delta^{15}N$ can be related to increased dentrification, which in turn is controlled by the climate induced productivity increase (Ganeshram et al., 1995).

2.2.5. Trace metals as paleo-redox proxies

The redox condition of marine sediments is the cumulative response of organic carbon and bottom water oxygen concentration. High organic carbon flux to the sediment and low bottom water oxygen concentrations favor the development of anoxic conditions close to the sediment-water interface (McKay et al., 2007). This redox condition can be traced by the trace metal distribution in sediments. Many trace elements are redox-sensitive and become moderately to highly enriched under anoxic bottom water conditions, making them useful as indicators of past redox conditions. The redox environment prevalent during the deposition of marine sediments is reconstructed using the geochemical behavior of redox-sensitive trace metals such as Mo, Cu, Zn, Ni, Co, V, and Cr (Jones and Manning 1994; Tribovillard et al., 2006).

In marine sediments, Mo is considered as a proxy of redox conditions because of its conservative behavior in oxygenated waters and enrichment in anoxic sediments. The ratio R = (Cu + Mo) /Zn has been proposed by Hallberg (1976), as an indicator of the oxygenation of bottom waters. The basic principle behind the use of this ratio lies in the fact that in reduced environment with H_2S in bottom water, the precipitation of Cu

is favored over Zn in the sediments, which is the result of differences in the solubility product of their sulfides in the reduced environments (Hallberg, 1976 and references therein). Hence, this ratio is expected to increase under anoxic conditions and decrease under oxidizing conditions.

In oxic environments, Nickel behaves as a micronutrient, which occurs as soluble Ni^{2+} or $NiCl^{+}$ ion (Tribovillard et al., 2006). Nickel complexation with organic matter accelerates scavenging in the water column and thus its enrichment in sediments (Calvert and Pedersen, 1993). Unlike Ni, Cobalt behaves similarly as Mn in seawater and sediments, i.e. it can diffuse out of sediments under reducing conditions (Heggie and Lewis, 1984) and hence increase the Ni/Co ratio.

In oxic water, vanadium is present in the pentavalent state as vanadate oxyanions (HVO_4^{2-} and $H_2VO_4^{-}$). In pelagic and hemipelagic sediments, V is strongly coupled with the redox cycle of Mn (Tribovillard et al., 2006). The V/Cr ratio is a redox indicator, which reflects changes in the scavenging efficiency as a function of redox conditions (Gallego-Torres et al., 2010; Jones and Manning, 1994; Riquier et al., 2006). Under oxic conditions vandate adsorbs more strongly than chromate, whereas in reducing condition Cr (III) forms stronger surface complexes than VO^{2+}.

2.3. Isotope Systematics

2.3.1. What are stable isotopes?

Atoms consist of the subatomic particles protons, electrons and neutrons. Protons are positively charged, electrons are negatively charged and neutrons have no charge. The mass of a neutron is about equal to that of a proton and the mass of an electron is

negligible relative to protons and neutrons. Therefore, the total number of protons and neutrons determines the mass of an atom. The number of protons in its nucleus defines an element. In a neutral atom, the number of protons is balanced by an equal number of electrons, which are present as a negatively charged cloud around the nucleus. The configuration of the electron cloud imparts to the atom its gross chemical properties. For a given element, the number of protons (atomic number) is always the same, but the number of neutrons (neutron number) may vary. The mass number is the sum of atomic number and neutron number. An isotope of a given element differs from another isotope of the same element by the number of neutrons in its nucleus. The number of neutrons in the nucleus of an element does not affect the gross chemical properties of the element and its compounds, but mass differences due to changing neutron number can cause subtle chemical and physical differences which results in isotopic fractionation. It is these small differences comprise the subject of this discipline.

2.3.2. Isotope Effects

(a) Kinetic isotope effects

Kinetic isotope effects are common both in nature and in the laboratory and their magnitudes are comparable to and often much larger than those of equilibrium isotope effects. Kinetic isotope effects are irreversible, and normally associated with fast, incomplete, or unidirectional processes like evaporation, diffusion, and dissociation reactions. Biological reactions such as photosynthesis are clearly irreversible, defying tradition thermodynamics, which assume chemical equilibrium. Classical kinetic theory tells us that the average kinetic energy (K.E.) per molecule is the same for all gases at a given temperature. Consider, for example, the molecules $^{12}C^{16}O$ and $^{12}C^{18}O$

that have molecular weights of 28 and 30, respectively. Equating their kinetic energies at some T.

$$\text{K. E. } (^{12}C^{16}O) = \text{K. E. } (^{12}C^{18}O) \qquad \ldots(1)$$

and

$$\text{K.E.} = 1/2\ mv^2 \qquad \ldots(2)$$

Where m is mass and v is velocity. Substituting the masses of these isotopologues of CO, the above equations reduce to

$$1/2(28)(v_{28})^2 = 1/2(30)(v_{30})^2 \qquad \ldots(3)$$

$$v_{28} = \sqrt{30/28}v_{30} = 1.035\ v_{30} \qquad \ldots(4)$$

That is, regardless of T, the average velocity of $^{12}C^{16}O$ molecules is 3.5 per cent greater than the average velocity of $^{12}C^{18}O$ molecules in the same system. Such velocity differences can lead to isotopic fractionations in a variety of ways. For example, isotopically light molecules will preferentially diffuse out of a system and leave the reservoir enriched in the heavy isotope. In the case of evaporation, the greater average translational velocities of isotopically lighter water molecules allow them to break through the liquid surface preferentially and diffuse across a boundary layer, resulting in an isotopic fractionation between vapor and liquid that is superimposed on the equilibrium isotopic fractionation between liquid and gaseous H_2O. Attesting to this phenomenon is the fact that water vapor over the oceans or over a large lake has $^{18}O/^{16}O$ and D/H ratios that are significantly lower than the ratios that would obtain at equilibrium (at 100% relative humidity). These lower ratios arise from kinetic isotope effects associated with evaporation.

While it is important to be aware of kinetic isotope effects, they are relatively rare in

high-temperature processes occurring on Earth. By contrast, transient processes can occur whereby differing rates of isotopic exchange between coexisting minerals themselves, or between the minerals and an external fluid, can result in assemblages that are grossly out of isotopic equilibrium. Such examples are explained, not by kinetic isotope effects, but rather by a series of equilibrium isotope exchange reactions.

(b) Equilibrium isotope effects

Equilibrium isotope effects can be considered in terms of the effect of atomic mass on bond energy. Substituting a light for heavy isotope in a molecular site does not affect the nuclear charges or electronic distribution of the molecule. It does, however, affect the bond strength. The energy required to break a bond is slightly higher for a heavy isotope than it is for a light one. This subtle difference in bond strength results in a predictable isotope fractionation between any two phases. The magnitude of this equilibrium isotopic effect is related to the bonding environment of the phases in question. Most importantly, the fractionation is dependent on temperature, so that for appropriate systems, such as calcite-water, the equilibrium oxygen isotope fractionation between the two phases is a function of temperature alone. Equilibrium isotopic fractionation between two substances or between two phases of the same substance is the basis of stable isotope thermometry. The temperature dependence on isotope fractionation spawned the first major application of stable isotope chemistry to geological problems: the calcite oxygen isotope thermometer, first used for paleotemperature estimates over 50 years ago (Urey et al., 1948; Epstein et al., 1951; Urey et al., 1951).

2.3.3 Isotopes, Isotopologues, Isotopomers and Mass Isotopomers

The word **isotope** is defined as atoms whose nuclei contain the same number of protons but a different number of neutrons. All stable isotope studies report the stable isotope composition of a particular element in a molecule or compound. For example, we measure the carbon and oxygen isotope composition of CO_2 or calcite. According to recommendations made in 1994 by the International Union of Pure and Applied Chemistry (IUPAC), **isotopologues** are molecules that differ from one another only in isotopic composition. It is therefore appropriate to talk about the different 'isotopologues' of CO_2, but not the different 'isotopes' of CO_2 because CO_2 doesn't have isotopes – its constituent elements C and O do. Isotopologues can have the same or different masses. For example, $^{16}O^{13}C^{16}O$, $^{17}O^{12}C^{16}O$, $^{16}O^{12}C^{17}O$ has the same mass i.e 45. Although they have the same mass, they are distinctly different isotopologues of carbon dioxide. **Isotopomers** are isotopologues that differ from one another only in the positions or locations of the isotopic elements. Studies of isotopomers is common in pharmaceutical and biochemical research, where the position of atoms provides important information about metabolic processes. Isotopomers always comprise the same number of each isotope and thus always have the same mass. They differ from one another in the positions or locations of the isotopic elements. In mass spectrometry, mass isotopomer is used to describe a family of isotopologues that have the same mass. Mass isotopomers are collected simultaneously on the same collectors of a mass spectrometer.

2.3.4. The Delta Value

Relative differences in isotopic ratios can be determined far more precisely than absolute isotopic ratios. McKinney et al. (1950) introduced the delta (δ) notation to

report stable isotope data. The delta value (δ) is used to express the relative difference of a ratio of the numbers (or the amounts) of two isotopes in a specimen compared with that of a standard (Coplen, 2011). The delta value is given by $\delta = [(R_x\text{-}R_{std})/R_{std}]$ or equivalently $\delta = [(R_x)/(R_{std}) - 1]$ where *R* is the ratio of the abundance of the heavy to light isotope, *x* denotes the sample, and *std* is an abbreviation for standard. For the elements, carbon, oxygen, and nitrogen, *R* is given by $^{13}C/^{12}C$, $^{18}O/^{16}O$ (and $^{17}O/^{16}O$), and $^{15}N/^{14}N$ respectively. δ-value is a dimensionless quantity as it is the ratio of the two quantities of the same kind. Since δ-value is a small quantity, so it is multiplied by extraneous numerical factors like 10^3 and expressed in "per mil" (‰) units for the sake of readability and ease of comprehension. Likewise, when it is multiplied by 10^4, it shall be expressed in "pptt" (parts per ten thousand). These extraneous factor do not form a part of the definition of the delta value and hence has been recommended to avoid its usage in the formula (Coplen, 2011). A positive δ value means that the ratio of heavy to light isotope is higher in the sample than it is in the standard, and a negative δ value has the opposite meaning. A sample with a $\delta^{18}O$ value of +19.7 ‰ has an $^{18}O/^{16}O$ ratio that is 19.7 per mil, or 1.97 per cent, higher than that of the standard. Similarly, a negative $\delta^{18}O$ value of –19.7 ‰ means that the $^{18}O/^{16}O$ ratio of the sample is 19.7 per mil or 1.97 per cent lower than that of the standard. The delta notation provides a very convenient means to express the small relative differences in isotopic ratios between samples and standards that are measured by isotope ratio mass spectrometry.

2.3.5. Reference Standards

Very precise comparisons of isotopic compositions of materials can be determined in a given laboratory, but to allow for accurate inter-comparisons of data obtained in

different laboratories, an internationally accepted set of reference standards is available to all workers in the field. The measured isotopic composition of any substance should be the same in all laboratories after calibrations have been made with these international reference standards. Beginning in the 1970s, committees of stable isotope geochemists convened periodically in Vienna to select standard materials and to establish protocols for calibrating mass spectrometer analyses and presenting stable isotope data (Coplen and Clayton, 1973; Hut, 1987; Coplen, 1996). Reference materials are available from the National Institute for Standards and Technology (NIST) in Gaithersburg, Maryland and from the International Atomic Energy Agency (IAEA) in Vienna. International reference standards are in limited supply and are not intended for use as working standards. They are provided in small quantities to allow workers to establish larger supplies of secondary reference materials that in turn can be used on a daily basis as working standards.

The history of stable isotope reference materials is long and complex. The early Chicago group reported $\delta^{13}C$ and $\delta^{18}O$ values of carbonates relative to the carbon and oxygen isotope compositions of a powdered specimen of *Belemnitella americana* (a species of extinct Belemnites belonging to Class Cephalopoda) from the Upper Cretaceous Peedee Formation of South Carolina. They called this calcite standard PDB (PeeDee Belemnite). When the original supply of this material became exhausted, another sample was prepared and named PDB II, a standard that was later replaced by PDB III. In each case the new standard was carefully calibrated against the isotopic composition of the original sample of PDB. Despite the fact that the original supply of PDB is exhausted, PDB remains the standard used in reporting all carbon isotope analyses and most of the oxygen isotope analyses of low-temperature

carbonates. Secondary standards have been developed with isotopic compositions that are calibrated to the original PDB. Many other accepted standards are available from the IAEA, so that standardization procedures are now relatively routine and stable isotope analyses made anywhere in the world are, for the most part, easily comparable. An outline of the reference materials for selected elements used in this thesis is given below.

(a) Carbon

Carbon isotope ratios are reported relative to the PDB standard described above and, by definition, the $\delta^{13}C$ value of PDB is 0 ‰. Several secondary carbonate standards (e.g. Carrara marble and Solenhofen limestone) were measured relative to PDB in the early years and these standards are still in use in some older laboratories. The international isotope reference standard NBS-19 (and most recently IAEA-603) is now the accepted means of calibrating to the PDB scale. NBS-19 was originally the TS (Toilet Seat) limestone working standard used in the laboratory of Irving Friedman and colleagues at the U. S. Geological Survey (Friedman et al., 1982). It has a $\delta^{13}C$ value of +1.95‰ relative to PDB and VPDB. In other words, the $\delta^{13}C$ value of NBS-19 = +1.95‰ on the VPDB scale. NBS-19 is now out of stock due to consumption over time, and a new calcite standard IAEA-603, a sample of the Carrara marble is available with a $\delta^{13}C$ value of +2.46‰ ± 0.01 on the VPDB scale.

(b) Nitrogen

The reference standard for nitrogen isotope analyses is atmospheric nitrogen and is called Air-N_2. The $\delta^{15}N$ value of atmospheric nitrogen is almost constant everywhere on Earth and is 0 ‰ by definition (Mariotti, 1983). One N_2 gas standard called

NSVEC (^{15}N = -2.8‰ vs AIR) is distributed by IAEA. Several other solid standards (nitrates) are also available from IAEA. Any laboratory can produce their own nitrogen lab-standards by purifying air. Oxygen is removed by combusting the air sample with Cu metal, but contaminant Ar in the product can interfere with the nitrogen isotope analyses.

(c) Oxygen

Two international reference standards are used to report variations in oxygen isotope ratios, VPDB and VSMOW. SMOW was originally defined in terms of NBS-1. Use of the PDB standard for reporting oxygen isotope compositions is restricted to analyses of carbonates of low-temperature origin (oceanic, lacustrine, or pedogenic) in studies of paleoclimate, paleoceanography and carbonate diagenesis. As mentioned above, oxygen isotope compositions of carbonates are determined by analyses of CO_2 generated from them by reaction with 100% H_3PO_4 at a fixed temperature. It is emphasized that the PDB standard is the solid carbonate, not the acid-liberated CO_2 that is actually introduced to the mass spectrometer. The ^{18}O of PDB is 0 ‰ on the VPDB scale by definition and analysis of NBS-19 is the accepted means of relating oxygen isotope analyses to VPDB. The ^{18}O value of NBS-19 is 2.20 ‰ on the VPDB scale. Additional international secondary reference standards for carbonates are also available and relating analyses to PDB no longer poses any ambiguities.

2.3.6. Isotope Ratio Mass Spectrometry

The mass spectrometer is the heart of nearly all-stable isotope laboratories. Some labs are beginning to employ laser spectroscopy systems, but for the last century, most analyses have been made using a mass spectrometer. The foundations of the mass

spectrometer can be traced to the Cavendish Laboratory, University of Cambridge, where noted scientists including J.J. Thomson, E. Rutherford and F.W. Aston developed some of the first mass spectrographs. By 1927, Aston had built a second generation machine that allowed for the discovery of isotopes and accurate determinations of their atomic weights. A description of Aston's early machine is discussed in detail and is worth reading (Aston, 1927). In the early to mid-20th century, most isotope ratios were determined gravimetrically, where the mass of a sample was determined using a precise density balance. The difference in the atomic weight of oxygen in air and water – the basis for the 'Dole Effect' – was determined in this way (Dole, 1936). Major improvements were made in the sensitivity and precision of mass spectrometers in the 1940's so that variations in the isotopic composition of natural materials could be measured with the necessary precision. These machines were operated by talented physicists, and extracting high-quality data required skilled practitioners. Only starting in the 1970s and 80s did the mass spectrometer manufacturers begin to offer mass spectrometers that could be used without a great deal of training and infrastructure. Today, there is a wide range of mass spectrometers available, from simple desktop units for low-precision analyses used for simple tracer experiments, to complex doubly- focusing machines that have high sensitivities and mass resolution for analyses of exotic isotopologues from natural samples. At the same time, there is a growing industry of laser spectroscopy systems in which the isotope ratios are measured based on the absorption of infrared radiation by the different isotopologues of a particular gas, such as CO_2, H_2O, CH_4 and N_2O.

All mass spectrometers are based on the principle of deflecting an energetic, focused

ion beam in a magnetic and/or electrostatic field. The degree of deflection is a function of mass and charge. The relative intensities of the ion beams of different masses can then be used to calculate isotopologue masses or isotope ratios. The mass spectrometer consists of three primary components: 1) the source, where a sample is ionized, accelerated to a given energy and collimated into a well-focused beam; 2) the analyzer, which acts to deflect the ion as a function of mass. It is the 'prism' of the system; and 3) the collector assembly for measuring the relative intensities of the different ion beams. In addition, the mass spectrometer system also has an inlet system for introducing the gas into the source without fractionation.

2.4. Analytical technique used for sample analysis

2.4.1. Elemental and Isotopic abundance of C and N in sedimentary organic matter

For elemental and isotopic analysis of carbon and nitrogen, each sub-sample was oven dried at 40°C and then homogenized by finely grinding it in an agate mortar. For total organic carbon (TOC) concentration and $\delta^{13}C_{org}$ estimation, carbonate was removed from sub-sample by adding 2N hydrochloric acid. The samples were then completely rinsed by adding deionized water five times and again oven dried at 40°C. Given the known problems of loss of nitrogen compounds from the sedimentary organic matter on acidification of samples, resulting in bias in nitrogen content and $\delta^{15}N$ values (Brodie et al., 2011), untreated samples were used for total nitrogen (TN) and $\delta^{15}N$ analysis. A portion of the grinded sample was wrapped in a tin capsule and combusted using an Elemental Analyzer coupled to an Isoprime stable isotope ratio mass spectrometer at the Marine Stable Isotope Lab (MASTIL) of National Centre for Polar and Ocean Research (NCPOR), Goa, India. Samples were run along with the

blank and known standards. Standards were prepared by weighing 0.4–0.6 mg of IAEA cellulose standard (IAEA- CH-3) of certified isotopic composition ($\delta^{13}C$ = −24.74 ‰ vs. VPDB) for carbon isotopic composition and 0.5–1.0 mg of IAEA ammonium sulphate (IAEA N1) of certified isotopic composition ($\delta^{15}N$ = 0.4 ‰) for nitrogen isotopic composition. Sulphanilamide was used as reference standard for %TOC and %TN measurements. Data quality control was checked by running a reference standard after every six samples. Stable isotope abundance is reported in terms of δ-values and expressed in per mil (‰). Analytical precision for isotopic composition for carbon and nitrogen is based on repeat measurements of the reference standard (IAEA- CH-3 for carbon and IAEA N1 for nitrogen). Analytical precisions for the TOC and TN measurements are based on repeat measurements of the reference standard (Sulphanilamide).

2.4.2. Oxygen isotopes and trace element analysis of foraminiferal tests

The oxygen isotope ratio ($\delta^{18}O$) of planktic foraminifera (size range: 250–420 μm) was measured in the Marine Stable Isotope Lab of National Centre for Polar and Ocean Research (NCPOR), Goa, India, using a stable isotope ratio mass spectrometer (IRMS) in dual-inlet mode. The $\delta^{18}O$ values are reported with respect to the V-PDB. The reference standard used for normalizing to V-PDB scale is NBS-19. The precision of the $\delta^{18}O$ measurement is obtained by repeatedly running NBS-19. For Mg/Ca ratio in planktic foraminifera, around 70-80 visibly clean tests were picked under microscope and subjected to cleaning following the protocol of Elderfield and Ganssen (2000), which is modified by Barker et al. (2003). The calcite fragments were then repeatedly washed with ultrapure water followed by methanol to remove clays. The organic coating was removed by treating the clay-free fragments in

buffered H_2O_2 in a boiling water bath. To remove any secondary calcite deposition on the tests, the Mg-polishing was done by treating the clay and coating free fragments with 0.001 N HNO_3. Before the final dissolution in 1 ml of suprapure 0.75 M HNO_3, the cleaned fragments were examined under the microscope to ensure that only pristine calcite is taken for dissolution. The final solutions were than analyzed using ICP-OES following standard calibrations technique (De Villiers et al., 2002).

2.4.3 Trace Metal analysis in sediments

For inorganic elemental chemistry sediments were dissolved following acid digestion procedure by Balaram and Rao (2003). The powdered sediment samples were weighed accurately (50 mg), transferred to clean Teflon beakers and subjected to open acid digestion. The sediments were repeatedly digested by treating with a mixture of HF, HNO_3, and $HClO_4$ in the ratio of 6:3:1. Finally, the extract was brought to a standard volume (50 ml). All elements were analyzed using inductively coupled plasma mass spectrometry at National Centre for Polar and Ocean Research, Goa. Analytical accuracy was determined through analysis of a suite of internationally recognized Standard Reference Material (NIST 2702). The relative standard deviation estimates are based on repeated analysis of standards.

The analytical techniques mentioned above have been explained in more detail in the corresponding chapters.

Chapter 3

Multi-centennial scale SST and Indian summer monsoon precipitation variability since the mid-Holocene and its nonlinear response to solar activity

3.1. Introduction

The formation of an atmospheric pressure gradient between the Indian Ocean and South Asia and northward displacement of the Intertropical Convergence Zone (ITCZ) during boreal summer produces the ISM (Webster, 1987). Modern observations point to sea SST anomalies in the Indian Ocean as a key factor in determining ISM intensity; however, complex interactions are also predicted with changes in tropical Pacific SSTs, El Niño Southern Oscillation (ENSO), and temperature anomalies in Asian land mass (Meehl and Arblaster, 2002). Importantly, a weak but positive correlation is observed between the ISM precipitation and solar variability in the 20th century (Bhattacharya and Narasimha, 2005; Hiremath and Mandi, 2004; Mehta and Lau, 1997). However, such observations on sunspot activity–ISM precipitation relationship are based on data sets spanning only a few decades and hence are uncertain. A few speleotherm records from Oman – a region that receives very little precipitation – reveal the coherence between monsoon and solar variability, but only for early Holocene (Fleitmann et al., 2003; Neff et al., 2001). Additionally, most of the earlier paleomonsoon studies have focused on the western Arabian Sea, where surface ocean productivity is driven by the intense summer monsoon winds through upwelling; typical wind proxies were thus used for detecting past monsoon variations, for example, abundance of *Globigerina bulloides* (surface-dwelling foraminifera) or mineral dust (Anderson et al., 2010; Gupta et al., 2013; Ivanochko et al., 2005; Naidu and Malmgren, 1996; Sirocko et al., 1993; Tiwari et al., 2010, and references therein). However, these records reflect the monsoon wind intensity and not the monsoon precipitation, which is more relevant to human society and is the basis of the livelihood of the millions of people living in South Asia. The reconstructions are also disadvantaged given that climatological studies have shown

that the relationship between ISM wind over the Arabian Sea and precipitation can be nonlinear as higher precipitation can result because of moisture convergence despite the weakening monsoonal flow (Shukla and Misra, 1977). SEAS, in contrast, is uniquely suited to reconstruct precipitation records from proxies, particularly in documenting subtle Holocene climatic oscillations. First, monsoon signals are highly amplified within the SEAS as major changes in salinity occur because of orographic precipitation and runoff along the southwestern coast of India (Schott et al., 2009). Fig. 2 depicts the seasonal profile of climatological salinity and temperature as per the World Ocean Database (Boyer et al., 2009) at 12°30′N, 74°30′E, very near the core location.

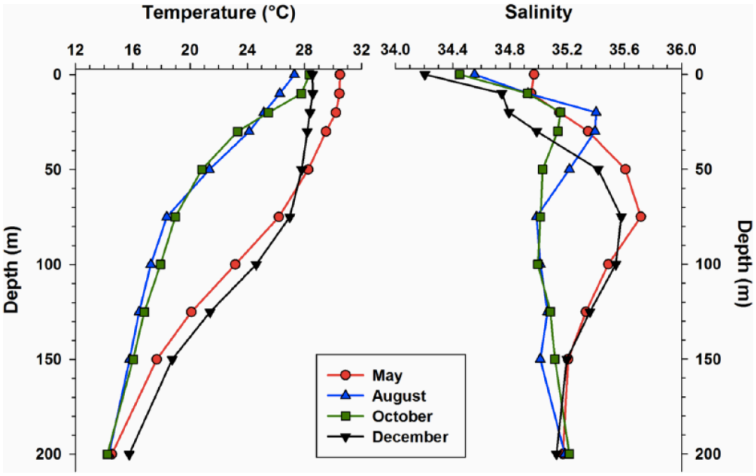

Figure 2: Present-day temperature and salinity profiles near the core location. It reveals clear seasonality with maximum sea surface salinity and temperatures (SSS and SST) during the period corresponding to the pre-summer monsoon (depicted by the month May). The minimum SST is noticed during the summer monsoon period (shown by August) indicating the effect of moderate upwelling during that period. The SSS also reduces during the summer monsoon period because of the surface runoff and overhead precipitation. The salinities reduce further during the post-summer monsoon period as the Northeast monsoon wind driven North East Monsoon Current (NEMC) brings lower salinity waters (fresher due to input from the Ganges–Brahmaputra–Irrawaddy River system mainly fed by summer monsoon precipitation) from the northern Bay of Bengal. This figure is based on the World Ocean Database 2009 (Boyer et al., 2009).

Here, sea surface salinity reduces by 0.5 during the summer monsoon period (mean represented by August values) because of surface runoff and overhead precipitation. Also, the salinity decreases by up to 0.8 during the post-monsoon period because of the transport of lower salinity waters from the northern Bay of Bengal (fresher due to input from the Ganges–Brahmaputra–Irrawaddy River system mainly fed by summer monsoon precipitation) via the wind driven North East Monsoon Current. Additionally, the moderate upwelling causes SST to fall to a minimum of 27.5°C during the summer monsoon period from a high of 30.5°C during the pre-monsoon (mean depicted by May in Fig. 2). These relatively large salinity and temperature changes in the study site make it uniquely suitable for reconstructing paleomonsoon precipitation. Second, a perennial oxygen minimum zone (OMZ) (Naqvi and Noronha, 1991) occurs in the Arabian Sea at depths of 100/150 to 1000 m. The core site of the present study lies at a depth of 589 m, the middle of the OMZ. Bioturbation effects in such sediments are minimal (Smith et al., 2000), and sediments also accumulate rap- idly in such coastal locations; both the factors enable a high-resolution study. The utility of the $\delta^{18}O$-salinity method for monsoon reconstructions in the southeastern Arabian Sea has been demonstrated by recent studies employing this method on glacial–interglacial and millennial timescales (Anand et al., 2008; Govil and Naidu, 2010; Kessarkar et al., 2013; Saraswat et al., 2013, and references therein). Although a few earlier paleoclimatological studies from the SEAS have linked ISM precipitation with solar variability on centennial to multi-centennial timescales (Chauhan et al., 2009; Tiwari et al., 2005, 2006), it remains speculative primarily because of the lack of records with properly resolved SST and salinity component in monsoon reconstructions. In view of this, a sediment core from the coastal SEAS from the OMZ is analyzed to reconstruct the SST and the salinity on

centennial timescale. We further compare our more precise (i.e. temperature corrected), high-resolution summer monsoon reconstruction since mid-Holocene with recent periods of low Total Solar Irradiance (TSI) (e.g. Maunder, Spörer, Oort, Wolf, and beyond) to explore the role of solar activity on such timescales in driving tropical convection. We confirm our results statistically using Continuous Wavelet Transform (CWT) and Squared Wavelet Coherence analysis between different time series.

3.2. Core details and chronology

The sediment core used in this study, SN-6, was collected in 2010 during the return leg of the Fourth Indian Southern Ocean Expedition from the SEAS from a water depth of 589 m (12°29′12″N; 74°7′59″E; location shown in Fig. 3).

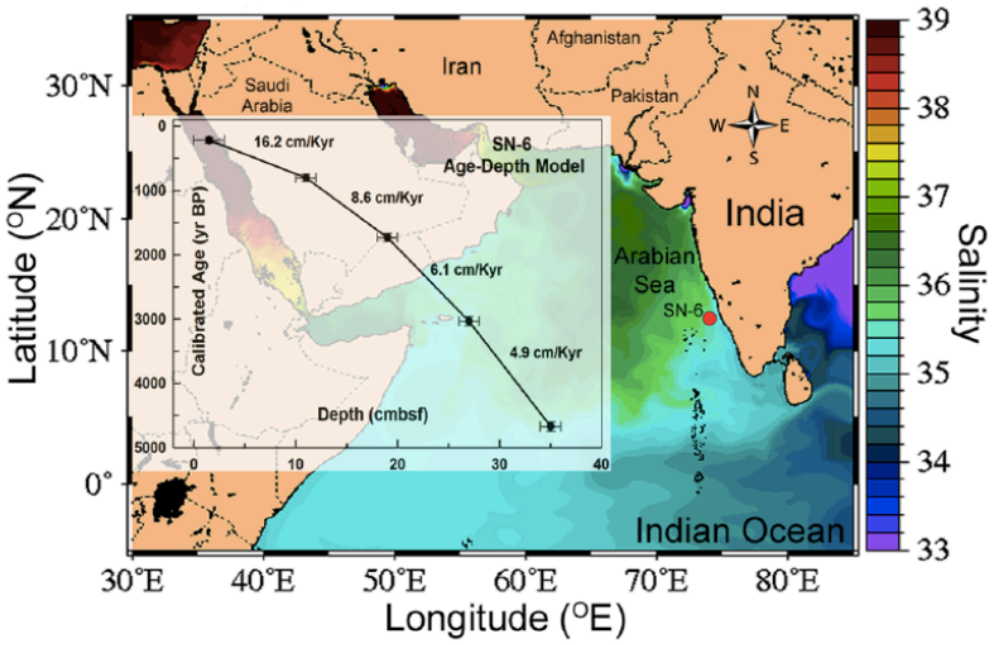

Figure 3. Location of the Core SN-6 with surface salinity contours and its Age–Depth Model. The core (shown by closed circle) is strategically located to determine the salinity fluctuations due to precipitation variability as it receives copious rainfall and surface runoff during the summer monsoon season. The salinity changes rapidly away from the west coast of India. Age–Depth model (inset) is based on five radiocarbon dates approximately at every 9 cm on selected species of planktic foraminifera; sedimentation rates are also shown (underlined; in cm/kyr).

The total length of the core was 36 cm and was sampled at every centimeter to obtain high temporal resolution. The sedimentation rates observed for the top 11 cm is 16.2 cm/kyr yielding a sub-centennial scale resolution of ~62 years per sample which increases to centennial scale in the later part of the core (Fig. 3, Age–Depth Model in inset); average sedimentation rate is 8.96 cm/kyr while the average resolution is ~112 years per sample. These high temporal resolutions and the fact that the core has experienced relatively less bioturbation as it is raised from the middle of the OMZ allow us to reconstruct the SST and the salinity at high resolution. The chronology of the core was obtained on an average at every 9 cm through five radiocarbon dates on selected species of planktic foraminifera (Globigerinoides ruber, Globigerinoides sacculifer; size range: 250–420 μm) using accelerator mass spectrometer (AMS) at the NSF AMS Facility at University of Arizona. The radiocarbon ages were calibrated using the program CALIB 6.0 (Stuiver and Braziunas, 1993) with the global reservoir age correction of 400 years following previous studies from this region (Chauhan et al., 2009; Govil and Naidu, 2010). Also, Butzin et al. (2005) yield the reservoir age based on a three-dimensional global ocean circulation model for the core location as 373 years (available at http://radiocarbon.LDEO.columbia.edu), which is very near to the global reservoir age. This is an estimate of the modern ocean radiocarbon reservoir ages based on the physics of the ocean circulation (Cao et al., 2007) compared with previous tentative estimates based on a few data points from far-off regions (Dutta et al., 2001; Southon et al., 2002). The top of the core (0– 3 cmbsf) yields an age of 154 yr BP (years before present; present denotes AD 1950) while the full core spans up to 4772 yr BP.

3.3. Oxygen isotope and trace element ratio analysis

The oxygen isotope ratio ($\delta^{18}O$) of *G. ruber* (white; d'Orbigny; morphotype sensu stricto; size range: 250–420 μm) was measured in the Marine Stable Isotope Lab of National Centre for Polar and Ocean Research (NCPOR), Goa, India, using a stable isotope ratio mass spectrometer (IRMS) in dual-inlet mode. The $\delta^{18}O$ values are reported with respect to the V-PDB. The reference standard used for normalizing to V-PDB scale is NBS-19. The precision of the $\delta^{18}O$ measurement is ±0.08‰ (1σ standard deviation) obtained by repeatedly running NBS-19 (n = 25). The past SST variations were determined using an independent parameter, that is, Mg/Ca content of the shells of the planktic foraminifera – *G. ruber* (white; d'Orbigny; morphotype sensu stricto; size range: 250–420 μm). The core is from a shallow location, and hence the foraminiferal tests had detrital particles sticking on shells and filling pore spaces. Therefore, removing the contaminating phases with care to avoid altering the original Mg/Ca ratio was very important in the present study. The cleaning was carried out following Barker et al. (2003) that included removal of alumino-silicates, which were the biggest source of contamination followed by removal of organic matter using an oxidizing agent (using hot alkali-buffered solution of H_2O_2) and removal of manganese and iron oxide coatings using reductive treatment (using buffered solution of hydrous hydrazine). Mg/Ca ratios were measured on samples comprising 70–80 shells of the foraminifera G. ruber. Usually, 30–35 shells of G. ruber are enough to yield sufficient material for Mg/Ca analysis, but due to high levels of detrital contamination in the present case much larger number of shells was needed to be cleaned. The use of a larger number of shells also helps in avoiding the problem of the biological variability. Therefore, every sample required extensive cleaning of each shell of foraminifera (submerged in methanol) under high-power

stereozoom microscope. Each shell was broken using a surgical scalpel and the contaminating phases/detrital particles were sucked away using a dropper. The shells were thereafter ultrasonically cleaned and observed again under the microscope. If any contamination was observed, above steps were repeated unless pristine fragments of shells were only present. Samples were analyzed using an ICP-OES in the School of Geosciences, University of Edinburgh, UK, using the methods described elsewhere in detail (De Villiers et al., 2002). To monitor residual contamination, the criterion chosen was to reject any sample with Fe/Mg ratio exceeding 1 mol/mol (Barker et al., 2003). The precision obtained for Mg/Ca values through repeated measurements of carbonate reference material ECRM 752-1 over the period of analysis is 0.02 mmol/mol (1σ standard deviation) corresponding to a precision of 0.06°C. The calibration equation used to convert Mg/Ca ratio to SST is as follows: SST = (1/0.09) × LN{(Mg/Ca)/0.38} (Anand et al., 2003). The inherent error in the calibration equation yields an accuracy of ±1.2°C (Anand et al., 2003). The $\delta^{18}O$ of seawater was constructed from the SST and the $\delta^{18}O$ of *G. ruber* using the following equation: $\delta^{18}O_{seawater} = 0.27 + \{(SST - 17 + 4.59 \times \delta^{18}O_{ruber})/4.59\}$ (linear regression of the Erez and Luz (1983) data as given in equation (6) of Bemis et al. (1998)). $\delta^{18}O$ values of seawater were converted into salinity using the following equation: Salinity = $(\delta^{18}O_{seawater} + 8.6)/0.26$ pertaining to the northern Indian Ocean (Singh et al., 2010) that compiles data collected during different cruises from 1987 to 2009 (n = 152). The error in the estimate of $\delta^{18}O_{seawater}$ is ±0.3‰ corresponding to an accuracy of 2.3 in salinity reconstruction after including the uncertainties in the SST calibration equation, $\delta^{18}O_{ruber}$ measurement, and temperature–$\delta^{18}O_{ruber} - \delta^{18}O_{seawater}$ conversion.

3.4. ISM precipitation variability since the mid-Holocene

SEAS experiences two periods of salinity reduction – first during the summer monsoon season and thereafter during the post-summer monsoon season (Fig. 2; Boyer et al., 2009; Schott et al., 2009). Therefore, it is important to select a species representative of the season of interest, which is summer in this case. The percentage of *G. ruber* among all the species may decline during the summer monsoon, but its absolute number increases signifying the fact that it mostly represents summer monsoon conditions (Curry et al., 1992). Guptha et al. (1994) also found a high number of *G. ruber* in six vertical plankton tows in the SEAS during the summer monsoon period. In fact, several previous paleoclimatological studies from the SEAS have used *G. ruber* to reconstruct past summer monsoon conditions (e.g. Govil and Naidu, 2010; Kessarkar et al., 2013; Saraswat et al., 2013; Thamban et al., 2001; Tiwari et al., 2006, and so on). Also, *G. ruber* dwells predominantly in the surface mixed layer and is therefore a very good representative of surface conditions (Field, 2004). Therefore, we chose *G. ruber* to calculate the past SST and surface salinity of the SEAS during the summer monsoon season. Fig. 4a–c depicts the oxygen isotope ($\delta^{18}O$), SST, and the salinity values, respectively. The bands depict the periods of high salinity/reduced ISM precipitation (Fig. 4c). As there are no ice-melting episodes of significance during the period of the study (Peltier and Fairbanks, 2006), no ice-volume correction is applied to the $\delta^{18}O$ values. Dark gray lines in Fig. 4a show the precision of the $\delta^{18}O$ruber measurement (±0.08‰). Dark gray lines in Fig. 4b and c show the boundaries of the calibration uncertainty in the SST (±1.2°C) and the $\delta^{18}O_{seawater}$ (±0.3‰) reconstruction. Calibration uncertainty affects the accuracy and not the precision. So, the trends are real, but the absolute SST and $\delta^{18}O_{seawater}$ values have errors introduced by calibration. That is to say, if we repeat our analysis, we will

come up with the same curve, but the curve will move up or down depending on the uncertainties in the calibration equation.

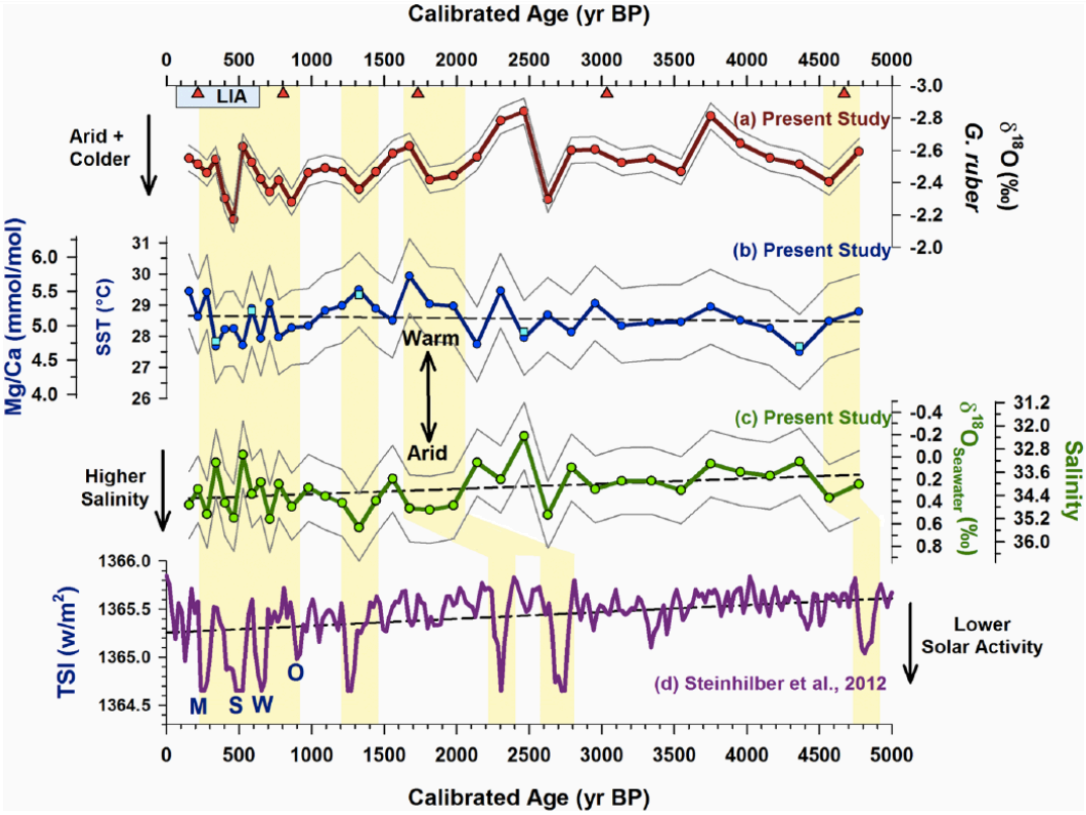

Figure 4. SST and salinity variability of the southeastern Arabian Sea since mid-Holocene. Bands depict the periods of higher salinity/reduced Indian Summer Monsoon precipitation; dashed lines depict the long-term trend determined through linear regression (least square method): (a) $\delta^{18}O$ values of Globigerinoides ruber, which is a function of temperature and salinity (closed triangles indicate the position of the Accelerator Mass Spectrometer (AMS) radiocarbon dates); (b) SST values derived from the Mg/Ca ratio of the G. ruber (closed squares depict the repeat values; see text for more details); (c) ISM precipitation intensity shown by salinity fluctuations in the southeastern Arabian Sea; note that the salinity scale is reversed; (d) solar activity indicated by TSI variability (Steinhilber et al., 2012); the capital alphabets depict the Maunder, Spörer, Oort, and Wolf minima. Dark gray lines in panel 'a' show the precision of the $\delta^{18}O_{ruber}$ measurement while those in panels 'b' and 'c' show the calibration uncertainty in the SST and the $\delta^{18}O_{seawater}$ reconstruction (see text for more details). LIA: Little Ice Age.

Since the mid-Holocene, the SST in the SEAS during the ISM period has varied from a maximum of 29.9°C to a minimum of 27.5°C – a range of 2.4°C (Fig. 4b). To check

the consistency, five sample-extracts were re-run that yield identical values confirming the results (shown as closed squares in Fig. 4b). The study site is a shallow location near the coast that experiences moderate upwelling during the ISM season, which could reduce the SST by up to 3°C as shown by the present-day climatological data (Fig. 2). In the past, during the episodes of reduced ISM strength, the upwelling could have reduced resulting in the amplitude observed in the present study. Previous high-resolution studies from the nearby region have not observed such high SST fluctuations during the Holocene probably owing to their deeper locations farther away from the coast where the effect of upwelling reduces. For example, Kessarkar et al. (2013) from water depth of 800 m reported amplitude of up to 2°C since the mid-Holocene, while another study by Saraswat et al. (2013) from a deeper location (water depth of 1245 m) observed variability in SST by up to 1.5°C during the same period. The long-term trend as determined by linear regression (least square method) is that of an increase in SST since mid- Holocene (shown by the dashed line in Fig. 4b). In the case of salinity, the long-term trend as determined by linear regression (least square method) is of an increase in salinity/aridity (shown by dotted lines in Fig. 4c) implying that the mid-Holocene period experienced higher monsoon precipitation than present. Earlier studies from Asia and Africa have also reported a more humid mid-Holocene period than present because of the south-ward migration of the boreal summer position of the ITCZ in response to the changes in the distribution of the solar irradiance due to orbital forcing (Gasse, 2000; Wanner et al., 2008, and references therein). The present-day salinity during the peak ISM period (August) in the study region is 34.5 (Fig. 2; Boyer et al., 2009). The salinity in the present study varies from a maximum of 35.5 (arid) to a minimum of 32.4 (wet; Fig. 4c). It indicates that there have been several periods when the monsoon precipitation

was much stronger than present. But there have been multi-centennial scale periods since mid-Holocene when the summer monsoon was much weaker than present resulting in prolonged periods of aridity/droughts. The first period of aridity in the present record is centered at 4600 yr BP with salinity values similar to present. The salinity reduced slightly for the subsequent 900 years indicating moderate ISM. We observe a major period of high salinity/aridity starting at 2000 yr BP, which was accompanied by increasing SST. This severe arid event is widely reported using diverse proxies such as $\delta^{18}O$ of planktic foraminifera from the SEAS (Chauhan et al., 2009; Thamban et al., 2001; Tiwari et al., 2006) and northern Arabian Sea (Staubwasser et al., 2003); $\delta^{18}O$ of speleothems from the eastern India (Yadava and Ramesh, 2005), Arabian peninsula (Fleitmann et al., 2003) (hiatus in speleothem deposition), and the Andaman Islands from the Bay of Bengal (Laskar et al., 2013); varve thickness from the northern Arabian Sea (Von Rad et al., 1999); and *G. bulloides* abundance from the western Arabian Sea (Anderson et al., 2010). Subsequently, another episode of aridity is observed at ~1300 yr BP accompanied by high SST. During the 'Little Ice Age' and a couple of centuries prior to that, the salinity values increased in the southeastern Arabian Sea indicating reduced monsoon precipitation. Interestingly, there were wide fluctuations in salinity and SST values during that period indicating highly variable ISM precipitation. The arid events identified in this study are well constrained chronologically as AMS dates (shown by triangles in Fig. 4a) are closely available for the periods corresponding to the arid events. On comparing the long-term trends (dashed lines in Fig. 4b and 4c), we observe that temporally, SST correlates with salinity; higher salinity/reduced monsoon intensity is accompanied by higher SST. This pattern is also observed at shorter timescales at ~500, ~1300, and ~2000 yr BP. This is consistent with modern

observations in the SEAS (Fig. 2), where basin-wide wind forcing results in moderate upwelling of colder waters (Schott et al., 2009) resulting in the lowering of SST by up to 3°C during the summer monsoon season (Boyer et al., 2009). During past episodes of aridity, when the monsoon system was weak, the upwelling also reduced resulting in higher SST giving rise to the correlation between the salinity and the SST observed in the present study. The relationship between the SST and the salinity is further explored by spectral analysis to get a time–frequency representation. We carried out CWT using Morlet wavelets to look at the inherent periodicities (Fig. 5).

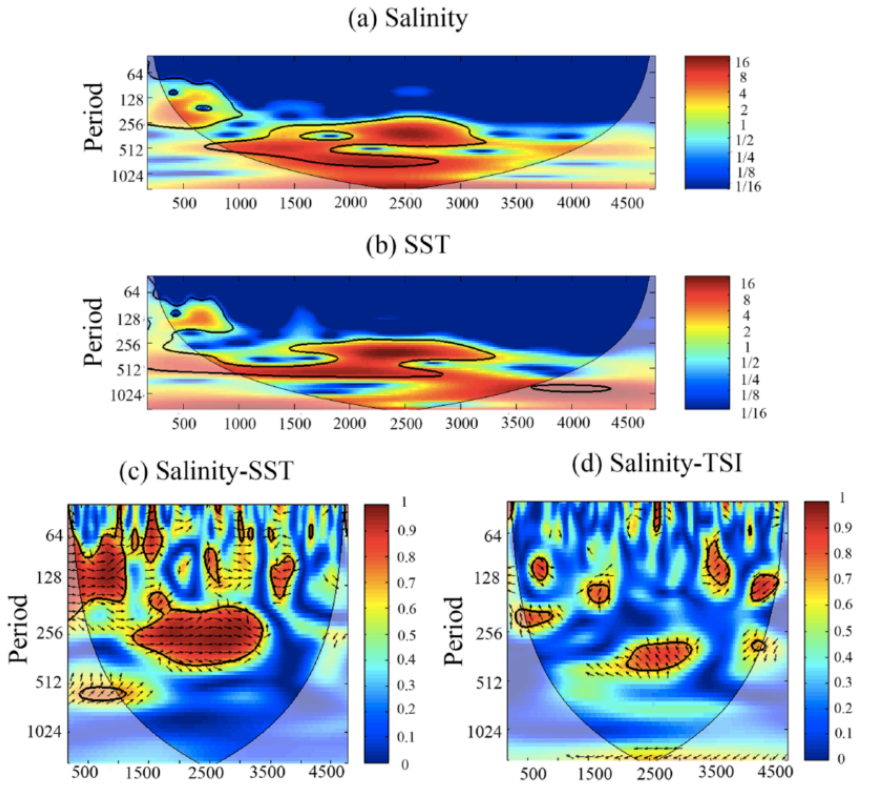

Figure 5. Spectral analysis including the Continuous Wavelet Transform (CWT) and the Squared Wavelet Coherence. Panels ‘a’ and ‘b’ show the CWT power spectrum for the salinity and the SST, respectively. Squared Wavelet Coherence between the salinity and SST is shown in panel ‘c’, while panel ‘d’ represents the Squared Wavelet Coherence between salinity and TSI. The 5% significance level against red noise is shown as a thick contour. Phase arrows pointing right means in-phase, left means anti-phase, down means salinity leading by 90°, and up means salinity lagging by 90°. The lighter shades depict the cone of influence (see text for details).

The area between the thin black line and the time axis is the cone of influence where zero padding (to diminish wraparound effects) has reduced the variance. Fig. 5a and 5b represents the wavelet spectrum for the salinity and SST, respectively, in the SEAS. The CWT spectra of both the salinity and the SST show high power in the periodicities between 256 and 512 years and also at 128 years implying strong coherence between them. To further confirm it, Squared Wavelet Coherence and phase analyses between the SST and salinity time series were performed following Grinsted et al. (2004). Periods of significant coherence (5% significance level) are found near the 256 and 128 year periodicity bands during different time periods. From 3500 to 1500 yr BP, the 256 year periodicity band dominated, while from 1200 yr BP onward the shorter periodicity band of 128 years dominated the coherency spectrum. The phase difference between the salinity and SST time series is revealed by the vector; the right pointing arrows show that the phase difference between the salinity and the SST is 0°, that is, they covary (higher SST accompanies higher salinity), confirming the visual observations of Fig. 4.

3.5. ISM precipitation versus solar activity

We compare the salinity record representing the ISM precipitation with a new TSI reconstruction (Fig. 4d) (Steinhilber et al., 2012). This particular TSI reconstruction uses a new cosmic ray record by combining ^{10}Be data from ice cores from Greenland and Antarctica with those of the global ^{14}C tree ring record. This combined approach minimizes the effect of climate, carbon cycle, and accumulation/transport-related changes that skew the individual radionuclide-based earlier TSI records. The dashed line in Fig. 4d represents the long-term trend in the TSI variability determined through linear regression (least square method). We find that the long-term trends for

both the TSI and the ISM precipitation (Fig. 4c) show similar pattern; both decline from mid-Holocene toward the present. We further note that, except for a couple of data points, salinity in the southeastern Arabian Sea was higher during the recent periods of strong TSI minima such as Maunder, Spörer, Wolf, and Oort indicating reduced ISM precipitation within the constraints imposed by the relatively coarser resolution achievable by the marine sediments. The TSI minima centered at ~1300 yr BP was also accompanied by reduced ISM precipitation. In fact, salinity exhibits greater and more frequent fluctuations concurrent with TSI variability during the last 1000 years compared with the rest of the time period under study. Previous studies have shown prominent correspondence between ISM and solar activity for early Holocene and beyond (e.g. Fleit- mann et al., 2003; Gupta et al., 2013; Kessarkar et al., 2013; Neff et al., 2001; Singh et al., 2011; Staubwasser et al., 2003) but are weak and inconclusive during the recent periods of the strong solar minima. Moreover, many of the earlier studies have focused on proxies related to the monsoon winds (e.g. Anderson et al., 2010; Gupta et al., 2013) or precipitation over the Arabian Peninsula (e.g. Fleitmann et al., 2003; Neff et al., 2001). A few high-resolution studies from the SEAS reported a correlation with some of the recent periods of solar minima, but they covered a very short time period (e.g. Agnihotri et al., 2002; Tiwari et al., 2005) or have not corrected for the effect of SST on the oxygen isotope ratio of foraminifera (Chauhan et al., 2009; Tiwari et al., 2006). In this scenario, the present study provides important evidence by demonstrating the close correspondence between the reduction in the ISM precipitation during the recent major periods of low solar activity (Maunder, Spörer, Oort, Wolf, and at ~1300 yr BP). But this relationship changes toward the older part of the record; periods of aridity near 2000 and 4600 yr BP appear to be lagging behind the prominent periods of TSI minima

(Fig. 4c and 4d). TSI variability leads the monsoon changes by a few hundred years during the older parts of the record. To check whether the visually perceived coherence between the salinity and the solar activity on multi-centennial timescale is statistically significant or not, we carried out wavelet coherency analysis as well as the phase analysis for the salinity and the TSI time series following Grinsted et al. (2004). We find that the salinity/ISM precipitation is statistically significantly coherent (5% significance level) with TSI over the approximately 300-, 200-, and 128-year periodicity band during the different parts of the time series as shown in Fig. 5d. The phase difference is represented by the vector; the upward direction shows that the TSI leads the salinity by approximately 90°, which we observe beyond 1300 yr BP. This again confirms the visual observations. Several mechanisms have been proposed to explain how the small TSI variability can affect terrestrial climate (for a review, see Gray et al., 2010; Tiwari and Ramesh, 2010), which basically falls into two categories: Direct and Indirect. The most widely accepted Indirect mechanism, also known as top-down approach, relating TSI changes to precipitation is via heating of the Earth's stratosphere by the increased absorption of the solar ultraviolet (UV) radiation by ozone during periods of enhanced solar activity (Haigh, 1994). Solar irradiance variability is much higher in the UV region. For example, during the 11-year solar cycle, variations of up to 6% in irradiance near 200 nm where oxygen dissociation and ozone production occur and up to 4% in the region 240–320 nm where absorption by stratospheric ozone takes place are reported, which are much higher compared with ~0.07% variation in TSI integrated over all the wavelengths (Gray et al., 2010). The TSI Modeling studies show that the stratospheric heating is transferred to the troposphere, mostly through the action of large-scale atmospheric waves (Haigh, 1999). This anomalous heating affects the circulation in the

troposphere, for example, increased Hadley circulation is reported during enhanced solar activity (Haigh, 1994; Labitzke and van Loon, 1995), which affects the distribution of atmospheric moisture (Kodera, 2004). Direct mechanisms, also known as bottom-up approach, argue that enhanced irradiance absorption takes place over the subtropical oceans during periods of solar maxima (Cubasch et al., 2006). It results in enhanced evaporation and the transport of moisture into the precipitation zones, causing enhanced precipitation and associated upward vertical motions. Consequently, the trade winds and equatorial Pacific Ocean upwelling strengthen accompanied by colder SSTs, which is consistent with stronger Hadley and Walker circulations (Meehl et al., 2008). Furthermore, a positive feedback takes place as strengthened circulation enhances the subtropical subsidence causing lesser cloud cover and thus further increasing solar absorption at the surface (Meehl et al., 2008). A recent study based on numerical simulation shows that the increase of 0.1% in TSI from solar minima to solar maxima will result in an increase in the atmospheric precipitable water by up to 200% (Hiremath et al., 2015). They further observed that the response of monsoon precipitation to the solar activity is physically a nonlinear phenomenon, which was also noted by previous studies (Weng, 2012 and references therein). In the present study, the changing phase relationship between the ISM precipitation and the solar activity toward mid-Holocene indicates the possible influence of the varying dynamics of the tropical coupled ocean–atmosphere phenomenon like ENSO and Indian Ocean Dipole (IOD) (Berkelhammer et al., 2010; Emile- Geay et al., 2007). The mid-Holocene is believed to be a period of lower ENSO activity and stronger positive IOD events than present as shown by paleoclimatological observations (Abram et al., 2007; Gagan et al., 2004; Wanner et al., 2008, and references therein) and models (Clement et al., 2000; Liu et al., 2004).

It is proposed that during the periods of lower TSI, ocean–atmosphere interactions modulate the solar forcing to produce persistent ENSO-like SST anomalies that could have reduced the ISM precipitation on centennial to millennial timescale (Emile-Geay et al., 2007). Such influences need to be confirmed using modeling efforts including multiple ensembles. Model output matching with observation will be an important step forward toward understanding the response of ISM precipitation to the complex interplay of various forcing factors.

3.6. Marine versus terrestrial records of ISM precipitation during past periods of TSI minima

Recently, there have been various studies from both marine and terrestrial realms that have attempted to reconstruct the ISM precipitation at high resolution (centennial scale or higher) during the Holocene (Berkelhammer et al., 2010; Chauhan et al., 2009; Laskar et al., 2013; Prasad et al., 2014; Sinha et al., 2007; Tiwari et al., 2006; Von Rad et al., 1999; Yadava and Ramesh, 2005, etc.). The comparison of marine and terrestrial records is difficult as diverse paleo-archives accumulate at different rates and thus have different resolutions, which is further complicated by sampling frequency and error in the chronologies including those in the reservoir age corrections with errors up to a few decades. Keeping these limitations in mind, we compare the arid periods identified in the salinity record of the present study (shown by gray bars in Fig. 6) with the arid periods recognized by earlier studies from various parts of the Arabian Sea and the Indian subcontinent (Fig. 6) on multi-centennial timescale. We also compare these records with the TSI record (Steinhilber et al., 2012) to look at the regional picture of ISM precipitation fluctuations vis-à-vis the past periods of low TSI (Fig. 6).

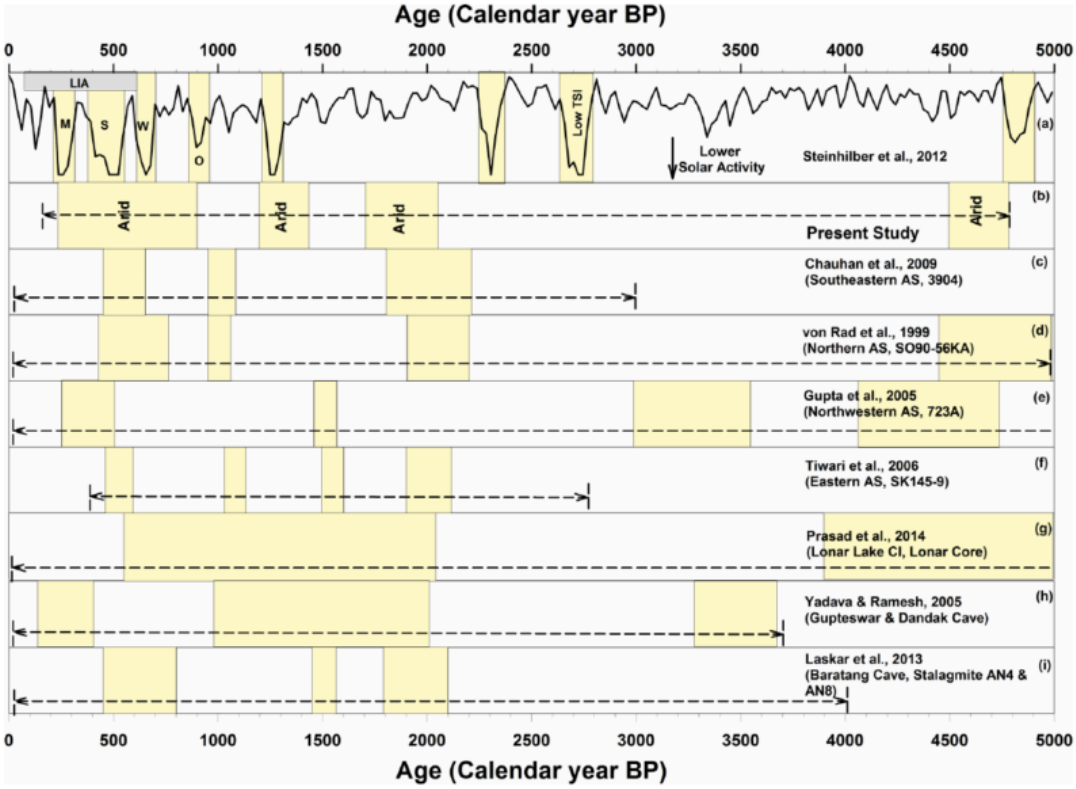

Figure 6. Marine-versus terrestrial-based high-resolution studies and their relation to the periods of TSI minima. The gray bands depict the major period of aridity observed by various studies. The gray bands in panel 'a' depict the periods of low solar activity. Panels 'b'–'f' show the marine-based studies, while panels 'g'–'i' show the terrestrial-based reconstruction of the ISM precipitation.

Tiwari et al. (2006) (Fig. 6f) and Chauhan et al. (2009) (Fig. 6c) reconstructed the ISM precipitation from the eastern Arabian Sea based on δ18O values of planktic foraminifera. Von Rad et al. (1999) deciphered the past variations in the ISM precipitation intensity from the northern Arabian Sea based on the varve thickness (Fig. 6d). In contrast, Gupta et al. (2005) studied the concentration of the planktic foraminifera *G. bulloides* related to the upwelling induced by ISM winds. They identified four periods of aridity during the past 5000 years as shown in Fig. 6e. From terrestrial realm, a few high-resolution studies using speleothems (Laskar et al., 2013; Yadava and Ramesh, 2007) and lake sediments (Prasad et al., 2014) from India since the mid-Holocene are available. Prasad et al. (2014) from the Lonar Lake, central

India, report two major periods of aridity (Fig. 6g) between 4600– 3900 and 2000–600 yr BP. Yadava and Ramesh (2005) analyzed speleothems spanning the past 3500 years from the Gupteshwar and Dandak caves from central India that show periods of aridity during the 'Little Ice Age', a prolonged period of aridity starting from ~2000 yr BP, and another period at ~3500 yr BP as shown in Fig. 6h. Laskar et al. (2013) (Fig. 6i) reconstructed the ISM precipitation intensity for the past 4000 years using two stalag- mites from Baratang cave in Andaman Islands. They reported periods of aridity during 1800–2100 yr BP and also around 1500 and 400–800 yr BP. Despite the huge spatial separation among these studies relying on different proxies and chronologies, we find reduced precipitation during the 'Little Ice Age', Wolf and Oort minima, and at ~1300 yr BP. Furthermore, on an average, all these records also show major periods of aridity at ~2000 yr BP and at ~4500 yr BP exhibiting similar lag to the TSI minima as observed in the present study.

3.7. Conclusion

The SST in the southeastern Arabian Sea during the ISM period has varied from a maximum of 29.9°C to a minimum of 27.5°C – a range of 2.4°C – since the mid-Holocene. Based on accurate reconstruction of salinity by accounting for SST from the $\delta^{18}O$ values of *G. ruber*, we find several high-frequency (multi-centennial scale) oscillations with periods of high salinity/aridity during the 'Little Ice Age' (and a few centuries prior to it) and at 1300, 2000, and 4600 yr BP. SST correlates statistically significantly (5% significance level) with salinity; higher SST is accompanied by high salinity/reduced ISM intensity. This study reveals that even for a short duration of the past ~5000 years, the SST contribution to $\delta^{18}O$ of foraminifera is considerable in the southeastern Arabian Sea and should be accounted for accurate paleoclimatic

reconstructions. We also find statistically significant coherence between the ISM precipitation and the TSI on multi-centennial timescale; ISM precipitation reduces during recent periods of major TSI minima like Maunder, Spörer, Oort, and Wolf corresponding to the 'Little Ice Age' and at ~1300 yr BP. But this relationship changes beyond ~1300 yr BP, and the TSI variability leads summer monsoon precipitation change by a few hundred years – confirmed through wavelet analysis and comparison with earlier marine- and terrestrial-based studies. This nonstationary phase relationship possibly illustrates the nonlinear response of the monsoon system to the influence of tropical coupled ocean– atmosphere phenomenon like ENSO and IOD that needs to be confirmed using multiple ensembles.

Chapter 4

Organic carbon preservation in Southeastern Arabian Sea sediments since mid-Holocene: Implications to South Asian Summer Monsoon variability

4.1. Introduction

The South Asian Summer Monsoon (SASM) variability on different timescales is an intense area of research due to its influence on the life and economic conditions of billions of people. Despite a large number of studies to decipher its past variability, the consensus has not yet evolved for the SASM variability after attaining the orbital forcing induced mid-Holocene (~5–6 ka) maximum. General circulation model ensemble (Chevalier et al., 2017) as well as paleo-proxy data (deMenocal et al., 2000; Russell et al., 2003; Weldeab et al., 2007) show that the northern African summer monsoon was stronger than present during the mid-Holocene due to the higher amount of heat received by the northern tropics during summer because of the precessional forcing. Likewise, model ensemble studies have also proposed stronger than present mid-Holocene East Asian Summer Monsoon (EASM) (Jiang et al., 2013) and the SASM (Joussaume et al., 1999). Present day orbital configuration is of precession maximum implying perihelion during northern hemisphere winters. Therefore, the northern tropics would receive lower insolation during summer than mid-Holocene leading to decreasing monsoon intensity since then. But, based on various proxy records from different regions, various authors have reported contrasting trends in the overall SASM variability with a few arguing for declining trend (Fleitmann et al., 2003; Sinha et al., 2005; Gupta et al., 2005; Kessarkar et al., 2010; Saraswat et al., 2013; Tiwari et al., 2015a) while others reporting increasing trend based on oxygen isotope ratio of planktic foraminifera (Sarkar et al., 2000; Thamban et al., 2001; Tiwari et al., 2006; Azharuddin et al., 2016) and TOC concentration of sediments (Thamban et al., 1997; Bhushan et al., 2001; Tiwari et al., 2010) since the mid-Holocene maximum. The different trends in SASM variability can be because of the fact that the proxies used are affected by multiple factors. For

example, the $\delta^{18}O$ value of foraminifera is affected by salinity, temperature, and ice-volume effect (Tiwari et al., 2015b, and references therein). Likewise, TOC concentration of sediments is influenced by preservation depending on the prevailing redox conditions and sedimentation rate (e.g., Calvert and Pedersen, 1993). The TOC concentration is a widely used proxy in the Arabian Sea for reconstructing the SASM variability (Thamban et al., 2001; Kessarkar and Rao, 2007; Kessarkar et al., 2010; Singh et al., 2011). The Arabian Sea is characterized by intense phytoplankton production during summer monsoon seasons making it one of the highest productivity zones in the world oceans (Banse, 1987; Nair et al., 1989; Qasim, 1997). The majority of organic matter produced in the euphotic zone is remineralized while settling through the water column (e.g., Berger et al., 1989). This process consumes dissolved oxygen while settling to the bottom (Nair et al., 1989). This accompanied by a moderate rate of thermocline ventilation by Indian Ocean Central Water, Red Sea Water, and Persian Gulf Water masses, result in massive mid-depth (150–1200 m) oxygen minimum zone (OMZ) in the Arabian Sea (Wyrtki, 1971; Naqvi, 1987; Helly and Levin, 2004). Consequently, by far, the largest part of organic matter produced in the photic zone of the ocean (i.e., 90–99%) is ultimately recycled back to inorganic carbon (Hedges and Keil, 1995). After the organic matter settles down to the bottom, benthic organisms further consume it and finally, less than 1% of the overhead surface productivity is preserved in the sediments, which is called as Sedimentary Organic Matter (SOM) (e.g., Hedges and Keil, 1995). TOC concentration of the SOM in marine sediment cores is widely used as a proxy for overhead surface paleoproductivity; high/low TOC value is related to high/low paleoproductivity (Reichart et al., 1997; Schulz et al., 1998; von Rad et al., 1999a, 1999b). But, preservation depending on the redox conditions and sedimentation rates along with

detrital dilution in the SEAS also plays an important role in determining TOC concentration (Sarkar et al., 1993; Pattan et al., 2005; Narayana et al., 2009). Thus, the possible cause for TOC increase in different regional settings is still debated. Earlier studies from the SEAS primarily using TOC as a proxy suggested decreased productivity during the LGM (Pattan et al., 2003; Avinash et al., 2015, and references therein). This low productivity was attributed to weaker summer monsoon wind induced upwelling. Pattan and Pearce (2009) have reported enhanced sub-oxic conditions in the SEAS over the last 140 kyr during the stadials and the glacial periods, which could have caused better preservation of TOC (Paropkari et al., 1991). Additionally, studies on TOC enrichment suggests that the formation of oxygen deficient conditions, either in the oxygen minimum zone (OMZ) at intermediate water depths, or in silled basins, would have allowed better preservation and consequent enrichment of TOC in marine sediments (Dow, 1978; Demaison and Moore, 1980). Thus, a complex interaction between overhead surface productivity, oxygen conditions, and preservation complicate the use of TOC as a productivity proxy. In view of this, we analyzed multiple geochemical proxies viz., TOC, C/N, $\delta^{13}C_{org}$, $CaCO_3$ and major and trace elements in a sediment core from upper continental slope from the SEAS to (i) identify the sources of the SOM, (ii) determine the applicability of TOC concentration as a paleoproductivity indicator in such settings, (iii) investigate the factors responsible for TOC enrichment especially on the slope sediments that have been reported to be dominated by organic carbon maxima in this region (Calvert et al., 1995), and most importantly, (iv) to decipher the long-term SASM variability since mid-Holocene. This study will have major implication toward the interpretation of TOC variability in future studies from the slope sediments from the SEAS.

4.2. Modern Oceanographic Conditions at the Study Site

Coastal circulation in the SEAS undergoes a complete reversal associated with the two different mon- soons (Shetye and Gouveia, 1998; Naqvi et al., 2006). The West Indian Coastal Current (WICC) flows pole-ward during winter (northeast monsoon) causing downwelling off the western coast of India and a well-oxygenated water column over the shelf. In contrast, circulation in summer (southwest monsoon) is typical of an eastern boundary - an equatorward flowing WICC, a poleward undercurrent, and moderate coastal upwelling. What makes this region unique, apart from the seasonally reversing WICC, is that it receives enormous orographic precipitation and runoff along the southwestern coast of India in just 4 months (Schott et al., 2009) during the summer monsoon season. This results in the reduction of salinity as shown by the vertical profiles of salinity near the core-site (Fig. 7a).

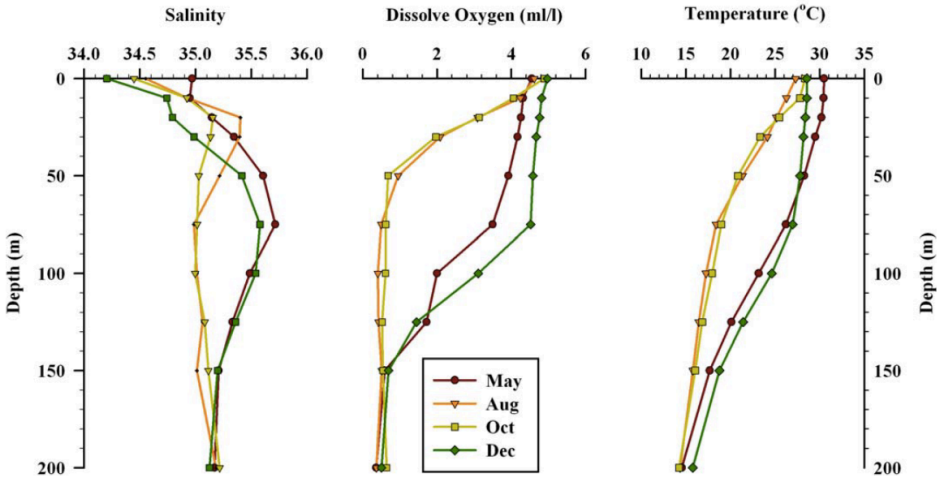

Figure 7. Modern salinity, dissolved oxygen, and temperature profiles (monthly average) near the core location. The months of August and December represent the summer and winter monsoon periods, respectively. The conditions prevailing inter-monsoon periods are represented by the months of May and October. This figure is based on the World Ocean Database 2009 [Boyer et al., 2009].

Owing to the high nutrient concentrations in the freshly upwelled water (as shown by the reduction in SST by ~3^{o}C; Fig. 7c), the productivity is high (Naqvi et al., 2006). During summer monsoon chlorophyll maximum (up to 7.8 μg/L) are observed in the SEAS (Banse, 1987). Also, the sediment traps in the Eastern Arabian Sea have registered a doubling of the total export flux to approximately 200 mg/m^2/d (Nair et al., 1989) for the same season. The fairly high production is sustained till October to November (Radhakrishna, 1969; Swallow, 1984). Consequently, the high oxygen demand for degradation of this copious organic matter leads to intense oxygen deficiency close to the surface during the summer and post-summer monsoon season (Fig. 7b). An intense OMZ from ~150 to 1200 m exists year-round supported by high productivity, advection of water masses with a high amount of organic matter from the western Arabian Sea, and flow of intermediate water masses with low oxygen content.

4.3. Core details and chronology

A 36 cm long gravity core named SN-6 was retrieved from the upper continental slope of the SEAS (12°29'021"N: 74°07'966"E; water depth 589 m) during the return-leg of the 4th Indian Southern Ocean Expedition (Fig. 8). The core was subsampled at 1 cm interval. The Accelerator Mass Spectrometer (AMS) ^{14}C chronology of the core was obtained from the National Science Foundation-AMS Laboratory, University of Arizona, USA. The details of the chronology have been reported in Tiwari et al. (2015a). The Age-depth model (Fig. 8) shows that the core-top (0–1 cm) is dated at 15±44 yr BP (1sigma) while the last dated section (35–36) age is 4772 yr BP. The sedimentation rates observed for the top 11 cm in the present study is 16.2 cm/kyr (i.e., a resolution of ~62 years/cm) while the average resolution

is 127 years/cm yielding, thus, a centennial scale resolution.

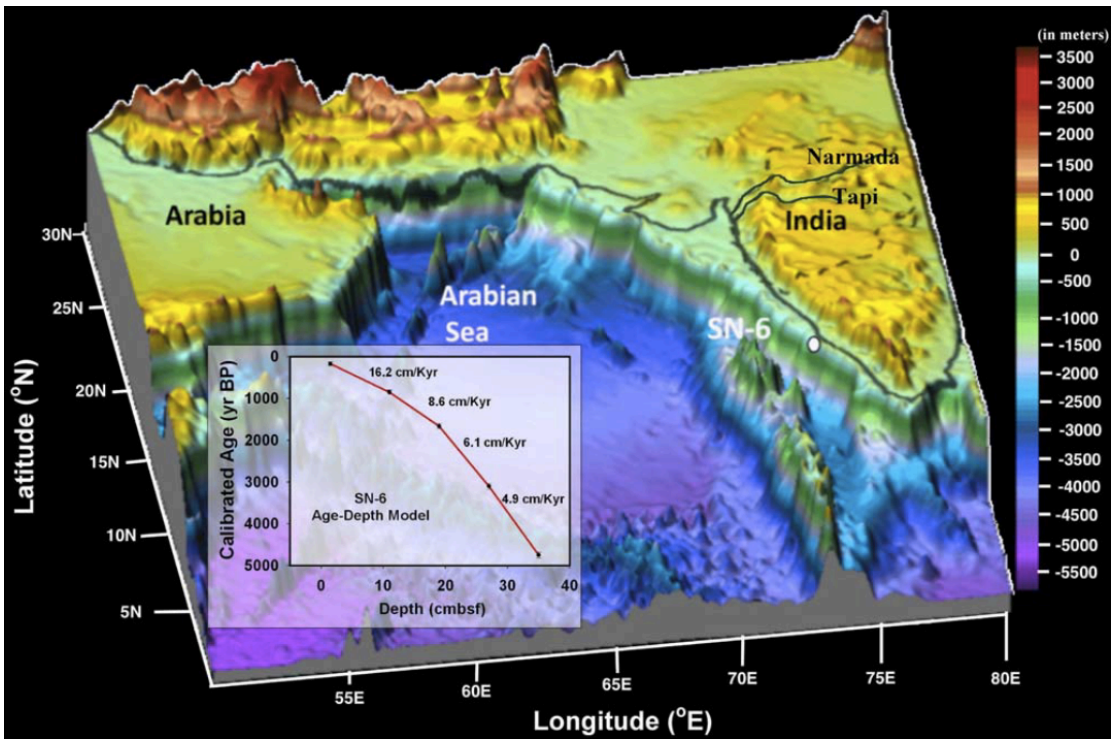

Figure 8. Location of the core (shown by the closed circle) and the bathymetry of the study area. Core SN-6 is from the upper continental slope of India. The inset shows the age-depth model based on five radiocarbon dates approximately at every 9 cm on selected species of planktic foraminifera; sedimentation rates are also shown (in cm/kyr).

4.4. Elemental Analysis of Total Organic Carbon and Total Nitrogen

For %TOC and %TN analysis, each subsample was oven dried at 40°C and then homogenized by finely grounding it in an agate mortar. For %TOC, carbonate was removed from the subsample by adding 2N hydrochloric acid. The samples were then completely rinsed by adding deionized water for around five times and again oven dried at 40°C. In the case of %TN analysis, untreated samples were used. A portion of the ground sample was then wrapped in a tin capsule and combusted using an Elemental Analyzer at the Marine Stable Isotope Lab (MASTIL) at National Centre for Polar and Ocean Research (NCPOR), Goa, India. The analytical precision based

on repeated measurements (n=18) of the reference standard Sulphanilamide for %TOC and %TN measurements is ±0.2% and ±0.3%, respectively. The $CaCO_3$ content of the sediment was calculated by first calculating the inorganic carbon by subtracting the TOC from the Total Carbon and then multiplying by 8.33 to convert to $CaCO_3$ content ($CaCO_3$ (%) = (Total Carbon - TOC) x 8.33). The analytical precision based on standard error propagation techniques is ±0.3% for the $CaCO_3$ content. The Mass Accumulation Rate (MAR) of various geochemical proxies ($CaCO_3$, TOC) has been calculated by multiplying concentration by dry bulk density (DBD) and sedimentation rate. The DBD has been calculated using the empirical equation derived by Clemens et al. (1987).

4.5. Carbon Stable Isotope Ratios

For the analysis of stable isotope of carbon ($\delta^{13}C_{org}$), carbonate-free samples were used. $\delta^{13}C_{org}$ values were determined using an Isoprime stable isotope ratio mass spectrometer after high-temperature flash combustion in an elemental analyzer at 950°C. Samples were run with blank and known standards. Standards were prepared by weighing 0.4–0.6 mg of IAEA cellulose standard (IAEA-CH-3) of certified isotopic composition ($\delta^{13}C$ = -24.74‰ versus VPDB). Data quality control was checked by running reference standard after every six samples. Stable isotope values were reported in per mil (‰) while the delta notation is defined as $\delta^{13}C$ (‰) = $[(R_{Sample} - R_{Standard})/R_{Standard}]$ x 1000‰; where R_{sample} and $R_{reference}$ are the isotopic ratios ($^{13}C/^{12}C$) of sample and reference, respectively. Analytical precision based on repeated measurements of the reference standard (n=18) was better than 0.02‰.

4.6. Inorganic Elemental Analysis

For inorganic elemental chemistry, sediments were dissolved following acid digestion procedure by Balaram and Rao (2003). The powdered sediment samples (n=36) were weighed accurately (50 mg), transferred to clean Teflon beakers and subjected to open acid digestion. The sediments were repeatedly digested by treating with a mixture of HF, HNO_3, and $HClO_4$ in the ratio of 6:3:1. Finally, the extract was brought to a standard volume (50 ml). All elements were analyzed using inductively coupled plasma mass spectrometry at National Centre for Polar and Ocean Research, Goa. Analytical accuracy was determined through analysis of a suite of internationally recognized Standard Reference Material (NIST 2702). The relative standard deviation estimates based on repeated analysis of standards for all elements discussed here are better than ±10%.

4.7. Enhanced Reducing Conditions in the SEAS Since Mid-Holocene

We studied a suite of inorganic metals (Al, Ti, Fe, Mn, Cr, V, Mo, Cu, Zn, Ni, and Co) to investigate the role of past geochemical changes on the preservation of organic matter (e.g., Morford and Emerson, 1999). The abundances of most of these elements are controlled by (1) terrigenous fraction (fluvial and aeolian), (2) biogenic fraction - related to carbonates and organic matter, and (3) authigenic fraction - composed of insoluble oxyhydroxides and sulfides (Riquier et al., 2006). Aluminum is commonly used as a proxy for land derived aluminosilicate fraction of the sediments with very little affinity to move during diagenesis (Brumsack, 1989; Calvert and Pedersen, 1993) and calcium carbonate is primarily considered as the biogenic product of marine origin. So, in order to identify the origin (detrital, biogenic, or authigenic) of the studied elements in our core, correlation of aluminum and calcium carbonate with

selected elements was determined using linear regression (least square method) for 36 samples using the statistical package - SigmaPlot 12.0. A high regression coefficient (r^2) value of these metals with Al indicates the detrital source (Fig. 9) and with that of $CaCO_3$ indicates the biogenic source (Fig. 10) (e.g., Acharya et al., 2015).

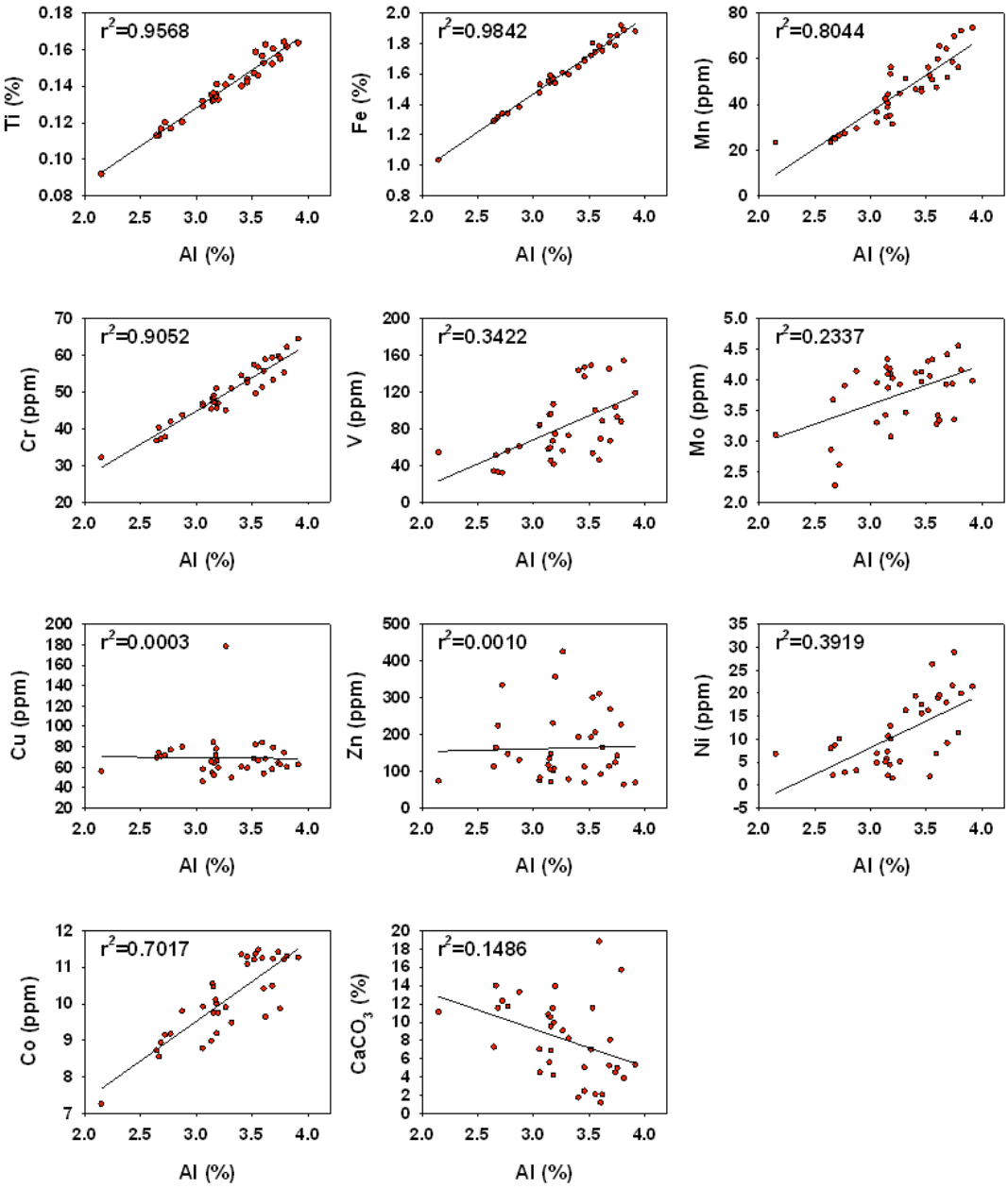

Figure 9. Correlation of Al with selected major and trace elements. Correlation coefficient is given by r^2 value.

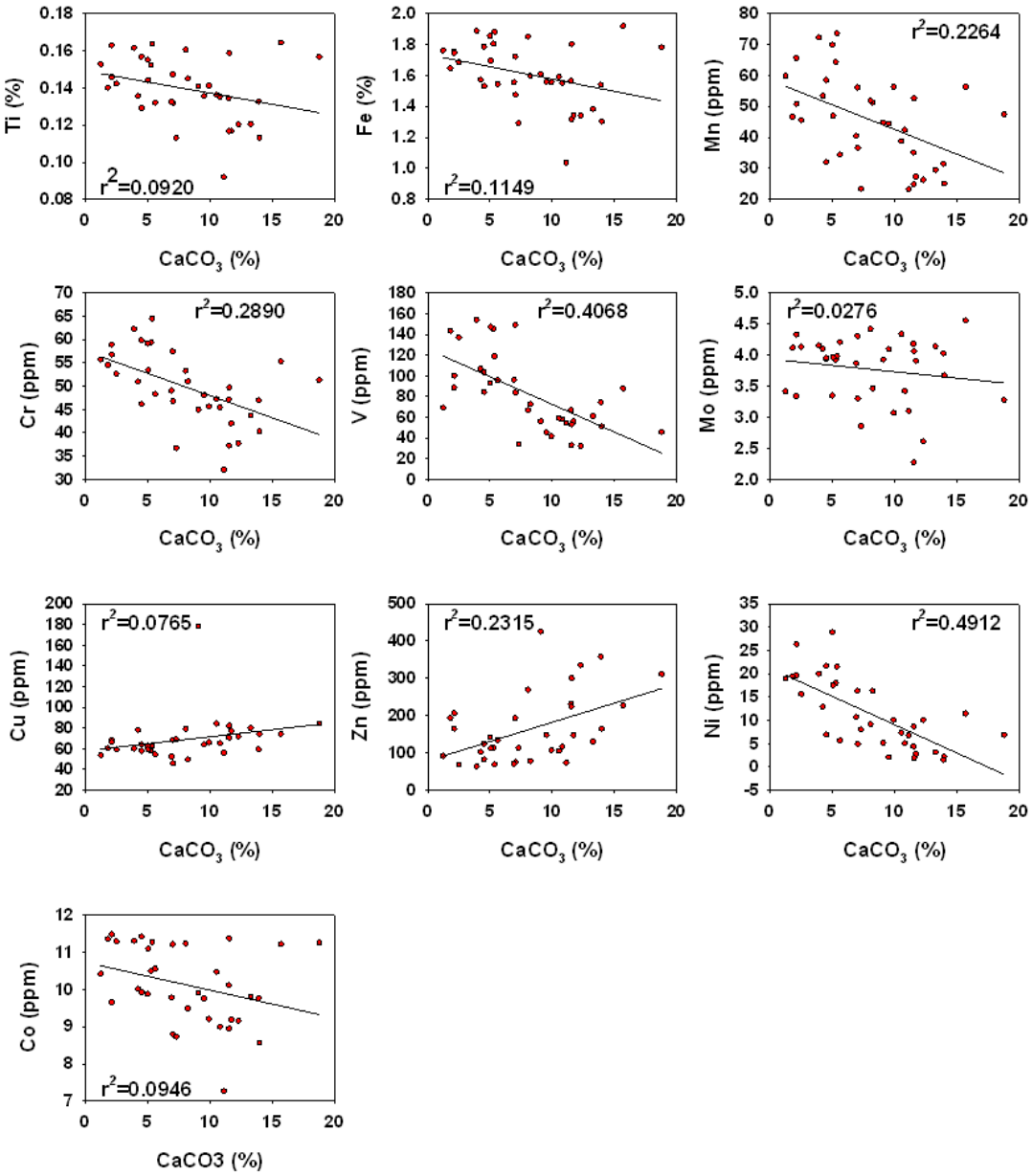

Figure 10. Correlation of $CaCO_3$ with selected major and trace elements. Correlation coefficient is given by r^2 value.

The regression coefficient values (Table 2) indicate that elements such as Ti, Fe Mn, Cr, and Co have a siliciclastic origin and their fluctuations in sediments can be explained in terms of the variation in the detrital influx. V and Ni show moderate regression coefficient values with Al and $CaCO_3$. While elements such as Mo, Cu,

and Zn show very poor correlation with Al and $CaCO_3$ thereby suggesting an authigenic source.

	Al		$CaCO_3$	
Elements	r^2	p	r^2	p
Ti	0.96	<0.0001	0.09	0.0721
Fe	0.98	<0.0001	0.11	0.0431
Mn	0.80	<0.0001	0.23	0.0034
Cr	0.91	<0.0001	0.29	0.0007
V	0.34	0.0002	0.41	<0.0001
Mo	0.23	0.0028	0.03	0.3327
Cu	0.00	0.9139	0.08	0.1024
Zn	0.00	0.8528	0.23	0.003
Ni	0.39	<0.0001	0.49	<0.0001
Co	0.70	<0.0001	0.09	0.0653
$CaCO_3$	0.15	0.0202	N.A	N.A

Table 2: Regression Coefficients (r^2) of Al and $CaCO_3$ With Selected Major and Trace Elements and Level of Significance of Correlation Correlation (p) for 36 Samples.

In addition to the element/Al ratio, enrichment factors of selected trace metals (Table 3) have been evaluated to determine the redox conditions during the sediment deposition. The enrichment factor (EF) for an element X has been determined by the formula $EFX=(X/Al)_{sample}/(X/Al)_{average\ shale}$, where the average shale values were taken from Wedepohl (1971). Thus, the enrichment factor of redox-sensitive may, therefore, indicate anoxic/oxic conditions at the seafloor or within the sediment. Elements with siliciclastic origin show some enrichment with regard to its shale values thereby suggesting reducing environment during the time of deposition since mid-Holocene. Maximum enrichment shown by Mo, Cu, and Zn can be due to its authigenic source of origin as they show very poor correlation with Al and $CaCO_3$.

Trace Elements	Element/Al Ratio (ppm/%)			Average Shale	Enrichment Factor
	Core SN-6				
	Max	Min	Average		
Cr	16.49	13.80	15.24	10.2	1.45
V	42.49	11.81	24.51	15	1.65
Mo	1.44	0.71	1.11	0.15	7.73
Cu	27.86	14.89	19.87	5.1	4.21
Zn	109.37	16.77	44.64	11	4.58
Ni	12.31	0.46	4.1	7.7	0.43
Co	3.61	2.63	3.11	2.1	1.48

[a]The enrichment factors (EF) for various elements in studied samples are calculated wrt average shale.

Table 3: Average Redox-Sensitive Element/Al Ratio for SN-6 Sediments and Average Shale (Wedepohl, 1971)

Therefore, to estimate the fraction of elements that are not derived from the terrigenous input, the authigenic fraction was estimated for a trace metal X by the standard formula; Authigenic X= Total X - (Al sample x (X/Al) reference material). Average shale (Wedepohl, 1971) and Al are generally used as reference component to calculate the authigenic fraction of metals (Calvert and Pedersen, 1993; Morford and Emerson, 1999; Tribovillard et al., 2006). We used the ratio R=(Cu+Mo/Zn) proposed by Hallberg (1976), as an indicator of the oxygenation of bottom waters. The basic principle behind the use of this ratio lies in the fact that in reduced environment with H_2S in bottom water, the precipitation of Cu is favored over Zn in the sediments, which is the result of differences in the solubility product of their sulfides in reduced environments (Hallberg, 1976). Hence, this ratio is expected to increase under suboxic conditions and decrease under oxidizing conditions. The variation of R from a minimum value of 0.14 during mid-Holocene to the maximum value of 2.01 toward

present reflects the increasing reducing conditions since mid-Holocene. We further examined the interelemental relationships of redox-sensitive trace elements, as they become moderately to highly enriched under suboxic bottom water conditions, making them useful as indicators of paleoredox conditions. In marine sediments, Mo is considered as a proxy of redox conditions because of its conservative behavior in oxygenated waters and enrichment in anoxic sediments. In oxic environments, Nickel behaves as a micronutrient, which occurs as soluble Ni^{2+} or $NiCl^{+}$ ion (Tribovillard et al., 2006). Nickel complexation with organic matter accelerates scavenging in the water column and thus its enrichment in sediments (Calvert and Pedersen, 1993). Unlike Ni, Cobalt behaves similarly as Mn in seawater and sediments, i.e., it can diffuse out of sediments under reducing conditions (Heggie and Lewis, 1984) and hence increase the Ni/Co ratio. The V/Cr ratio is a redox indicator, which reflects changes in the scavenging efficiency as a function of redox conditions (Jones and Manning, 1994; Riquier et al., 2006; Gallego-Torres et al., 2010). Under oxic conditions, vandate adsorbs more strongly than chromate, whereas in reducing condition Cr (III) forms stronger surface complexes than VO^{2+}. Unlike V which starts precipitating in suboxic condition, Mo only starts to precipitate when dissolved sulfide (H_2S) is available (euxinic condition).

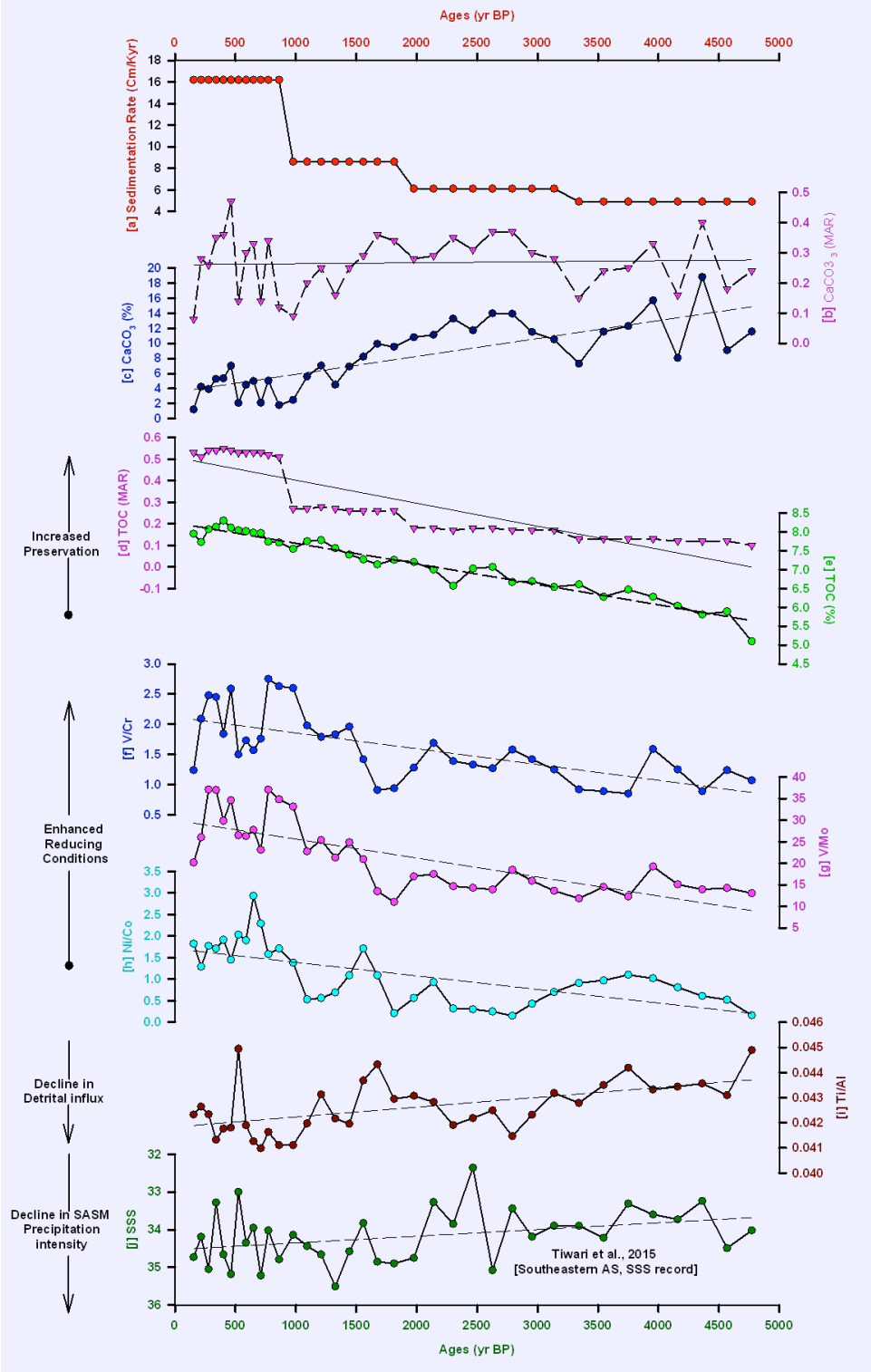

Figure 11. Downcore variation of geochemical proxies: (a) sedimentation rate; (b) $CaCO_3$ mass accumulation rate; (c) $\%CaCO_3$; (d) total organic carbon mass accumulation rate; (e) %total organic carbon as a function of preservation; (f)–(h) V/Cr, V/Mo, and Ni/Co indicating redox condition; (i) Ti/Al indicating decline in detrital influx since mid-Holocene; and (j) sea surface salinity showing SASM precipitation strength.

In the present study, Ni/Co, V/Cr, and V/Mo ratio ranges from 0.01 to 3.75, 0.85 to 2.75, and 8.43 to 37.12, respectively. All the three ratios show an increase in reducing conditions from 4772 to 3955 yr BP followed by a slight decline thereafter. Another episode of increase in reducing conditions is seen from 3342 to 2795 yr BP that is again followed by a decline in reducing conditions with the major decline seen at 1813 yr BP. After this period, we see an increase in reducing conditions till 278 yr BP with a slight decline in reducing periods observed between 1326-1093 and 710-525 yr BP. From 278 yr BP to present, we again see a slight decline in reducing conditions. Although, we see some declining periods of reducing conditions, the long-term trend shown by these redox proxies (Fig. 11f, 11g, and 11h) shows an increase in reducing conditions resulting in intensified OMZ conditions since mid- Holocene. Further, the persistent low Mn/Al ratio (mean=14.47 ppm/%), which is about a factor of 10 lower than that in shale value (106 ppm/% for Mn/Al) (Wedepohl, 1971) suggests that the bottom water remained suboxic at the studied location throughout the period of deposition. Mn/Al ratios in detrital materials of the river Narmada and Tapi, which drain into this region, are still higher, 147±20 ppm/%. Agnihotri et al. (2003a) based on low Mn/Al ratio since mid-Holocene to present in the core 3268G5 (water depth 600 m, 12.5°N, 74.2°E) near Mangalore offshore, also suggests that the bottom water remained suboxic at the studied location throughout the period of deposition. Naik et al. (2014) by using the enrichment of Mo and Cr reported the prevalence of suboxic depositional environment from late Holocene to present in the sediments from Goa offshore (Core AAS9/19; water depth of 367 m, 14°30'115"N; 73°08'515"E), which was also observed by Agnihotri et al. (2003a) as evidenced by increasingly higher $\delta^{15}N$ values. Recently, Saraswat et al. (2016) based on the relative abundance of the angular asymmetrical benthic foraminifera - an indicator of bottom water

oxygenation—showed a declining dissolved oxygen concentration since mid-Holocene.

4.8. TOC and $CaCO_3$ Concentration: Implications to SASM Variability Since Mid-Holocene

The accumulation of calcium carbonate on the seafloor is mainly controlled by the surface water biological production, rate of dissolution during its journey through the water column as well as on the seafloor and dilution by the non carbonate fraction and terrigenous matter. The regional lysocline depth in the study region is at 3800 m (Peterson and Prell, 1985) and the present sediment core was retrieved from 590 m water depth suggesting that dissolution of calcium carbonate is negligible in the SEAS. The % $CaCO_3$ in the present study varies from 18.79% to 1.23%. $CaCO_3$ mass accumulation rate does not show any trend (Fig. 11b) whereas the long-term trend shown by $CaCO_3$ concentration in the present study shows a decline since mid-Holocene (Fig. 11c) with the increasing sedimentation rate suggesting that terrigenous dilution could be cause for its variation. But, the terrigenous dilution as a possible cause for $CaCO_3$ variations is excluded based on the fact that the positive correlation between both variables is weak (r^2=0.15). The inverse relationship observed between the overall trend of $CaCO_3$ (%) and TOC (%) (r^2=0.57, p=0.0001, Fig. 11) can be due to the enhanced availability of CO_2 in the OMZ. Accumulation of remineralization end products in OMZs result in a Dissolved Inorganic Carbon (DIC) maxima, which is known as Carbon Maximum Zones (CMZ) (Paulmier et al., 2011). They can act as a local source of CO_2 (Paulmier et al., 2011) and can dissolve $CaCO_3$ on the seafloor (Naik et al., 2014). Therefore, we propose that the observed decline in $CaCO_3$ concentration in the present study is due to the dissolution of $CaCO_3$ as a result of

enhanced reducing conditions (low oxygen concentration, strengthened OMZ, and CMZ) since mid- Holocene. This is further supported by another study from a nearby core (AAS9/19) that observed a similar decline in $CaCO_3$ (%), which was attributed to the dissolution effect as a result of strengthened reducing conditions since mid-Holocene (Naik et al., 2014). Sedimentary TOC as a proxy of in-situ productivity related to the SASM intensity in coastal sediments of the SEAS possess an inherent limitation that whether they are of marine (in-situ produced) or terrestrial (transported via numerous streams/surface runoff) origin (Muller and Suess, 1979). Traditionally, source characterization of organic matter is done using carbon isotopes ($\delta^{13}C_{org}$) and atomic C/N wt. ratio. Fontugne and Duplessy (1986) reported typical $\delta^{13}C_{org}$ of terrestrial and marine organic matter of the Arabian Sea as -26‰ and -20‰, respectively (with respect to PDB). Likewise, mean C/N wt. ratio ranges ~8.0 ±2 for a typical marine organic matter in this region (Calvert et al., 1995; Bhushan et al., 2001). Despite heavy monsoonal precipitation runoff on the west coast of India, several studies reported majority of the organic matter is typically ‘‘marine’’ even in very shallow environment (Bhushan et al., 2001; Agnihotri et al., 2002, 2003a). In the present study, the $\delta^{13}C_{org}$ values vary between -22.35‰ and -221.17‰, with an average of -21.56‰. Whereas atomic C/N ratios show higher values ranging between 18.21 and 23.22 with an average of 20.38 revealing marine as well as terrestrial sources of organic matter. The plot of $\delta^{13}C_{org}$ versus atomic C/N (Fig. 12) shows a signal of mixed sources: marine organic matter, as well as significant amount of terrestrial organic matter, is present. It suggests that the traditional paleoproductivity proxy, i.e., TOC concentration, cannot be ascribed solely to the surface water productivity in such settings.

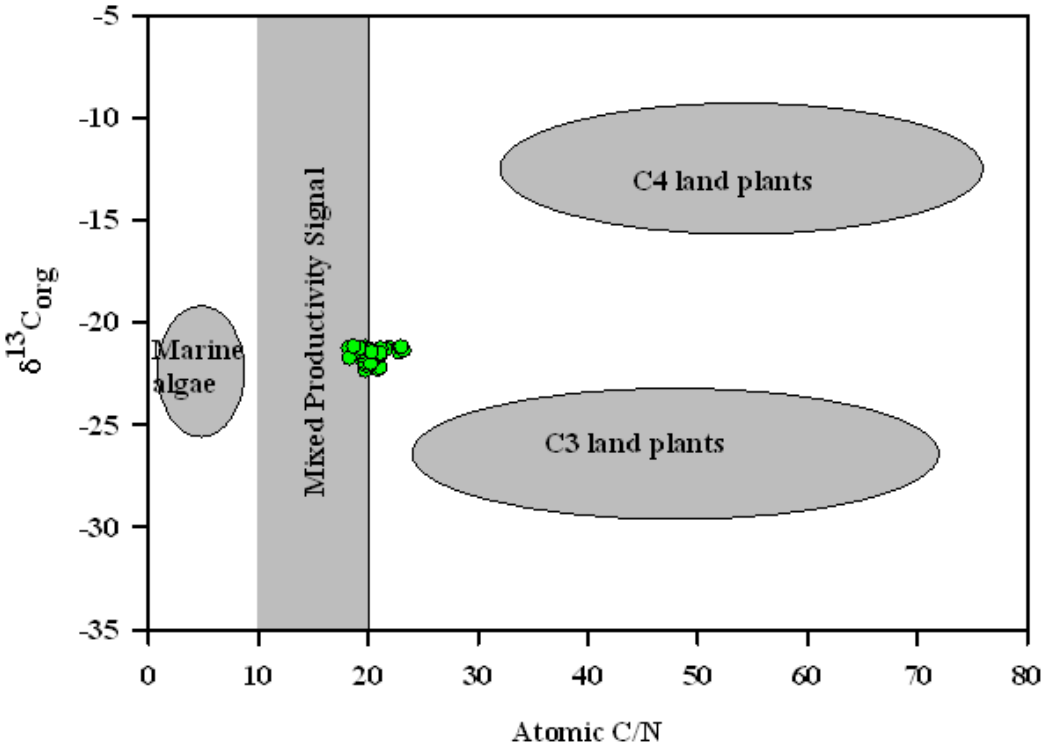

Figure 12. The plot shows the provenance of the SOM. Atomic C/N and $\delta^{13}C_{org}$ values show a mixed productivity signal i.e. presence of both marine as well as terrestrial source of the SOM.

The timing and the magnitude of change in the TOC concentration are attributed to regional oceanographic features, mainly productivity, surface current direction, terrigenous input, and dissolved oxygen that affect both the flux of autochthonous and allochthonous material, and its deposition and diagenetic alteration. The long-term declining trend shown by Ti/Al (Fig. 11i) in the present study suggests a decline in surface runoff/detrital influx resulting in a decline in terrestrial organic carbon input. So, enhanced runoff bringing more terrestrial organic matter is ruled out. The lack of an independent surface water productivity indicator in the present study does not allow us to examine the relative contribution of marine organic carbon. However, the previous study from the same region based on changes in relative abundance of planktic foraminifera *Globigerina bulloides* (an indicator of high productivity)

suggests a decline in marine productivity since mid-Holocene (Saraswat et al., 2016). Therefore, the increasing trend observed in the TOC mass accumulation rate and concentration (Fig. 11d and 11e) since mid-Holocene to present can be interpreted either in terms of the sedimentation rate variation and/or changes in redox conditions in bottom waters/ sediment-water interface. Both these factors can play a major role in the preservation of TOC, resulting in its deviation from the surface productivity trend. However, as discussed above in section 4.2, the periods of slight decline in reducing condition are not coeval with the enhanced TOC values observed in the present study since mid-Holocene to present. Canfield (1994) observed that the sediment deposition rate is overall the most important factor influencing TOC preservation, as it provides less time for organic matter to degrade. Canfield (1994) also proposed a similar preservation of TOC irrespective of presence or absence of bottom water oxygen, at sedimentation rates higher than ~40 cm/kyr in normal marine conditions. In the case of marine sediments depositing with sedimentation rates below 40 cm/kyr, enhanced preservation of TOC may be found under low bottom-water oxygen conditions. In the studied core, the high sedimentation rate of 16.2 cm/kyr is observed for the top 11 cm with the average sedimentation rate of 8.96 cm/kyr, which is much lower than 40 cm/kyr. Somayajulu et al. (1999) and Agnihotri et al. (2003b) also observed similar sediment accumulation rates (~20 cm/kyr) at 370, 600, and 1680 m water depths on the continental slope off Mangalore. Sediment cores lying outside the OMZ of the eastern Arabian Sea were found to have a much lower abundance of TOC contents due to much lower sedimentation rates and thereby longer exposure time to oxic waters at the sediment-water interface leading to a poor preservation (Agnihotri et al., 2003a). Therefore, the increased sedimentation rate observed in the present study along with the enhanced bottom-water reducing

conditions must have caused limited organic matter decomposition within the water column, resulting in enhanced TOC values in the SEAS and its deviation from the surface productivity trend. This is further corroborated by a strong correlation between TOC and TN (r^2=0.88) (Fig. 13).

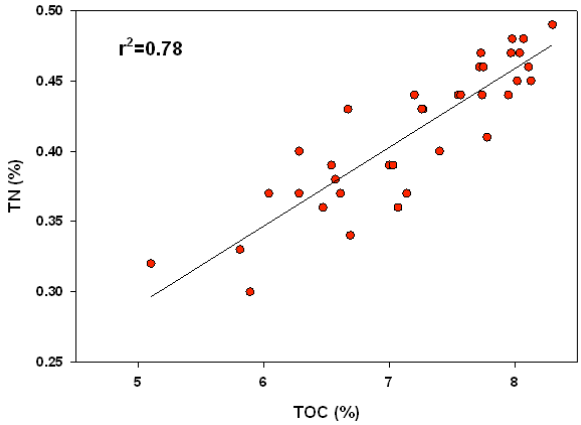

Figure 13. Correlation of TOC with TN. Correlation coefficient is given by r^2 value.

The qualitative changes in past SASM have been reconstructed from both the SEAS (Schulz et al., 1998; von Rad et al., 1999a, 1999b; Luckge et al., 2001; Altabet et al., 2002; Agnihotri et al., 2002; Anderson et al., 2002) and from the Indian subcontinent (Ramesh et al., 1985; Sinha et al., 2005; Yadav, 2013) at centennial to sub-centennial scale resolution. However, the quantitative estimates of SASM intensity (based on $\delta^{18}O$ of foraminifera, Mg/Ca, a proxy for seawater temperature) are limited and have coarse resolution (Saraswat et al., 2005; Anand et al., 2008; Banakar et al., 2010; Govil and Naidu, 2011; Saraswat et al., 2012). Recently, past salinity values determined from the same core used in the present study at a high-resolution of centennial scale has shown declining SASM precipitation intensity since mid-Holocene (Tiwari et al., 2015a) (Fig. 11j). This is further accompanied by the declining long-term trend shown by Ti/Al (Fig. 11i) in the present study, which suggests a decline in surface runoff/detrital influx with the declining SASM

precipitation intensity. The sedimentation rate in the present study has shown a gradual increase from 4772 to 977 yr BP, whereas the drastic change in the sedimentation rate is observed only after 1000 yr BP to present thereby showing an increasing long-term trend. However, the observed long-term trend shown by the sedimentation rates in the present study do not match with declining SASM intensity since mid-Holocene. But if we look at the short-term changes in Ti/Al, it shows an increase during the time of increased sedimentation rate, i.e., from 3342 to 3137 yr BP, from 1976 to 1813 yr BP, and from 977 yr BP to present thereby suggesting an increase in terrigenous influx with increasing sedimentation rate. Interestingly, this time intervals are further accompanied by a decrease in SSS suggesting an increase in SASM intensity. Thus, the non-consistent long-term trend of sedimentation rate observed in the present study is could be due to fewer numbers of dates and the same could be improved by dating few more number of samples in between to get a clear picture. Therefore, we note that, although there were few periods of enhanced SASM intensity, the long-term trend shown by surface run-off/detrital influx suggests decline in the SASM intensity since mid-Holocene, which corroborates the previously determined decline in SASM precipitation (Kessarkar et al., 2013; Saraswat et al., 2013; Tiwari et al., 2015a).

4.9. Response of Monsoon System to Precessional Forcing Since Mid-Holocene: Comparison Between South Asian, East Asian, and North African Summer Monsoon

The Indian monsoon represents the most typical monsoon climate, as it is characterized by (i) a robust annual reversal of the prevailing surface winds (summer south-westerlies and winter north-easterlies) and (ii) a sharp contrast between rainy

summer and arid winter, with 70–80% of the total annual precipitation falling in June-July-August-September (Webster, 1987). In general, it seems that the SASM precipitation since mid-Holocene transits between dry and wet conditions (e.g., Yadava and Ramesh, 2005; Laskar et al., 2013; Prasad et al., 2014; Tiwari et al., 2015a) but the overall trend since mid-Holocene is still debatable. The spectral analysis and numerical modeling indicate that the low-latitude climate and SASM variability are mainly caused by changes in precession (Molfino and McIntyre, 1990; Clemens et al., 1991; McIntyre and Molfino, 1996; Joussaume et al., 1999; Jiang et al., 2013). The precessional cycle does not change insolation's annual total, but rather influences its seasonality and in turn that of the monsoon, significantly. Since seasonal variations are out of phase between hemispheres, the insolation changes associated with precession are also out of phase, resulting in hemispheric contrasts in paleomonsoon records at the precessional timescale. The precession forcing of the monsoon is most evident in proxy records since mid-Holocene, given the richness of geological data archives and particularly the high-resolution terrestrial and marine records from the Indian, African, and East Asian monsoon regions. For example, a few of the SASM wind intensity, based proxies such as the relative abundance of *G. bulloides* from the ODP site 723-A from the western Arabian Sea (Gupta et al., 2005) (Fig. 14d) showed that the SASM has declined since mid-Holocene with the declining NH solar insolation. Recent study by Tiwari et al. (2015a), based on paired measurement of stable oxygen isotopic ratio and trace metal composition of surface dwelling planktic foraminifera for the same core SN-6, helps in estimating past salinity which is mainly controlled by local evaporation-precipitation, thus providing a good idea of monsoon intensity.

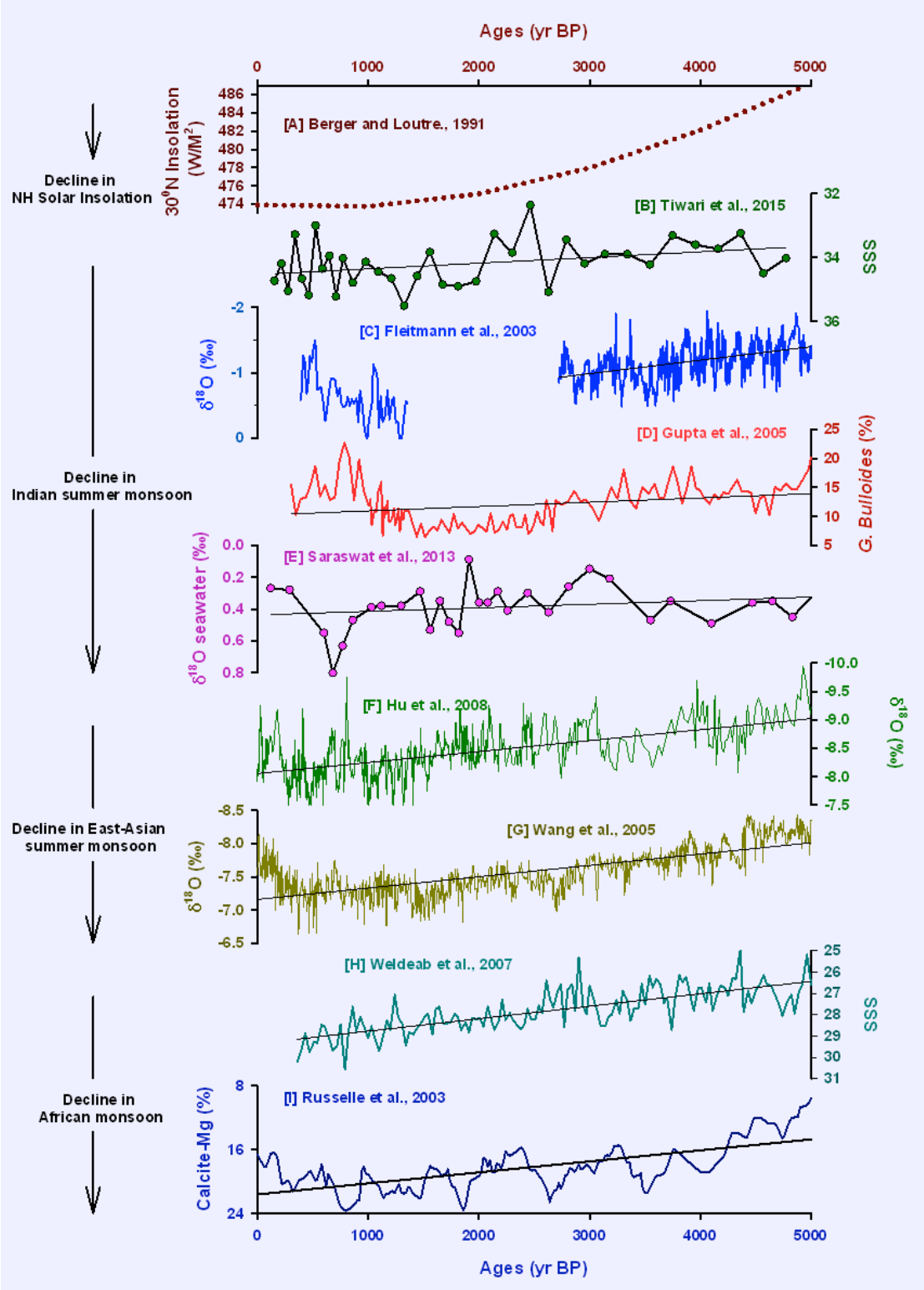

Figure 14. Comparing records of (b–e) Indian summer, (f and g) East Asian summer monsoons, and (h and i) African summer monsoon using diverse proxies from different regions and its response to precessional forcing. Figure 4a shows June insolation at 30°N.

Increasing values of SSS since mid-Holocene to present corresponds to weakened SASM conditions leading to arid climate (Fig. 14b). A similar decline in SSS in the SEAS is also shown by Kessarkar et al. (2013), suggesting declining SASM intensity since mid-Holocene. Sea surface salinity and $\delta^{18}O_{seawater}$ are directly linked to the local E-P balance, and in general, a good linear correlation can be found between these parameters for most of the global ocean (Craig and Gordon, 1965). Thus, by studying the $\delta^{18}O_{seawater}$, Saraswat et al. (2013) show the evidence of high saline surface water since mid-Holocene indicating a decline in freshwater runoff from the Western Ghats as a consequence of declining SASM intensity since mid-Holocene. Also, the terrestrial records from Qunf Cave, southern Oman (Fleitmann et al., 2003) (Fig. 14c), Timta Cave, northern India (Sinha et al., 2005), and Tianmen Cave, Tibet (Cai et al., 2012) suggest that the Indian monsoon has varied in concert with the declining Northern Hemisphere solar insolation after attaining maxima during mid-Holocene. Furthermore, stalagmites from East Asia exhibit a long-term trend that is broadly similar to changes in Northern Hemisphere solar insolation, with a general warm/wet period in NH monsoon regions at 5.0 kyr BP, which corresponds to the Holocene climatic optimum followed by cold/arid period since then (Fig. 14f and 14g). A similar pattern has also been observed in marine and terrestrial proxy records of the North African monsoon. Africa is presently the only continent that is divided by the Equator into two nearly equal parts, resulting in distinct monsoon systems in each hemisphere. Rich geological archives of the North African monsoon have been recovered from the East African Rift lakes (Gasse et al., 2008), the Mediterranean Sea (Ziegler et al., 2010), the North Atlantic (Pokras and Mix, 1987; Weldeab et al., 2007), as well as caves (Bar-Matthews et al., 2003). As a result, the history of the North African monsoon is better resolved by proxy data than its southern counterpart.

The precipitation record from the marine sediment core in the Gulf of Guinea (MD03–270), an indicator of relative changes in the outflow of the Niger and Sanaga rivers shows a decline since 5 kyr BP (Weldeab et al., 2007) (Fig. 14h). Likewise, Mg percentage in calcite from Lake Edward, an equatorial rift lake in central Africa, is used to reconstruct lacustrine paleohydrology and climate history. The Mg percentage in calcite rises during evaporative concentration of a lake because of increases in the $[Mg^{2+}]/[Ca^{2+}]$ ratio in lake water. The observed decline in Mg percentage in calcite suggest increased aridity since mid-Holocene (Russell et al., 2003) (Fig. 14i). Thus our inter-comparison study suggests that basic structures of variability for the Indian, East Asian, and African monsoons are remarkably similar. It exhibits a long-term trend broadly tracking the intensity of northern hemisphere summer insolation (Yuan et al., 2004; Wang et al., 2008; Cheng et al., 2009; Zhang et al., 2011; Cai et al., 2012) suggesting a decline in seasonal heating resulting in colder summer in the Northern Hemisphere since mid-Holocene. It is likely therefore that the NH summer monsoons are not only governed by a common set of processes, such as the enhanced east-west thermal contrast in the Indo-Pacific, but also by inter-hemispheric thermal asymmetries associated with their contrasting land extents that have potentially opposing effects on the NH and SH monsoons (Wang et al., 2012).

4.10. Conclusion

A suite of geochemical proxies, including major and trace elements, have been used to reconstruct past redox conditions and SASM variability from SEAS since mid-Holocene. Various redox proxies (viz. enrichment and interelemental relationships of redox-sensitive trace elements) indicate intensified reducing conditions there by suggesting the strengthening of the OMZ since mid-Holocene to the present. Atomic

C/N ratio versus the $\delta^{13}C_{org}$ plot shows that the core site has experienced mixed productivity signal since mid-Holocene thereby limiting the use of TOC as a productivity indicator in such settings. We find that the enhanced TOC values observed in the present study are a result of better preservation caused by increased sedimentation rate under the prevalence of enhanced suboxic bottom waters suggesting intensified OMZ since mid-Holocene. Past SASM variability as shown by Ti/Al in the present study indicates a decline since mid-Holocene, which matches with the previous studies. Thus, this study would help to understand past SASM variability more accurately in future studies from this region. The inter-comparison of monsoon records from different regions shows declining monsoon since mid-Holocene implying the influence of the precessional forcing. It suggests an increased/reduced seasonal heating during the northern/southern hemisphere summer during the mid-Holocene resulting in stronger/weaker summer monsoon in the northern/southern hemisphere and vice versa in winter. More of such studies involving quantitative estimates coupled with model ensemble are required to assess the role played by various forcing factors.

Chapter 5

Differential Response of Denitrification in the Southeastern Arabian Sea during Last Glacial Maximum and Holocene

5.1. Introduction

The Arabian Sea is one of the most productive regions of the world ocean, marked by a large-scale water-column denitrification in the oxygen OMZ. The expansion and intensification of declining oxygen concentration have become a topic of widespread interest because of its adverse effects on marine ecology and fisheries, and its potential to provide positive feedback to global warming through production of nitrous oxide, a potent greenhouse gas, through denitrification (Naqvi et al., 2000, Banse et al., 2014, Rixen et al., 2014). A recent trend of declining sub-surface oxygen levels almost everywhere in the open ocean (Joos et al., 2003), and the consequent expansion of major OMZs (Stramma et al., 2008, Banse et al., 2014, Rixen et al., 2014) is alarming. These declines are believed to reflect physical changes (ocean warming, stratification, and circulation) that seem to have already altered oxygen supply to subsurface waters. Denitrification occurs when the oxygen concentration in the OMZs falls below a threshold value of ~5 μmol/kg O_2 (e.g. Codispoti et al., 2001). During this process, NO_3^- acts as an electron acceptor and is reduced to primarily N_2 gas. In the ocean, denitrification occurs in organic-rich continental margin sediments and in intermediate waters within intense OMZs (200 – 1200 m). Of the later, The Arabian Sea supports approximately one-third of marine water-column denitrification (Howell et al., 1997). During denitrification, bacteria preferentially consume NO_3^- with a lighter isotope (^{14}N), thus enriching the residual nitrate in the heavier isotope (^{15}N) (Brandes et al., 1998). The ^{14}N-enriched NO_3^- is transported to the surface waters and is consumed by phytoplankton, which subsequently settles down and gets preserved in the sediments. The $\delta^{15}N$ of the sedimentary organic matter (SOM) faithfully records the $\delta^{15}N$ of the sinking organic matter (Altabet et al., 1999). Accordingly, $\delta^{15}N$ of the SOM has been widely used as a

tool to track past changes in subsurface denitrification (Ganeshram et al., 2000; Suthhof et al., 2001; Altabet et al., 2002; Agnihotri et al., 2003). During the last glacial maximum, denitrification was less intense than today as shown by the $\delta^{15}N$ records of the sedimentary organic matter (Galbraith et al., 2013). Models suggest- albeit with many uncertainties and unknowns - that both denitrification and nitrogen fixation were lower during the LGM (Deutsch et al., 2004; Eugster et al., 2013; Galbraith et al., 2013; Schmittner and Somes, 2016). However, due to a stronger reduction of denitrification than of nitrogen fixation, total export production was higher and increased the glacial oceanic nitrogen inventory by 10-50 % over that of the Holocene, affecting also the carbon storage in the ocean (Deutsch et al., 2004; Eugster et al., 2013; Schmittner et al., 2007). Distinct changes of sedimentary $\delta^{15}N$ values (Galbraith et al., 2013) during the deglaciation are interpreted to reflect the major changes in the nitrogen inventory. The decreasing iron supply at the end of the LGM may have significantly reduced nitrogen fixation, leading to a rise of $\delta^{15}N$ even during the LGM (Eugster et al., 2013). Enhanced upwelling at about 15 kyr BP led to abrupt increase of denitrification in the eastern tropical north and south Pacific as well as in the Arabian Sea (Altabet et al., 1995; Deutsch et al., 2004; Ganeshram et al., 2000; Ganeshram et al., 1995; Suthhof et al., 2001). The corresponding signal of enhanced $\delta^{15}N$values was registered in many parts of the global ocean from the late glacial to early Holocene due to increase of benthic denitrification caused by sea level rise and subsequent flooding of continental shelves followed by a smooth decline in $\delta^{15}N$ values (Deutsch et al., 2004; Galbraith et al., 2013; Ren et al., 2012). This sequence of events is very well recorded in cores from the east Pacific upwelling areas, but differs from the temporal pattern seen in sedimentary records from the Arabian Sea that show stable or increasing $\delta^{15}N$ values in the late Holocene

(Galbraith et al., 2013). Previous studies based on denitrification intensity have shown that the Arabian Sea OMZ was strongly developed during the Northern Hemisphere warm periods (Dansgaard-Oeschger interstadials), but weak (or absent) during the equivalents of North Atlantic cold spells (Heinrich Events, Younger Dryas and Dansgaard- Oeschger interstadials) (e.g. Schulz et al., 1998; Altabet et al., 2002). The previously long-held hypothesis was that, climate perturbations originate in the high-latitude North Atlantic and propagate globally via changes in the flux of North Atlantic Deep Water (NADW) (e.g. Broecker et al., 1985). However, an improved ice core chronology based on methane concentrations demonstrates that millennial-scale temperature variations occurred in Antarctica prior to their occurrence in Greenland (Blunier and Brook, 2001). Sediment cores from both hemispheres, through paired planktic and benthic records, confirm this was the case for water masses as well with changes in the Southern Hemisphere (or Antarctic Bottom Water) preceding those in the Northern Hemisphere (or NADW) (Charles et al., 1996; Shackleton et al., 2000). Reduced denitrification as a result of better ventilation of intermediate waters during the Younger Dryas and Heinrich Events is related to oceanic teleconnection with water masses advecting from the south (Suthhof et al., 2001). The paleoceanographic significance of most previous studies on denitrification intensity from the SEAS is limited by a rather low temporal resolution. Consequently, higher-resolution past denitrification records on continental slope sediments from this region are needed to allow a more detailed evaluation of environmental changes since the last glacial period. We have chosen a core (SK274-4G) from the SEAS that experiences moderately high productivity during the SASM season. The core is located close to the boundary of the perennial denitrification zone (Fig. 15). The present study attempts to determine the influence of oceanic

circulation changes on the denitrification variability in the SEAS at a high-resolution (centennial scale) for the past ~43 kyrs and the underlying mechanisms.

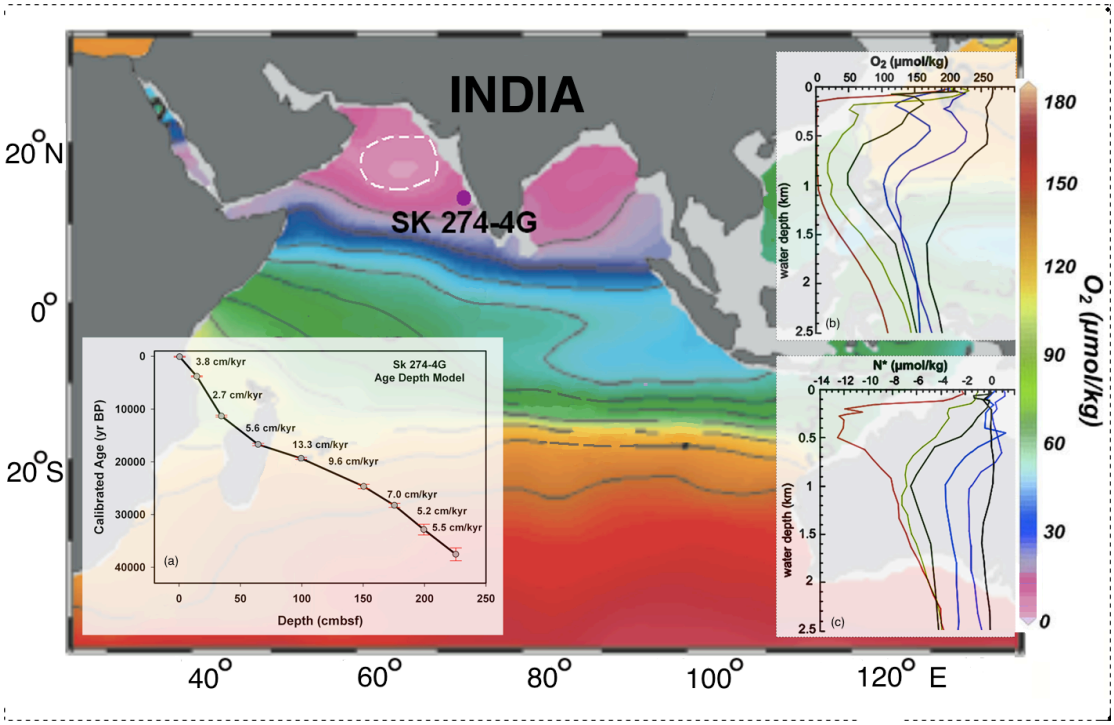

Figure 15. Location of the core SK 274-4G with oxygen contours showing oxygen concentration at 300 m depth. White dashed line indicates nitrite maximum (>0.5 µM/L; Naqvi, 1991) coinciding with lowest oxygen concentration. The pink color indicates permanent OMZ (O_2 <20 µM/kg). Purple circle in the figure shows the location of the core SK 274-4G. Age-depth model (inset; shown in panel a) is based on 9 radiocarbon dates on selected species of planktic foraminifera; sedimentation rates are also shown (underlined; in cm/kyr). Present-day water column characteristics of the Indian Ocean are shown (inset; panel b and c). Oxygen concentration and nitrate deficit, N* data are from the World Ocean Circulation Experiment (WOCE) stations I07N-819 (20°N 64°E; shown by red line), I01–910 (11°N–53°E; shown by light green line), I07N-716 (14°S–55°E; shown by blue line), I08N-346 (19°S–88°E; shown by purple line), I08S/I09N-23 (40°S–95°E; shown by black line) and a GEOSECS station (0–44.5°E; shown by dark green line) (http://cdiac.esd.ornl.gov/ oceans/glodap/Glodap_home.htm).

5.2. Regional Setting

The SEAS is characterized by a seasonal reversal of monsoon winds, resulting in large seasonal and spatial pattern in physical/hydrographic/biological/chemical variations in the water column (Wyrtki, 1973; Nair et al., 1989). Coastal circulation in the SEAS undergoes a complete reversal associated with the monsoons twice a year (Shetye and Gouveia, 1998; Naqvi et al., 2006). During winter monsoon (Northeast Monsoon), the West Indian Coastal Current flows poleward, causing downwelling off the west coast of India and a well-oxygenated water column over the shelf. During SASM, the circulation is along the eastern boundary – an equatorward flowing West Indian Coastal Current, a poleward undercurrent, and moderate coastal upwelling. The spatial variability of upwelling along the western continental margin of India can be inferred from the water column productivity. The water column productivity measured during July 1995 was 440 mg C m^{-2} day^{-1} at 18°N 70°E, 1760 mg C $m^{-2}day^{-1}$ at 12°N 73°E and 660 mg C m^{-2} day^{-1} at 10°N 75°E [Bhattathiri et al., 1996]. Whereas, the same measured during February 1995 was 335 mg C m^{-2} day^{-1} at 11°N 64°E, 807 mg C m^{-2} day^{-1} at 21°N 64°E and 643 mg m^{-2} day^{-1} at 21°N 67°E (Madhupratap et al., 1996). During the winter monsoon, northeast winds are too weak to induce any significant offshore Ekman transport in the SEAS (Fontugne and Duplessy, 1986, Madhupratap et al., 1996). This moderate to high surface productivity coupled with a sluggish renewal of intermediate waters has resulted in the development of oxygen-depleted conditions, which are also evident from the presence of denitrification in the water column at these locations (Naqvi, 1991, 1994). The main water sources at the intermediate depth of the Arabian Sea are the outflows from the marginal seas (Red Sea Water (RSW), Persian Gulf Water (PGW)) in the north and Indian Ocean Central Water (IOCW) from the south (Olson

et al., 1993). The latter is a mixture of intimately linked aged SAMW–AAIW and the Indonesian Intermediate Waters (IIW) (You, 1998). In the modern Arabian Sea, RSW and PGW settle at water depths of ~800 m and ~300 m, respectively (Shapiro and Meschanov, 1991, Prasanna Kumar and Prasad, 1999). The northern extent of these waters is marked approximately by the latitude of 18°N (Shetye et al., 1994) and their occurrence is also reported from 10°S (Shenoi et al., 2004). Oxygen concentrations in the northern and southern water masses are equally low but the volume-transported across the equator with the southern waters is 1 order of magnitude larger than that contained in the northern source inflow (Swallow, 1984). During SASM, poleward undercurrent carries well-oxygenated waters off the Indian margin. As monsoon wind reverses in winter, Arabian Sea high-salinity waters flow equatorward. Therefore, the renewal of the oxygen-deficient subsurface waters is more vigorous during the SASM than the winter Monsoon. Seasonal change in monsoon circulation drives significant changes of oxygen-deficient waters in the eastern Arabian Sea (Naqvi, 1991). Oxygen replenishment occurs mostly along the southern and western boundaries of the Arabian Sea and hence water severely impoverished in oxygen bathe the northeastern part of the basin. The $\delta^{15}N_{NO3-}$ values (Fig 16) at a water depth of 100–150 m, which correspond to the bottom depth of the euphotic zone (Olson et al., 1993), from different stations fall within a narrow range of 7–9‰ despite wide denitrification intensity underneath. Water column denitrification causes the $\delta^{15}N$ of nitrate to be significantly higher than the mean ocean nitrate value of 4.5–6% (Sigman et al., 1997). As a consequence, $\delta^{15}N_{NO3-}$ at 300 m depth reaches 18% in the northeastern Arabian Sea and 12 % in the western Arabian Sea (Brandes et al., 1998; Naqvi et al., 1998; Altabet et al., 1999), further highlighting the clear regional heterogeneity.

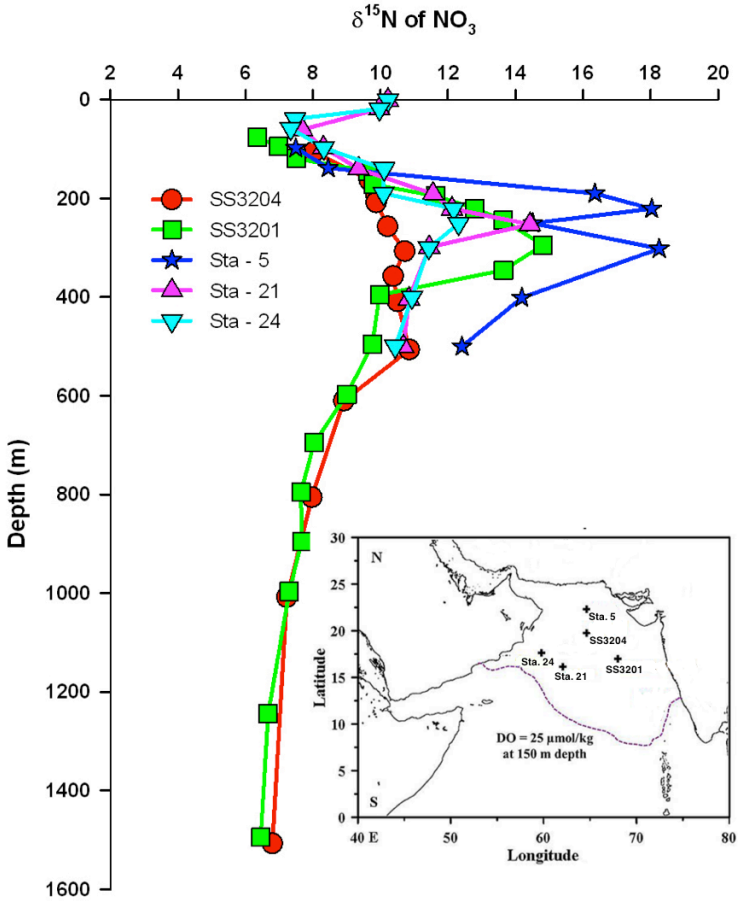

Figure 16. Shows the depth profile of nitrogen isotope of NO_3^- in the Arabian Sea water column. Inset shows the station locations; the dotted curve depicts dissolved oxygen concentration.

5.3. Chronology and Sedimentation Rate

Core SK-274-4G (13°59'N and 72°E; 1290 m water depth; 2.60 m length) was retrieved from the SEAS from the lower boundary of the OMZ (Fig. 15). The chronology of the core is based on nine radiocarbon dates on mixed planktic foraminifera (*Globigerinoides ruber, Globigerinoides sacculifer*; size range: 250–420 µm) using accelerator mass spectrometer (AMS) at the NSF AMS Facility at University of Arizona. The ^{14}C dates were calibrated using the marine dataset (Marine 09), (Reimer et al., 2009) in Calib 6.0 (Stuiver and Reimer, 1993), employing

a reservoir age correction of 355 years determined by Butzin et al., (2005) based on a three-dimensional global ocean circulation model for the core location (available at http://radiocarbon.LDEO.columbia.edu). These modern ocean radiocarbon reservoir age estimates are based on the output from a three-dimensional global ocean circulation model (Cao et al., 2007) that improves previous estimates based on data points from distant regions (e.g., Southon et al., 2002). The core spans the last ~ 43 kyr BP, and the core top shows an age of ~0.08 kyr BP. The sedimentation rate (Fig. 15a), as inferred from the calibrated AMS ^{14}C dates, averages 6.6 cm/kyr and varies from 2.7 to 13.3 cm/kyr between for the last 43 kyrs. The maximum sedimentation rate of 13.3 and 9.68 cm/kyr was seen between 16.7 to 19.3 and 19.3 to 24.6 kyrs intervals respectively. The average sample resolution is ~188 yr.

5.4. Elemental and Isotopic analysis of Sedimentary Organic Carbon and Total Nitrogen

For elemental and isotopic analysis of carbon and nitrogen, each sub-sample was oven dried at 40 °C and then homogenized by finely grinding it in an agate mortar. For total organic carbon (TOC) concentration and $\delta^{13}C_{org}$ estimation, carbonate was removed from sub-sample by adding 2N hydrochloric acid. The samples were then completely rinsed by adding deionized water five times and again oven dried at 40°C. Given the known problems of loss of nitrogen compounds from the sedimentary organic matter on acidification of samples, resulting in bias in nitrogen content and $\delta^{15}N$ values (Brodie et al., 2011), untreated samples were used for total nitrogen (TN) and $\delta^{15}N$ analysis. A portion of the grinded sample was wrapped in a tin capsule and combusted using an Elemental Analyzer coupled to an Isoprime stable isotope ratio mass spectrometer at the Marine Stable Isotope Lab (MASTIL) of

National Centre for Polar and Ocean Research (NCPOR), Goa, India. Samples were run along with the blank and known standards. Standards were prepared by weighing 0.4–0.6 mg of IAEA cellulose standard (IAEA- CH-3) of certified isotopic composition ($\delta^{13}C$ = −24.74 ‰ vs. VPDB) for carbon and 0.5–1.0 mg of IAEA ammonium sulphate (IAEA N1) of certified isotopic composition ($\delta^{15}N$ = 0.4 ‰) for nitrogen. Data quality control was checked by running reference standard after every six samples. Stable isotope abundance is reported in terms of δ-values and expressed in per mil (‰). Analytical precision based on repeat measurements of the reference standard for isotopic composition (n=16) are better than 0.02 ‰ for carbon and 0.08 ‰ for nitrogen. Analytical precisions based on repeat measurements (n=16) of the reference standard (Sulphanilamide) for the TOC and TN measurements are ±0.2% and ±0.3%, respectively.

5.5. Micropaleontological Analysis

For the micropaleontological study, about 10g of dried sediment was washed through a 63-μm sieve and dried at 50°C. The dried samples (> 63 μm) were sieved through a 125-μm sieve. The relative abundance of planktic foraminifera was calculated in the >125-μm size fraction. To calculate the relative abundance of *Globigerina bulloides*, a minimum of 300 specimens of planktic foraminifera were picked from 125-μm-size fraction from each sample. The increased abundance of *G. bulloides* is indicative of cold and nutrient-rich water advected to the surface, resulting in increased biological productivity, which is generally associated with the summer upwelling in the Arabian Sea.

5.6. Spectral Analysis

Continuous Wavelet Transform (CWT) and the Squared Wavelet Coherence including the phase analysis was carried out in this study to check whether the visually perceived coherence between the two different physical processes is statistically significant or not, by following Torrence and Campo, (1998) and Grinsted et al., (2004). CWT is a common tool for analyzing localized intermittent oscillations in a time series, it is very often desirable to examine two time series together that may be expected to be linked in some way. In particular, to examine whether regions in time-frequency space with large common power have a consistent phase relationship and therefore are suggestive of causality between the time series. From two CWTs we construct the Cross Wavelet Transform, which will yield their common power and relative phase in time-frequency space. A wavelet is a function with zero mean and that is localized in both frequency and time. The idea behind the CWT is to apply the wavelet as a bandpass filter to the time series. The CWT has edge artifacts because the wavelet is not completely localized in time. It is therefore useful to introduce a Cone of Influence in which edge effects cannot be ignored.

5.7. Marine Dominated Source of Sedimentary Organic Matter

It is important to ascertain the sources of the organic matter and examine it for any other influence like diagenesis before using it for reconstructing the past denitrification variability. Atomic C/N ratios for marine organic matter (algae) typically varies between 4 and 10, whereas for terrestrial organic matter (vascular land plants) it is >20 (Premuzic et al., 1982; Meyers, 1994). Organic matter produced by marine algae from dissolved bicarbonate ($\delta^{13}C$ value of ~ 0 ‰) typically has $\delta^{13}C$ values between -22 and -20‰. Whereas, organic matter produced by land plants from

atmospheric CO_2 ($\delta^{13}C$ ~7 ‰) using the C3 pathway consequently has an average $\delta^{13}C$ value of ~ -27 ‰ and by those using the C4 pathway is ~ -14 ‰ (O'Leary, 1988; Farquhar et al., 1989). The SOM as identified by TOC concentration in the present study varied between 0.80 to 2.84 % with an average of 1.82 %. Atomic C/N and $\delta^{13}C_{org}$ varied from 13.01 to 22.77 and -19.95 to -18.30 ‰, respectively. The $\delta^{13}C_{org}$ and C/N values for SOM in the present study shows mixed source of sedimentary organic matter: marine (in-situ produced) as well as terrestrial organic matter (transported via various streams/surface runoff) at the study region (Fig. 17).

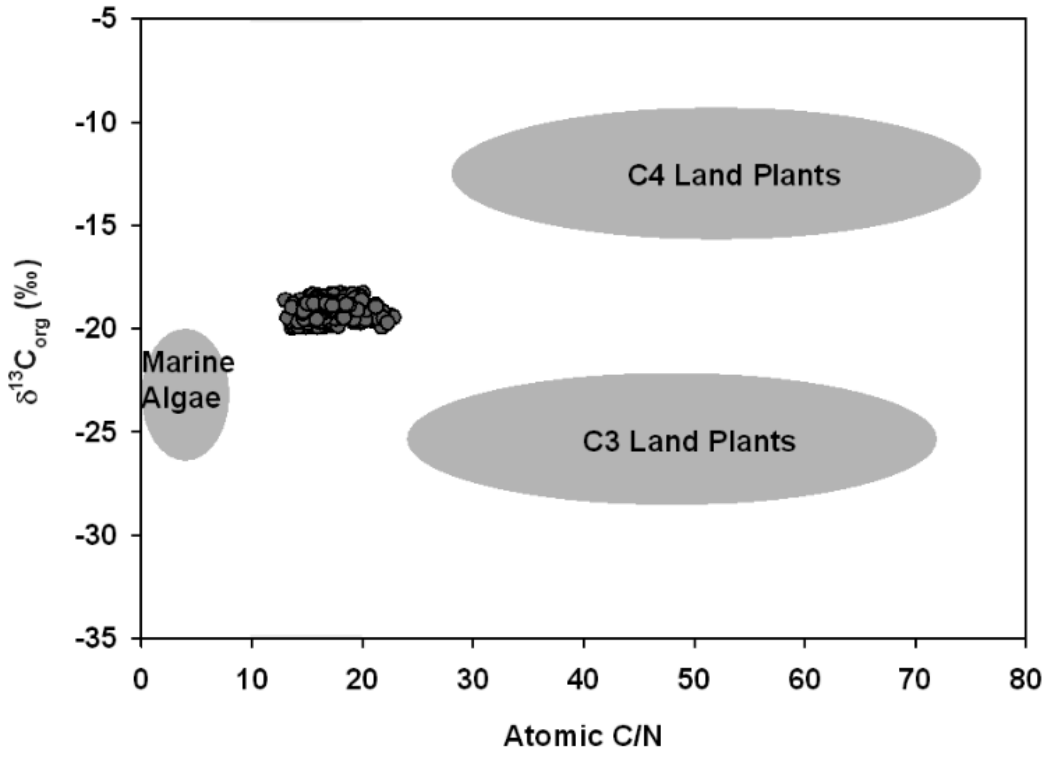

Figure 17. Shows mixed source of the sedimentary organic matter at our core location.

To assess the relative proportions of terrigenous and marine autogenous organic carbon present in the sediments, a simple $\delta^{13}C$-based two end-member mixing model based on the work of Calder and Parker (1968) and adopted by other researchers such

as Schluz et al., (1998) and Hu et al., (2006) was applied to this area. We assigned -13.0‰ (average value of the C4 plants) (Farquhar et al., 1989) as the $\delta^{13}C$ value of the terrestrial end-member ($\delta^{13}C_{terrestrial}$). We took the $\delta^{13}C$ values of the C4 plants as all the data points in the plot of $\delta^{13}C_{org}$ vs. atomic C/N of the present study (Fig. 17) fall on the mixing line between the marine and C4 end members. Likewise, we assigned -20.3‰ as the $\delta^{13}C$ value of the marine end-member ($\delta^{13}C_{marine}$) (Agnihotri et al., 2003). The terrestrial organic carbon contribution (f) was calculated by the following equation (Calder and Parker, 1968): f (%) = ($\delta^{13}C_{marine}$ - $\delta^{13}C_{measured}$) / ($\delta^{13}C_{marine}$ - $\delta^{13}C_{terrestrial}$) x 100 Then, the contribution of marine algae (f^m) to the TOC could be estimated by the following expression: f^m (%) = 100 - f. The resulting estimates for the contribution of the marine and terrestrial organic carbon suggest a dominance of the former (average 80.50 %) with a little contribution from the latter (average 19.50 %) since the last 43 kyr BP.

5.8. No Significant Effect of Terrestrial Input, Diagenesis, and Other Processes on the $\delta^{15}N$ Values

As the organic matter in the present study contains a small amount terrestrial organic matter, the possibility of it affecting the $\delta^{15}N$ values has been examined through the relationship between $\delta^{13}C_{org}$ and $\delta^{15}N$. If the terrestrial organic matter had any influence on $\delta^{15}N$ values then a positive correlation is expected between $\delta^{13}C_{org}$ and $\delta^{15}N$ (Peters et al., 1978). Varying proportions of terrestrial organic matter in the mixture will produce a mixing line in the $\delta^{13}C_{org}$ – $\delta^{15}N$ plot, with lower $\delta^{13}C_{org}$ corresponding to lower $\delta^{15}N$ values (Sweeney and Kaplan, 1980).

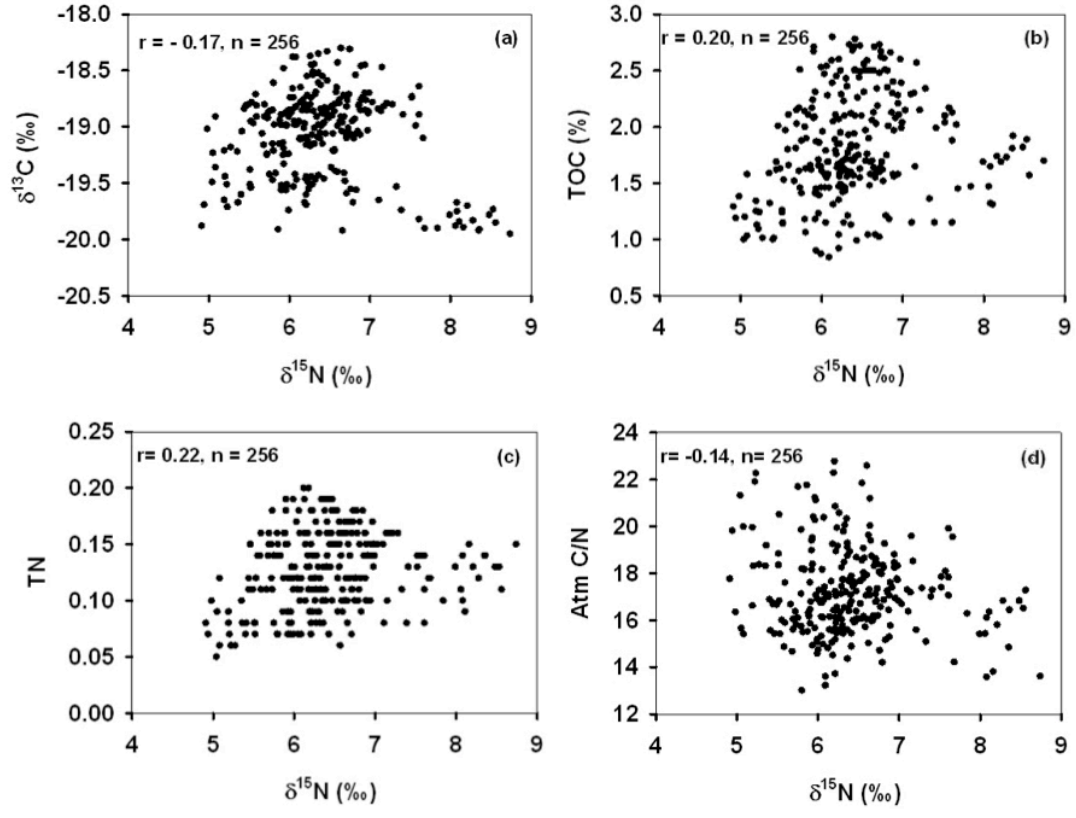

Figure 18. Shows the scatter plots of $\delta^{15}N$ with (a) $\delta^{13}C_{org}$, (b) TOC, (c) TN and, (d) atomic C/N, respectively, along with their respective r (correlation coefficient) and n (number of data points) values.

In the present study, scatter found in the $\delta^{15}N$ versus $\delta^{13}C_{org}$ plot (Fig. 18a) (r = - 0.17, n= 256) rules out the possibility that mixing of terrestrial and marine organic matter had any influence on $\delta^{15}N$ values. Further, the early digenetic effects if any, on the $\delta^{15}N$ were examined through relationships between $\delta^{15}N$ and TOC, TN and atomic C/N ratio. Early diagenetic degradation of organic matter tends to increase $\delta^{15}N$ (Agnihotri et al., 2003), resulting in anti-covariance with TOC and TN contents and covariance with atomic C/N ratios. However, such trends were not observed in the present study. We find that no relationship exists between $\delta^{15}N$ and TOC (r = 0.21, n = 256, Fig. 18b), TN (r= 0.22, n= 256, Fig. 18c), and atomic C/N ratio (r = - 0.14, n =256, Fig. 18d). Further, incomplete utilization of surface nitrate under

nutrient-rich conditions has been documented to have a very limited imprint on the $\delta^{15}N$ signal in the Arabian Sea (Schafer and Ittekkot, 1993). Moreover, biological nitrogen fixation develops either in stratified, oligotrophic surface waters or in denitrifying zones owing to relative phosphorus enrichment in thermocline waters that favors nitrogen fixing biota over other producers (Karl et al., 2002). Today, fixed nitrogen may account for a significant part of surface nitrate in the Arabian Sea where denitrification is exceptionally intense (Brandes et al., 1998; Deutsch et al., 2007), hence partially cancelling out the isotopic enrichment caused by denitrification. It is, however, questionable whether nitrogen fixation was more active in the SEAS during stadials and Heinrich events because (1) denitrification was reduced if not shut down (Reichart et al., 2004), and (2) surface waters were neither oligotrophic nor stratified during cold periods (Reichart et al., 2004). Hence, we infer that although nitrogen fixation occurs in the Arabian Sea and may contribute to lower nitrogen isotopic values during cold phases, the general relationship remains that the $\delta^{15}N$ value of surface NO_3^- decreases with decreasing water column denitrification. This suggests that the subsurface denitrification is the main governing factor of the $\delta^{15}N$ values of the SOM at our core site.

5.9. Surface Ocean Productivity Variability in SEAS for the Last 43 kyrs

Past changes in the productivity during the last glacial-interglacial transition and Holocene have been reconstructed from different parts of the Arabian Sea by several workers (Naidu and Malmgren, 1996; Agnihotri et al., 2003; Gupta et al., 2003; Tiwari et al., 2010; Singh et al., 2011; Saraswat et al., 2016; Naik et al., 2017; Nagoji & Tiwari, 2017). A majority of these inferences are based on changes in the relative abundance of the planktic foraminifera *G. bulloides*, which thrives in upwelling

influenced productive regions (Naidu and Malmgren, 1996). The possible post-depositional alteration of planktic foraminiferal assemblages, and thus the *G. bulloides* abundance, at the study location is unlikely because the core lies well above the foraminiferal lysocline (Cullen and Prell, 1984). Further, dissolution-susceptible planktic foraminiferal species are well preserved all along the western continental margin of India, suggesting negligible carbonate dissolution (Naidu et al., 1992). The *G. bulloides* abundance record of the present study shows low values during the glacial period and an increase during the deglaciation with a decline during the Holocene (Fig. 19a). However, during the Last Glacial Maxima and Henrich Events (H1 to H4), *G. bulloides* abundance shows low values suggesting decreased surface water productivity in the SEAS. Singh et al. (2006) from the core SK-17, off Goa, has also reported a decline in *G. bulloides* abundance during LGM. A major increase in *G. bulloides* abundance between 12-14.5 kyr BP suggests an increase in surface water productivity, similar to paleoproductivity changes estimated from other low and mid-latitude upwelling areas (Agnihotri et al., 2003). Although we see a decline in *G. bulloides* abundance starting from 11.5 to 8.5 kyr BP, the values are still higher compared to those seen after 7.5 kyr BP. This higher abundance of *G. bulloides* suggests comparatively higher productivity during the early Holocene, in SEAS. However, the abundance of *G. bulloides* uniformly decreases during the Holocene implying a gradual decrease in productivity, which is similar to that reported from the core ODP 723A, off Oman margin (Gupta et al., 2003), where proxy records including *G. bulloides* abundance suggest a progressive weakening of the SASM intensity also seen in salinity (Tiwari et al., 2015) and terrestrial input (Nagoji and Tiwari, 2017) reconstruction from the SEAS. A similar decline in *G. bulloides* abundance suggesting decreasing productivity during the Holocene period

has been also reported by Singh et al., (2006) from the core SK-17, off Goa, very close to our study location.

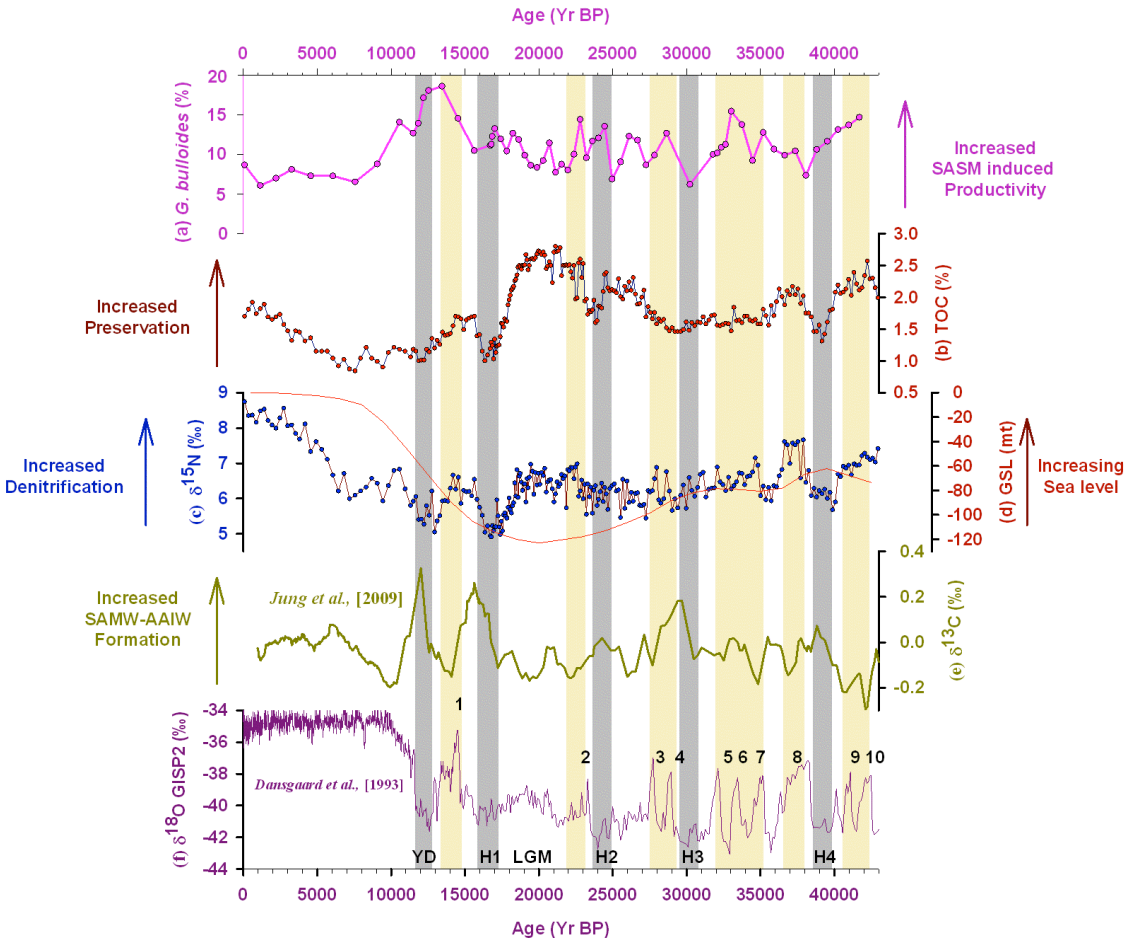

Figure 19. Comparison of geochemical proxies (panel a, b and c) of the present study with the GISP2 $\delta^{18}O$ record (panel f) (Dansgaard et al., 1993); $\delta^{13}C$ of benthic foraminifera record (panel e) shows millennial-scale changes in SAMW-AAIW formation rate (Jung et. al., 2009), and the global mean sea level variability is shown in panel 'd' (Siddal et al., 2003).

5.10. Decoupling of Surface Ocean Productivity and Denitrification in the SEAS

Using $\delta^{15}N$ of the SOM as a proxy for denitrification, studies have reported increase in denitrification intensity implying increased SASM intensity and productivity (e.g., Altabet et al., 1995, 1999, 2002; Ganeshram et al., 2000; Suthhof et al., 2001; Ivanochko et al., 2005; Reichart et al., 1998; Schulz et al., 1998). This increase in surface water productivity and associated oxygen demand for the degradation of

organic matter produced is therefore regarded as the main control on water column denitrification (Ganeshram et al., 2000; Ivanochko et al., 2005). However, high *G. bulloides* abundance of the present study, suggesting changes in the surface water productivity for the last 43 kyrs, is not always accompanied by a corresponding increase in $\delta^{15}N$ and TOC (Fig. 19c) especially during LGM and since early-Holocene in the SEAS. Naidu et al. (1992) and Calvert et al. (1995) from the western Arabian Sea inferred that TOC accumulation in the sediments could be used as an indicator of past productivity changes. However, in SEAS, decoupling between *G. bulloides* abundance and TOC as shown in the present study points towards factors other than productivity affecting TOC accumulation in sediments. Whereas, a similar trend observed between the $\delta^{15}N$ and the TOC suggests that accumulation of organic carbon in SEAS is mainly a response to better preservation under enhanced sub-oxic conditions in the OMZ rather than changes in primary productivity. Additional differences in productivity inferred from the *G. bulloides* abundance and TOC might also be related to the influence of sedimentation rate on TOC (Agnihotri et al., 2003). The TOC in a few cores collected from the eastern Arabian Sea did significantly increase during the LGM and was attributed to an increase in sedimentation rates leading to better TOC preservation during the Last Glacial Maxima (Agnihotri et al., 2003). Recently Nagoji and Tiwari (2017) has shown enhanced TOC values since mid-Holocene, which was attributed to increased preservation caused by enhanced reducing conditions in the SEAS, which is also observed by Naik et al., (2014) and Agnihotri et al., (2003). Overall, the Arabian Sea productivity is dominated by wind-driven upwelling of nutrient-rich subsurface waters in the southwest of the basin. However, strongest denitrification occurs in the northeastern Arabian Sea as shown by the nitrate deficit or N* minimum at 300 m depth (Naqvi, 1987, 1991) (Fig. 15c).

N* is calculated by using Redfield stoichiometry defined as $[NO_3^-]$ - 16* $[PO_4^{3-}]$ + 2.9 (Deutsch et al., 2001), quantifies excesses and deficits in NO_3^- relative to the globally derived $[NO_3^-]$ to $[PO_4^{3-}]$ relationship. These NO_3^- excesses and deficits indicate regions of fixed nitrogen input (e.g., N_2 fixation) and loss (e.g., denitrification). Negative values of N* are interpreted to show the net nitrogen loss whereas positive values show the net nitrogen fixation. Denitrification typically starts below a threshold value of ~5 μmol/kg O_2 (Codispoti et al., 2001). This condition is clearly met in the northeastern Arabian Sea, and correspondingly N* exceeds -12 μmol/kg at ~300 m depth (Fig. 15c). In the southwestern Arabian Sea, however, oxygen values never fall below 20 μmol/kg (Fig. 15b). Likewise, N* of -4 to -5 μmol/kg is observed at the same depth (Fig. 15c), which, however, cannot be explained solely by local denitrification, given a value of 50 μmol/kg O_2. Sarma (2002) proposed that combined circulation and productivity control perennial OMZ conditions in the northeastern Arabian Sea. Despite the strong variability in productivity, the thermocline waters of the Arabian Sea north of 12°N and east of 55°E develop an intense permanent OMZ throughout the year (Fig. 15), with peak oxygen depletion during the winter monsoon (Sarma, 2002; Pichevin et al., 2007). Even during the inter-monsoon, at low productivity and low organic carbon flux, the OMZ remains intense due to lateral inputs of water low in oxygen (Sarma, 2002). These features point to oxygen supply through oceanic ventilation as an additional control on denitrification. Model simulations indeed show that past changes in oxygen supply at intermediate depth by the AAIW can modulate denitrification in the OMZs such as the Arabian Sea (Schulte et al., 1999; Galbraith et al., 2004; Meissner et al., 2005; Schmittner et al., 2007). Given the regional decoupling between denitrification and productivity in the basin today, we propose to critically explore

the impact of ventilation on the intensity of the denitrification in the SEAS, through millennial-scale climate shifts and across the Holocene.

5.11. Regional Homogeneity in the $\delta^{15}N$ Variability

One crucial limitation in assigning clear causes to denitrification changes in the OMZs lies in the lack of definite proxies for either oxygen demand or its supply. It has been noted that denitrification is most intense in the northeastern Arabian Sea (Naqvi, 1987). By itself, this would suggest corresponding geographic gradients in the sediment $\delta^{15}N$ signature. The water column data, in contrast, indicate a regional homogenization of the $\delta^{15}N$ signal that reaches the euphotic zone (e.g. Altabet et al., 2002). Since the water column data may not represent long-term average conditions, a further test of the regional variability of the $\delta^{15}N$ signal is needed. In an attempt to compensate for this limitation, we compare our $\delta^{15}N$ record with other high-resolution sedimentary $\delta^{15}N$ record, from the western (core RC14 and RC 27-23) and the eastern (core MD04-2876) Arabian Sea covering the last 43 kyrs (Fig. 20) (Altabet et al., 2002; Reichart et al., 1998, Pichevin et al., 2007). This comparison shows a similar range (4- 9 ‰) and pattern as our $\delta^{15}N$ record, suggesting basin wide homogeneity in the $\delta^{15}N$ signals irrespective of regionally differing upwelling and productivity. This regional homogeneity in the $\delta^{15}N$ variations in the Arabian Sea brings out two important climate-driven biogeochemical aspects. The former suggests efficient horizontal mixing of thermocline water in the basin leading to the homogenisation of isotopic signals on glacial–interglacial timescale. The latter suggests that local decoupling of the productivity and denitrification occurred during the LGM and since the Holocene in the present study, probably due to effective ventilation of the thermocline in the SEAS.

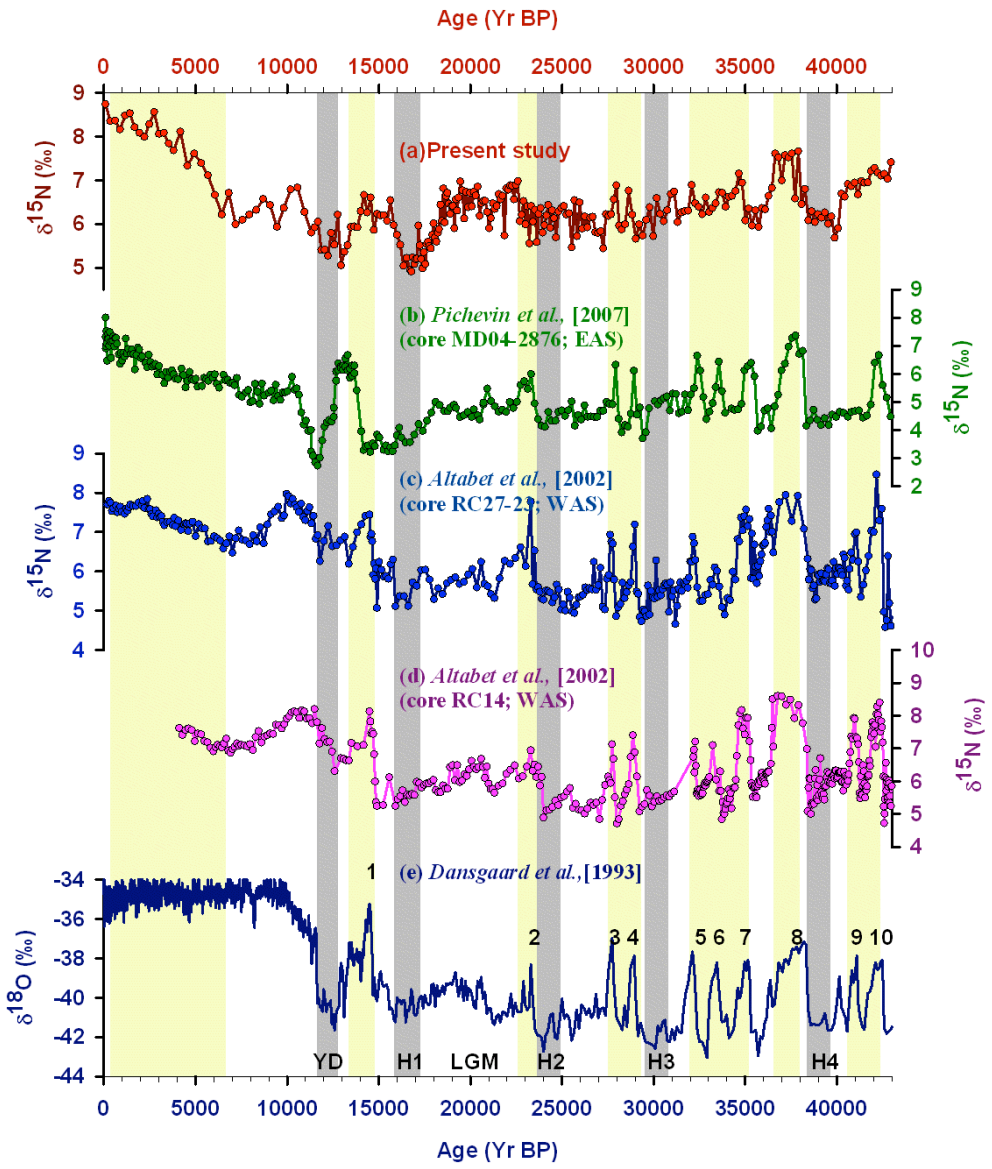

Figure 20. Regional comparison of $\delta^{15}N$ signal from the different parts of the Arabian Sea compared with $\delta^{18}O$ of GISP2 record (panel e). Panel (a) shows the $\delta^{15}N$ profile of the present study, panel (b) shows $\delta^{15}N$ profile from EAS; core MD04-2876, panel (c) shows $\delta^{15}N$ profile from WAS; core RC 27-23, and panel (d) shows $\delta^{15}N$ profile from WAS; core RC 14.

5.12. Ventilation Changes during the Last Glacial Period: Implications to Denitrification Intensity

Climatically driven increases in the supply of oxygen through enhanced ventilation

rates and cooling of the high-latitude surface ocean could contribute significantly to a higher subsurface oxygen during glacials and suppress suboxia and consequently reduce water column denitrification (Meissner et al., 2005). Recent observational and modeling studies from Indian and Southern Oceans have inferred that, higher oxygen was related to the increased production and northward spreading of intermediate waters (i.e. SAMW - AAIW) during North Atlantic Heinrich Events (e.g. Schulte et al., 1999; Pichevin et al., 2007; Schmittner et al., 2007). This phenomenon likely resulted from abrupt perturbations in North Atlantic Deep Water (NADW) formation generated by meltwater pulses over the North Atlantic (e.g. Vidal et al., 1997). The suppressed NADW formation most likely resulted in an increased formation of SAMW – AAIW to compensate for the changes in the meridional thermocline density gradient (Saenko et al., 2003). Therefore, to further investigate the influence of this southern sourced oxygen-rich intermediate depth water mass at our study region we compared our $\delta^{15}N$ record with the carbon isotopes of epibenthic foraminifera record of the core NIOP 905, off Somali coast (Fig. 19e) (Jung et al., 2009). $\delta^{13}C$ value of epibenthic foraminifera serves as a proxy for the ageing of the water mass along its flow path, i.e. the ventilation state of the ocean (Pahnke and Zahn, 2005). Although $\delta^{13}C$ -values of dissolved inorganic carbon (DIC) in the source areas of Glacial-AAIW have been modulated by the continuous addition of isotopically light organic carbon originating from remineralization of organic matter from the surface layers, the $\delta^{13}C$ - signature remains useful to identify water masses in the world ocean (Pahnke and Zahn, 2005). AAIW in the Indian and the Pacific Ocean, for example, has a high $\delta^{13}C$ -value of DIC in the modern ocean, (Charles and Fairbanks, 1992) and the $\delta^{13}C$ - value was probably also high in the past. Higher $\delta^{13}C$ value represents increased SAMW-AAIW formation. This comparison reveals

that the high/low peaks in $\delta^{15}N$ are concurrent with episodes of decreased/increased SAMW-AAIW formation. The Continuous Wavelet Transform (CWT) and the Squared Wavelet Coherence including the phase analysis was carried (Fig. 21) out to check whether the visually perceived coherence between the denitrification and the SAMW-AAIW formation is statistically significant (Torrence and Campo, 1998; Grinsted et al., 2004). The area between the thin black line and the time axis is the cone of influence where zero padding (to diminish wraparound effects) has reduced the variance. Figure 4a represents the wavelet spectrum for the $\delta^{15}N$ in the SEAS. The CWT spectra of the $\delta^{15}N$ show high power in the periodicities between 2000 and 4000 years. We find that the denitrification intensity is statistically significantly coherent (5% significance level) with SAMW-AAIW formation over the approximately 1000, 2000, 4000, and 8000 years periodicity band during the different parts of the time series as shown in Fig. 21c. The vector represents the phase difference; the left direction shows anti- phase, which confirms the visual observations. Our high-resolution $\delta^{15}N$ (Fig. 19b) record from the SEAS also correlates with that of the northern high latitude climate events identified in the GISP2 records (Fig. 19f). This is statistically compared by wavelet coherency analysis and phase analysis (Fig. 21b). We find that denitrification intensity and the GISP2 record is statistically significantly coherent (5% significance level) over approximately 1000, 2000, and 4000 years periodicity band. The phase difference is represented by the vector; the right direction shows in-phase, which confirms the visual observations. The decreased/increased conversions of SAMW-AAIW in the Southern Ocean during warm interstadials/cold stadials could have decreased/increased the oxygen inventory in the intermediate depth of the Arabian Sea (Schulte et al., 1999; Schmittner et al., 2007; Jung et al., 2009; Naidu et al.,

2014) resulting in higher/lower $\delta^{15}N$ values at our core location. Higher values observed in the $\delta^{15}N$ record during Last Glacial Maxima coincides with the major decline in the conversion of SAMW-AAIW in the Southern Ocean as evident from the $\delta^{13}C$ value of epibenthic foraminifera (Fig. 19e). Whereas the lowest $\delta^{15}N$ values observed during Heinrich Event 1 and during Younger Dryas suggest more northward expansion of this oxygen-rich water mass. Such a northward expansion of the SAMW-AAIW following perturbation of the thermohaline circulation (typical of Heinrich events) has been previously modeled and found to influence oxygen inventory at low latitudes (Schmittner et al., 2007) particularly in the Arabian Sea (Schulte et al., 1999).

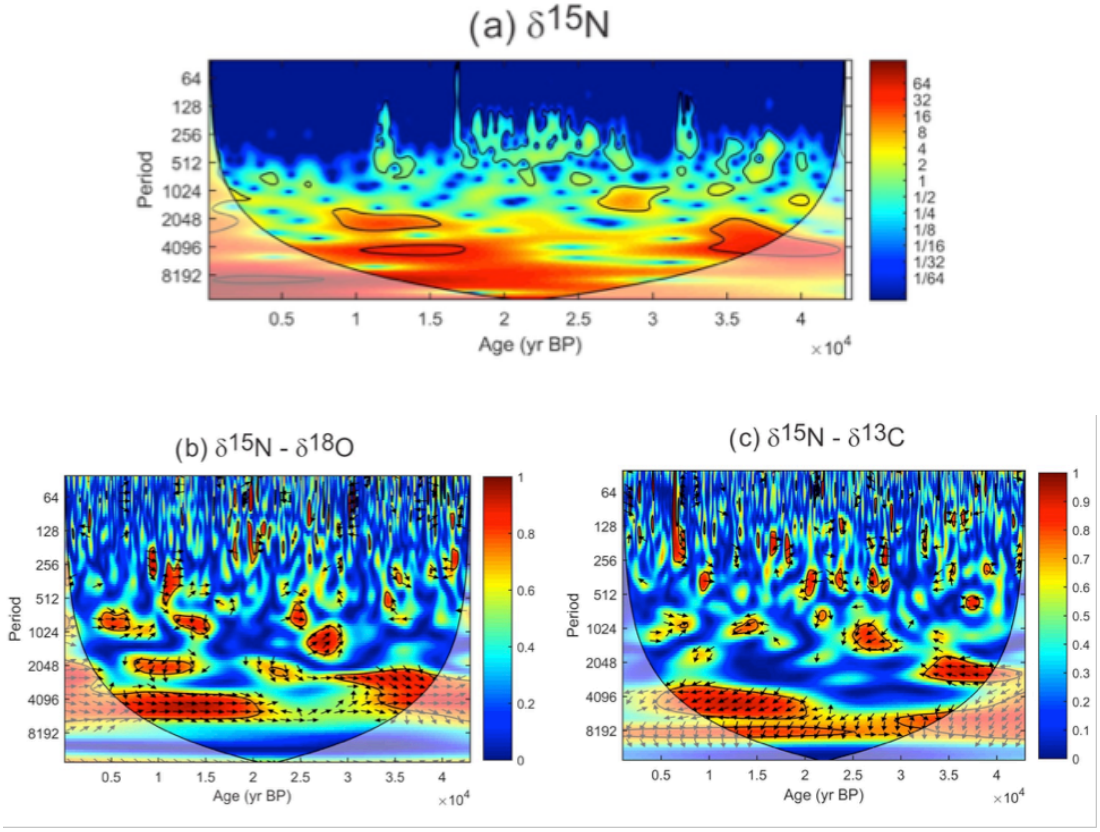

Figure 21. Spectral analysis including the Continuous Wavelet Transform (CWT) and the Squared Wavelet Coherence. Panels 'a' show the CWT power spectrum for the $\delta^{15}N$. Squared Wavelet Coherence between the $\delta^{15}N$ and $\delta^{18}O$ is shown in panel 'b', while between $\delta^{15}N$ and $\delta^{13}C$ is shown in panel 'c'. The 5% significance level against red noise is shown as a thick contour. Phase arrows pointing right means in-phase, left means anti-phase, down means $\delta^{15}N$ leading by 90°, and up means $\delta^{15}N$ lagging by 90°. The lighter shades depict the cone of influence.

5.13. Circulation Changes during the Holocene: Implications to Denitrification Intensity

During the early Holocene, we observe a decline in $\delta^{15}N$ values. This may be due to the increased inflow of low-density surface water having low $\delta^{15}N$ values from the Bay of Bengal (BOB) into the SEAS via the northeast monsoon current (Mahesh et al., 2014; Gaye et al., 2017). After precipitation declined and the sea level difference between the Bay of Bengal and the Arabian Sea dropped at about ~8 ka BP (Mahesh

et al., 2014; Gaye et al., 2017), the inflow of low density water to the eastern Arabian Sea decreased, which coincided with a rise in SEAS $\delta^{15}N$ values (Fig. 19c). Beyond the early Holocene (after ~8 kyr BP), the observed relation between the SAMW-AAIW flux and $\delta^{15}N$ weakens (Fig 19c and 19e). Today, the SAMW-AAIW spreads northward in the Indian Ocean up to 5°N where it feeds the IOCW (You, 1998). This meridional progression of oxygen-rich, southern water masses to the Arabian Sea is hampered owing to the low-salinity front created along the equator by the zonal Indonesian Intermediate Waters (< 500 m water depth) and the presence of very saline waters from the marginal seas north of the equator (Pichevin et al., 2007). During MIS 2 and probably MIS 3, however, both the inflows from the marginal seas and the Indonesian Intermediate Waters were strongly reduced owing to lower sea level (Kuhnt et al., 2004), favoring northward circulation of southern waters in the Arabian Sea and hence a greater contribution of the SAMW-AAIW to the Arabian Sea oxygen inventory. During the last glacial period when sea level was 120 m lower compared to today (Fig. 19d), the Red Sea outflow (separated from the open ocean by shallow and narrow sills of 137 m) and Persian Gulf outflow (separated from the open ocean by shallow and narrow sills of <100 m) was reduced by 85% (Rohling and Zachariasse, 1996). It reached to 50% at 10 kyr and increased progressively thereafter with sea level rise until it reached its present state at around 6 kyr BP (Fig. 19d) (Rohling and Zachariasse, 1996). Therefore, the enhanced $\delta^{15}N$ values observed in the present study since 8 kyr BP invoke a causal role for ventilation changes caused by the Red Sea and the Persian Gulf outflows as a result of a rise in global sea level. So, we propose that with the rise in the sea level, the oxygen-poor Red Sea and Persian Gulf Waters further prevented the reduced southern source water (SAMW-AAIW) from ventilating the Arabian Sea. It enabled a continuous build up of oxygen

deficiency and intensification of OMZ/denitrification in the intermediate depth of SEAS. It also implies that the denitrification increase during the Holocene, which is often interpreted as strengthening SASM, is in fact because of enhanced inflow of oxygen- poor water at intermediate depth. Thus, the above discussion shows that the denitrification reflects SASM induced productivity during the last glacial period and deglaciation but responds differently once the sea level rise is high enough to influence the intermediate depth circulation. During the Holocene, the denitrification does not reflect SASM induced productivity.

5.14. Conclusion

This study demonstrates that both the ventilation of the Sub Antarctic Mode Water - Antarctic Intermediate Water into the Southeastern Arabian Sea (SEAS) and the South Asian Summer Monsoon (SASM) induced productivity played a crucial role in modulating denitrification intensity. But importantly, during the Holocene and the LGM, denitrification increased despite reduced monsoon-induced productivity. During LGM, reduced ventilation of the intermediate waters of the SEAS due to the weakened thermohaline circulation resulted in the divergent response of the denitrification. During the Holocene, the decoupling between the denitrification and productivity is caused by the enhanced inflow of oxygen-depleted Red Sea Water and Persian Gulf Water into the intermediate depths of the SEAS due to the rising sea level. The increasing denitrification during the Holocene does not reflect strengthening SASM. The important role of oceanic oxygen supply implied by this study highlights how quickly global oceanic circulation can adjust to millennial-scale abrupt climate changes.

Chapter 6

Denitrification Variability in the Arabian Sea: Implications to Late Quaternary Nitrogen and Carbon Cycles

6.1. Introduction

Oxygen Minima Zones (OMZs) influence climate via regulating atmospheric nitrous oxide (N_2O) concentration (Agnihotri et al., 2006) or nitrogen inventory to modulate CO_2 sequestration through biological pump (Altabet, 2006). In the modern oceans, there exists three regions where perennial OMZs exist and pelagic denitrification takes place: Eastern Tropical South Pacific (ETSP), Eastern Tropical North Pacific (ETNP), and the Arabian Sea. Though OMZs occupy only ~4% of ocean volume, the denitrification process therein contributes remarkably to the nitrate loss, leaving excess phosphorous in the remaining water mass to stimulate nitrogen fixation while entering the euphotic zone (Morrison et al., 1998; Deutsch et al., 2007) and thus controlling the budget of bioavailable nitrogen in ocean. Denitrification occurs when nitrate is used as an oxidizing agent (electron acceptor) for respiration of the organic matter when dissolved oxygen concentration is lower than 0.2 ml/l (Naqvi et al., 2000). Denitrification leaves residual nitrate enriched in $^{15}NO_3^-$ that re-enters the euphotic zone resulting in high $\delta^{15}N$ values of the particulate organic matter (Sigman et al., 2001), whereas N_2 fixation introduces new bioavailable nitrogen with low $\delta^{15}N$ values (Capone et al., 1998). During denitrification, N_2O and N_2 are released into the atmosphere as the end product (Codispoti, 1995; Altabet, 2007). This process has the potential to affect the climate in an indirect fashion, since it partially modulates the total amount of nitrogen available for phytoplankton growth and hence the efficiency of the oceanic carbon sequestration, and directly by the production of the greenhouse gas N_2O. The estimated global rates of nitrogen removal were in the order of 100 $TgNyr^{-1}$ (Codispoti and Christensen, 1985), with a mean residence time for NO_3^- in the ocean of about 10^4 years (Liu, 1979). This timescale suggested a close link between changes in denitrification rates and the glacial-interglacial variations in

atmospheric CO_2 (McElroy, 1983). However, the present understanding points to a much more dynamic oceanic nitrogen cycle, with modern denitrification rates estimated in the order of 200–400 $TgNyr^{-1}$ and a mean NO_3^- residence time in the order of only 1500 - 3000 years (Codispoti, 1995; Codispoti et al., 2001; Brandes and Devol, 2002). Therefore, millennial-scale variations in the intensity of the denitrification in the OMZs during the last ice age, like those recorded in the nitrogen isotopic composition in the sediment's organic matter of the Arabian Sea (Suthhof et al., 2001; Altabet et al., 2002) and in the Pacific Ocean (Behl and Kennett, 1996; Emmer and Thunell, 2000; Thunell and Kepple, 2004), become of interest for climate studies, since they could lead to significant changes in the total amount of reactive nitrogen in the ocean, with potential consequences for the sequestration of CO_2 in the atmosphere (Altabet et al., 2002).

The Arabian Sea is one of the three largest OMZs in the world ocean with distinctive monsoon driven upwelling which accounts for at least one-third of the loss of marine fixed nitrogen (Codispoti and Christensen, 1985). The OMZ in the Arabian Sea occurs between 200 to 1000 m water depth (Codispoti 1995; Ganeshram et al., 2000). $\delta^{15}N$ signatures of marine sediments potentially provide the information about the biological processes in water columns, such as denitrification (Altabet et al., 1995; Ganeshram et al., 1995, 2000), nitrogen fixation (Haug et al., 1998), and the degree of nitrate utilization by phytoplankton (Altabet and Francois, 1994; Holmes et al., 1997; Robinson et al., 2004). In general, the average $\delta^{15}N$ value of global deep water is ~4.8 ‰ and increases with the degree of denitrification (Sigman et al., 2000). Earlier studies reported that, on an average, $\delta^{15}N$ value of sediment organic matter are

more than ~6 ‰ in the regions where denitrification occurs (Gaye-Haake, 2005; Tripathi et al., 2017; Kim et al., 2018).

Previous studies from the Arabian Sea based on sedimentary $\delta^{15}N$ measurements on various sediment cores and surface sediments revealed the following facts: (a) Complete utilization of near-surface NO_3^-, resulting in small isotopic fractionation between exported sinking particles and $\delta^{15}N$ of NO_3^- supplied to the euphotic zone (Altabet, 1988; Thunell et al., 2004); (b) monsoon wind-induced surface water productivity and related oxygen demand for degradation of sedimentary organic matter as one of the main governor of water column denitrification in the past (Ganeshram et al., 2000; Ivanochko et al., 2005); (c) Antarctic intermediate waters (AAIWs) can modulate the denitrification intensity by oxygen supply at intermediate depth in the northern Arabian Sea (Schulte et al., 1999; Schmittner et al., 2007; Pichevin et al., 2007). (d) $\delta^{15}N$ values of the sedimentary organic matter ($\delta^{15}N_{SOM}$) mainly reflects the relative intensity of water column denitrification (Altabet et al., 1995, 1999; Galbraith et al., 2013). Glacial-interglacial changes in denitrification in the Arabian Sea over the last 50 kyr are remarkably similar to ETNP and ETSP except during the Holocene where Arabian Sea-denitrification increases in contrast to the other regions. To understand the peculiar pattern of $\delta^{15}N_{SOM}$ variability in the Arabian Sea, detailed comparison between various records from different regions of the Arabian Sea needs to be carried out. But such a comparison is marred by the differing sedimentation rate and sampling resolution of different records. To overcome this, in the present study, we normalize and compare 61 sedimentary $\delta^{15}N$ records from different locations of the Arabian Sea (western, northern, eastern, and southeastern) along with our new $\delta^{15}N$ record from near the southern tip of India and

from ETNP and ETSP. The main objective of the present study is to investigate the reasons for the geographic differences in $\delta^{15}N_{SOM}$ values in the Arabian Sea, ETNP, and ETSP during different climatic periods to better understand the contrasting trend. Further, we try to assess the hypothesis of a global denitrification forcing on nitrogen and carbon cycle, and subsequently on global climate change on millennial timescale.

6.2. Present-day climate and surface hydrography

Seasonally reversing winds control the surface and near surface oceanographic conditions in the Arabian Sea. During the southwest monsoon, warm, moist air prevails, and a strong southwesterly wind jet runs diagonally across the Arabian Sea (Schott and McCreary, 2001). This wind forcing contributes to the development of a clockwise upper ocean circulation pattern in the Arabian Sea during summer and reverses to an anti-clockwise pattern during winter (Schott and McCreary, 2001). On the western side of the Arabian Sea, strong upwelling cells develop along the Somalian and Arabian coasts during the summer monsoon, when the winds blow from the southwest, parallel to the coast, resulting in a massive Ekman pumping. On the eastern side of the Arabian Sea off the Indian margin, prevailing winds blow from the west during the summer season. The summer productivity increase along the western coast of India is associated with a complex interplay of lateral advection, mixed-layer deepening and upwelling (i.e. Sharma, 1978; Shetye et al., 1990). By contrast, during the winter monsoon (December to March) winds from the Northeast evaporate and cool surface waters causing densification and convection, which deepens the mixed-layer from ~25 m during the summer monsoon to ~150 m depth during the winter monsoon. Such mixing leads to input of nutrients to the surface in the Northern basin (e.g. Madhupratap et al., 1996) generating a second productivity

maximum. Despite the high summer productivity peak, the particulate organic carbon flux seems to be equally high during summer and winter in the northern basin (Schulz et al., 2002). Thus, the monsoon-driven vertical mixing, coastal and open ocean upwelling shows an important basin-wide spatio-temporal variability resulting in a large variety of phytoplankton blooms (Levy et al., 2007). The circulation at the tip of India is affected by the westward flowing fresh water current known as North Equatorial Current (NEC) from the Bay of Bengal (e.g., Durand et al., 2007). During the boreal summer, in response to the monsoon wind reversal, the flow of the NEC reverses and combines with a weakened Equatorial Counter Current to form the South-West Monsoon Current. At the southern tip of India, however, the summer increase in productivity is chiefly associated with the development of a seasonal upwelling (Levy et al., 2007). It weakens during the winter season, when the winds reverse direction.

6.3. Thermocline circulation and Lateral ventilation within the Arabian Sea

The thermocline water of the Arabian Sea has three sources: (i) the intimately linked Subantarctic Mode and Antarctic Intermediate Waters (SAMW– AAIW), (ii) the Indonesian Intermediate Water (IIW) from the Indonesian Throughflow, and (iii) combined Persian Gulf and Red Seawaters (PGW–RSW). SAMW refer to the thick mixed-layers found directly north of the Subantarctic Front (McCartney, 1982). SAMW–AAIW roughly follow two pathways, an inner (western) branch within the subtropical gyre, and an outer (eastern) branch close to the West coast of Australia (You, 1998). North of the South Equatorial Current SAMW–AAIW are mixed with the frontal low-salinity tongue of the IIW at 300 m depth. Although more distant, the outer branch of SAMW–AAIW has an important influence on thermocline ventilation

of the Indian Ocean. Based on Chlorofluorocarbon (CFC) tracer distributions, Fine et al. (2008) recently concluded that the southeastern Indian Ocean represents the most likely ventilation source for the Arabian Sea south of 12°N. Not surprisingly, these data support the general idea that southern sourced intermediate waters effectively ventilate the thermocline Arabian Sea (Swallow, 1984; Olson et al., 1993; You, 1998). Low-latitude IIW and PGW–RSW indeed seem to represent minor ventilation sources (Swallow, 1984; You, 1998; Fine et al., 2008). However, the fact that upper thermocline waters at 12°N had CFC ages < 40 years (Fine et al., 2008) shows that the Arabian Sea must be ventilated very rapidly. SAMW–AAIW can be traced by its relatively high oxygen and low salinity. This is fully in agreement with You, (1998) who traced AAIW up to 5°N along the western boundary of the Indian Ocean. A mixture of SAMW–AAIW and IIW enters the southwestern Arabian Sea during the summer monsoon along the thermocline part of the Somali Current as Indian Ocean Central Waters (IOCW), whereby water masses drift towards the northeast. While the highly saline and oxygen poor PGW and RSW contribute to local intermediate water formation, their combined volume is one order of magnitude lower than the southern source (Swallow, 1984).

Naqvi, (1987), You, (1998) and Sarma, (2002) have suggested an equatorward transfer of thermocline water in the Arabian Sea, during the winter monsoon. Sarma, (2002) proposed that combined circulation (weak oxygen supply) and productivity (elevated oxygen demand) control perennial OMZ conditions in the northeastern Arabian Sea. Despite the strong variability in productivity the thermocline waters of the Arabian Sea north of 12°N and east of 55°E develop an intense permanent OMZ throughout the year (Sarma, 2002), with peak oxygen depletion during the winter

monsoon (Sarma, 2002; Pichevin et al., 2007). Even during the inter-monsoon, at low productivity and low organic carbon flux, the OMZ remains intense due to lateral inputs of waters low in oxygen (Sarma, 2002). In summary, these features clearly highlight the basin heterogeneity and demonstrate that southern oxygen supply and lateral mixing within the Arabian Sea are important factors which control thermocline (oxygen) as pointed out by Naqvi, (1987) and Olson et. al., (1993).

6.4. Sediment core details

A sediment gravity core, SK274/1G (8°N and 75.59°E) (Fig. 22), was collected at water depths of 1491 m located at the southern tip of India during the 274th cruise of ORV Sagar Kanya. Although the core MD77-191 locates further south in the Arabian Sea (Bassinot et al., 2011), SK274/1G is, so far, the southernmost core with reference to $\delta^{15}N$ record spanning last 43 kyr BP, at high resolution. The 1.50 m long core was sub- sampled at every 1 cm interval. All sub-samples were freeze-dried and ground into powder in an agate mortar with pestle. The chronology for core was based on four Accelerator Mass Spectrometer radiocarbon dates on mixed planktic foraminifera (*Globigerinoides ruber, Globigerinoides sacculifer*; size range: 250–420 μm) measured at the NSF, AMS Facility at University of Arizona. The ^{14}C dates were calibrated by using the marine dataset (Marine 09), (Reimer et al., 2009) and Calib 6.0 version (Stuiver and Reimer, 1993). We used the global reservoir age correction of 400 years as Butzin et al. (2005) yield the reservoir age based on a three-dimensional global ocean circulation model for the core location as 395 years, which is very near to the global reservoir age. This is an estimate of the modern ocean radiocarbon reservoir ages based on the physics of the ocean circulation (Cao et al., 2007) compared with previous estimates based on sparse data points from far-off

regions (Dutta et al., 2001; Southon et al., 2002). The core spans the last ~ 43 kyr BP and the core top is 5.5 kyr BP.

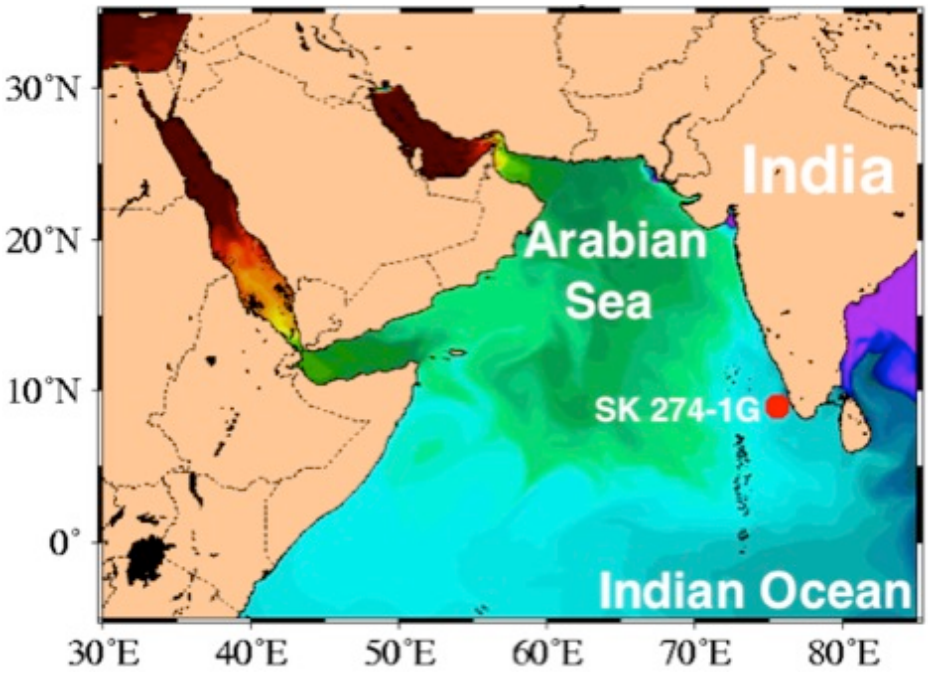

Figure 22. Map showing location of the core SK 274-1G shown by red circle

6.5. Elemental and Isotopic analysis of organic Carbon and total Nitrogen

Bulk sedimentary nitrogen content and $\delta^{15}N$ analyses were carried out using elemental analyzer connected to an isotope ratio mass spectrometer (EA-IRMS). Sediments for total organic carbon (TOC) analyses were acid-treated with 1N HCl for 16 h, and then centrifuged to remove carbonate. The acid-treated sediments were further dried at 60°C for TOC content and $\delta^{13}C_{som}$. Carbon and nitrogen isotopic data are presented in δ notation with respect to VPDB (Vienna Pee Dee Belemnite) and atmospheric nitrogen, respectively. IAEA cellulose standard (IAEA-CH-3), which has a certified isotopic composition ($\delta^{13}C$ = −24.74 ‰ vs. VPDB) for carbon and IAEA ammonium sulphate standards (IAEA N1) of certified isotopic composition ($\delta^{15}N$ = 0.4 ‰) for nitrogen were used to calibrate to the VPDB and atmospheric N_2

scale, respectively. The reproducibility of carbon and nitrogen isotopic measurements is better than 0.02 ‰ for carbon and 0.08 ‰ for nitrogen. The precisions of nitrogen and carbon content measurements were better than 0.2 and 0.3 %, respectively.

6.6. Normaliztion of $\delta^{15}N$ values

The normalized averaged $\delta^{15}N$ values were calculated for the SEAS, along with northern, western, eastern and the Oman and Somali upwelling systems for comparison. The data from the core SK274-1G is presented here for the first time and other $\delta^{15}N$ data is taken from the previous studies (Table 4). The data were combined in time slices of 1000 years for each individual sediment core and were averaged. Then, the $\delta^{15}N$ value of the 1000-year block for each individual sediment core was normalized by subtracting it from the average $\delta^{15}N$ value of the core. Finally, all the normalized $\delta^{15}N$ values of each 1000-year block for all the sediment cores in an area were averaged and presented as normalized $\delta^{15}N$ values for a that particular 1000-year block in that area. Each area composites are based on seven to twenty six different core records (details in Table 4).

Region	Core	Latitude	Longitude	Depth (m)	Reference
NAS	SO130-275KL	24.82N	65.91E	782	Böll et al. 2014
	NAST	19.99N	65.68E	3170	Möbius et al. 2011
	MD04-2879	22.54N	64.04E	920	Jaeschke et al. 2009
	MD 04-2876	24.84N	64.00E	828	Pichevin et al. 2007
	SO90-111KL	23.07N	66.48E	775	Suthhof et al. 2002
	NIOP 464	22.25N	63.58E	1470	Reichart et al. 1998
	NIOP455	23.55N	65.95E	1002	Reichart et al. 1998
EAS	EAST	15.59N	68.58E	3820	Möbius et al. 2011
	SK117/GC-08	15.48N	71.00E	2500	Banakar et al. 2010
	SK126-39	12.63N	73.33E	1940	Kessarkar et al. 2010
	CR-2	14.90N	74.00E	45	Agniihotri et al., 2008
	MD76-131	15.53N	72.56E	1230	Ganeshram et al. 2000
	SS3268G5	12.5N	74.20E	600	Agnihotri et al., 2003
	SK 274-4G	13.59N	72.E	1290	Unpublished data
	SK 274-1G	8.0N	75.59E	1491	Present Study
WAS	NIOP-905P	10.76N	51.95E	1586	Ivanchko et al. 2005
	SS4018G	13.21N	53.25E	2830	Tiwari et al. 2010
	M74-SL163	21.93N	59.80E	650	Gaye et al., 2017
	ODP724C	18.28N	57.46E	600	Möbius et al. 2011
	RC27-14	18.25N	57.65E	596	Altabet et al. 2002

	RC27-23	17.99N	57.59E	820	Altabet et al. 2002
	MC2-GOA6	14.98N	53.76E	2416	Isaji et al., 2015
	MC2/GOA4	12.82N	46.92N	1474	Isaji et al., 2015
	ODP 722B	16.61N	59.8E	2028	Möbius et al. 2011
	SO42-74KL	14.32N	57.34E	3212	Suthhof et al. 2002
ETNP	MR06-04 PC24A	60.26N	179.4E	852	Kim et al. (2011)
	St-11	57.04N	176.9E	3650	Nakatsuka et al. (1995)
	DR-16	54.50N	176.0E	3750	Nakatsuka et al. (1995)
	ODP 887	54.37N	148.4E	3647	Galbraith et al. (2004)
	IODP U1340	53.40N	179.5E	1324	Schlung et al. (2012)
	HLY 0202 JPC17	53.93N	178.6E	2209	Brunelle et al. (2007)
	DR-13	53.16N	177.3E	3930	Nakatsuka et al. (1995)
	ODP 882	50.35N	167.5E	3244	Galbraith et al. (2008)
	MD 02-2496	48.97N	127.0E	1243	Chang et al. (2008)
	JT96-09	48.90N	126.8E	920	McKay et al. (2004)
	ODP 1033	48.59N	123.5E	345	Calvert et al. (2001)
	W8709-8 PC	42.26N	127.6E	3111	Kienast et al. (2002)
	W8709-8 TC	42.26N	127.6E	3111	Kienast et al. (2002)
	W8709-13 PC	42.12N	125.7E	2712	Kienast et al. (2002)
	ODP 1019	41.68N	124.9E	977	Ivanochko et al., (2004)
	ODP 1017	34.53N	121.2E	955	Hendy et al. (2004)
	ODP 893	34.28N	120.0E	576.5	Emmer et al., (2000)
	ODP 1012	32.28N	118.4E	1772	Liu et al. (2008)
	NH15P	22.68N	106.4E	420	Ganeshram et al. (2000)
	NH22P	22.518	106.5E	2025	Ganeshram et al. (1995)
	MD 02-2519	22.51N	106.6E	955	Arellano-Torres (2010)
	NH8P	22.38N	107.0E	1018	Ganeshram et al. (1995)
	ME0005A-11PC	15.71N	95.29E	574	Hendy et al., (2006)
	MD 02-2520	15.66N	95.30E	719	Pichevin et al. (2010)
	ME0005A-03JC	15.65N	95.28E	740	Thunell et al., (2004)
	MD 02-2524	12.00N	87.91E	863	Pichevin et al. (2010)
ETSP	ODP 1228	11.06S	78.07E	273	Agnihotri et al. (2006)
	W7706-40	11.25S	77.96E	186	Higginson et al., (2004)
	W7706-41	11.35S	78.11E	410	Higginson et al., (2004)
	W7706-37	13.63S	76.85E	370	Higginson et al., (2004)
	CD 38-02	14.93S	77.06E	2525	Ganeshram et al. (2000)
	MW8708-PC2	15.10S	75.70E	270	Chazen et al. (2009)
	GeoB 7139	30.20S	71.98E	3269	De Pol-Holz et al. (2007)
	ODP 1234	36.21S	73.68E	1015	Robinson et al. (2007)
	ODP 1233	41.00S	74.45E	838	Martinez et al. (2006)
	E11-2	56.04S	115.0E	3094	Robinson et al. (2005)

Table 4: List of 61 $\delta^{15}N$ records from the Arabian Sea, ETNP, and ETSP used in this study.

6.7. Downcore Variability in Nitrogen and carbon contents and their isotopes

Temporal variations of geochemical proxies in the core SK274/1G spanning the last ~43 kyrs are shown in Fig. 23. The values of $\delta^{15}N$ bulk ranged from minimum value of 4.30 ‰ near ~31 kyr BP to 7.55 ‰ near ~9 kyr BP, with significantly lower values seen during the MIS 2 and highest during MIS 1 period (Fig. 23c). The record shows substantial changes throughout MIS 2 to 3 and a sharp transition from low to high

values at the early stages of the deglaciation (Fig. 23c). During MIS 3, the $\delta^{15}N$ values increased rapidly since ~ 43 kyr BP, with a peak at ~ 41 kyr BP, followed by gradual decline till ~ 38 kyr BP. Slight increasing trend in $\delta^{15}N$ values is seen between 38 to 32 kyr BP. Another gradual decline in $\delta^{15}N$ values is seen after 32 kyr BP showing a lowest value of 4.30 ‰ at ~ 30 kyr BP. During MIS 2, from ~ 29 kyr BP till 20 kyr BP, there was not much change in $\delta^{15}N$ values, the values remains very low ranging between 4.30 to 5.32 ‰. From 20 to 16 kyr BP we see slightly higher values similar to the time period between 38 to 32 kyr BP. The $\delta^{15}N$ values increased rapidly after 16 kyr BP. During MIS 1 $\delta^{15}N$ value shows an increasing trend with a peak at 9 kyr BP, followed by a slight decline thereafter. Bulk nitrogen content (TN), TOC content and atomic C/N ranged from 0.13 to 0.31 % (Fig. 23a), 0.14 to 6.49 % (Fig. 23b), and 1.15 to 33.27 (Fig. 23d), respectively. All three showed similar trends over the last 43 kyrs BP with maximum concentration seen during MIS 2 and lowest during MIS 1.

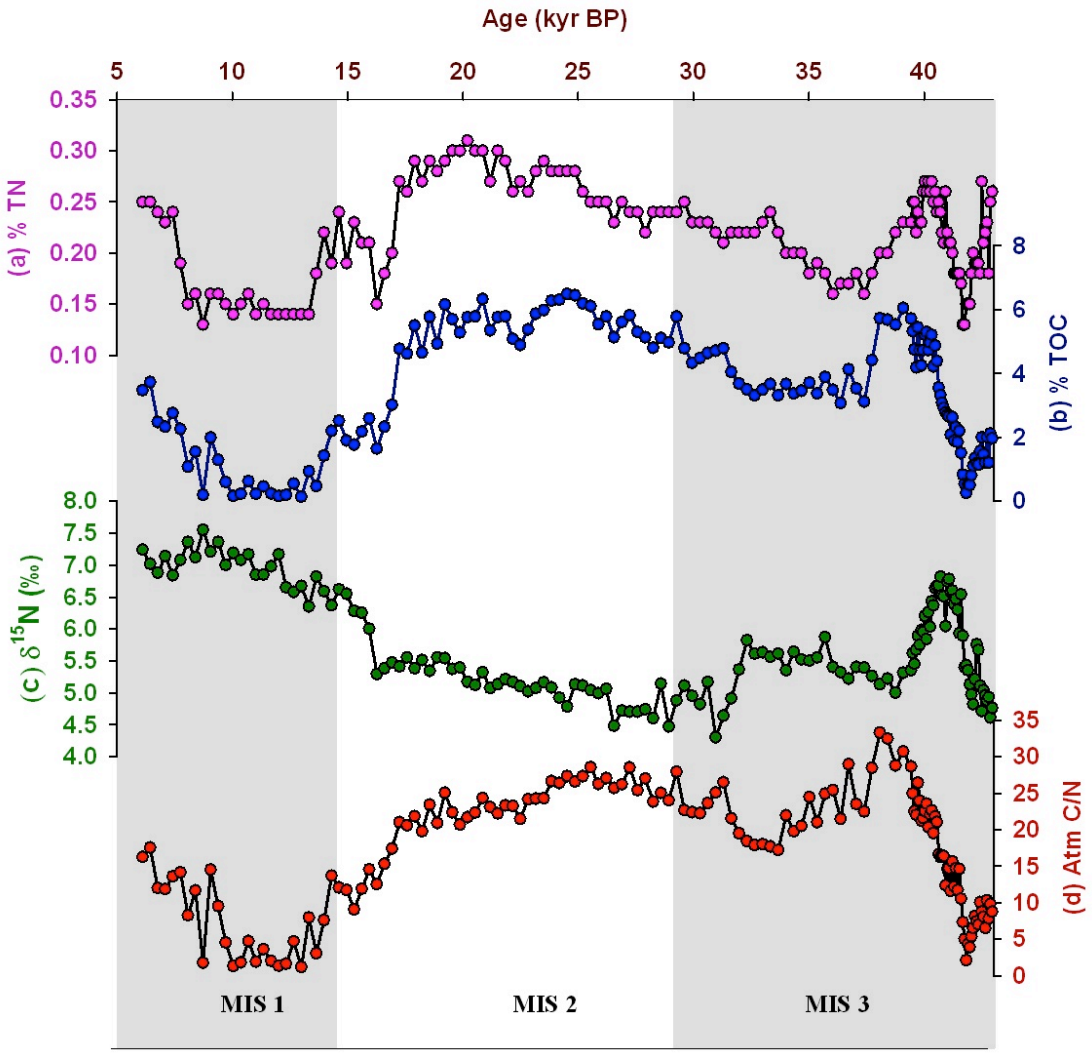

Figure 23. Downcore variation of geochemical proxies: (a) TN (%), (b) TOC (%), (c) $\delta^{15}N$, and (d) atomic C/N profile.

6.8. No alteration of nitrogen isotope composition of the sediments at core site

Before the interpretation of the past denitrification variability using the sedimentary $\delta^{15}N$ record an examination of the potential factors affecting the nitrogen isotope composition of the sediments is required. Among them are: the contributions of isotopically lighter terrestrial borne organic (Peters et al., 1978; Sweeney and Kaplan, 1980) and inorganic nitrogen (Schubert and Calvert, 2001), changes in the degree of

nitrate utilization at the surface by phytoplankton (Altabet and Francois, 1994), isotopic alteration during the particle settling to the ocean floor and during early diagenesis (Haake et al., 2005), and finally, changes in the isotopic composition of the upwelled nitrate. It has been shown than terrestrial organic material is characterized by relatively low $\delta^{15}N$ values (2-4 ‰) (Sweeney and Kaplan, 1980, Sigman et al., 2001) and therefore different admixtures of material could influence the downcore $\delta^{15}N$ record.

The elevated atomic C/N ratios during MIS 3 and MIS 2 would normally indicate presence of land plant derived organic matter. Therefore, the possibility of terrestrial organic matter contributing to total organic matter and affecting $\delta^{15}N$ values has been examined through the relationship between $\delta^{13}C_{org}$ and $\delta^{15}N$. If organic matter in sediment is an admixture of marine and terrigenous organic matter, then a good correlation is expected between $\delta^{13}C_{org}$ and $\delta^{15}N$ (Peters et al., 1978). Varying proportions of terrestrial organic matter in the mixture will produce a mixing line on the $\delta^{13}C_{org}$ – $\delta^{15}N$ plot, with lighter $\delta^{13}C_{org}$ corresponding to lighter $\delta^{15}N$ (Sweeney and Kaplan, 1980). We did not find any such relation; scatter found in the $\delta^{15}N$ versus $\delta^{13}C_{org}$ plot during MIS 3 ($r = -0.14$; Fig. 24c), MIS 2 ($r = -0.25$; Fig. 24b) and MIS 1 ($r = 0.28$; Fig. 24a) rule out the possibility that terrestrial organic matter may have had any influence on $\delta^{15}N$ values of the present study.

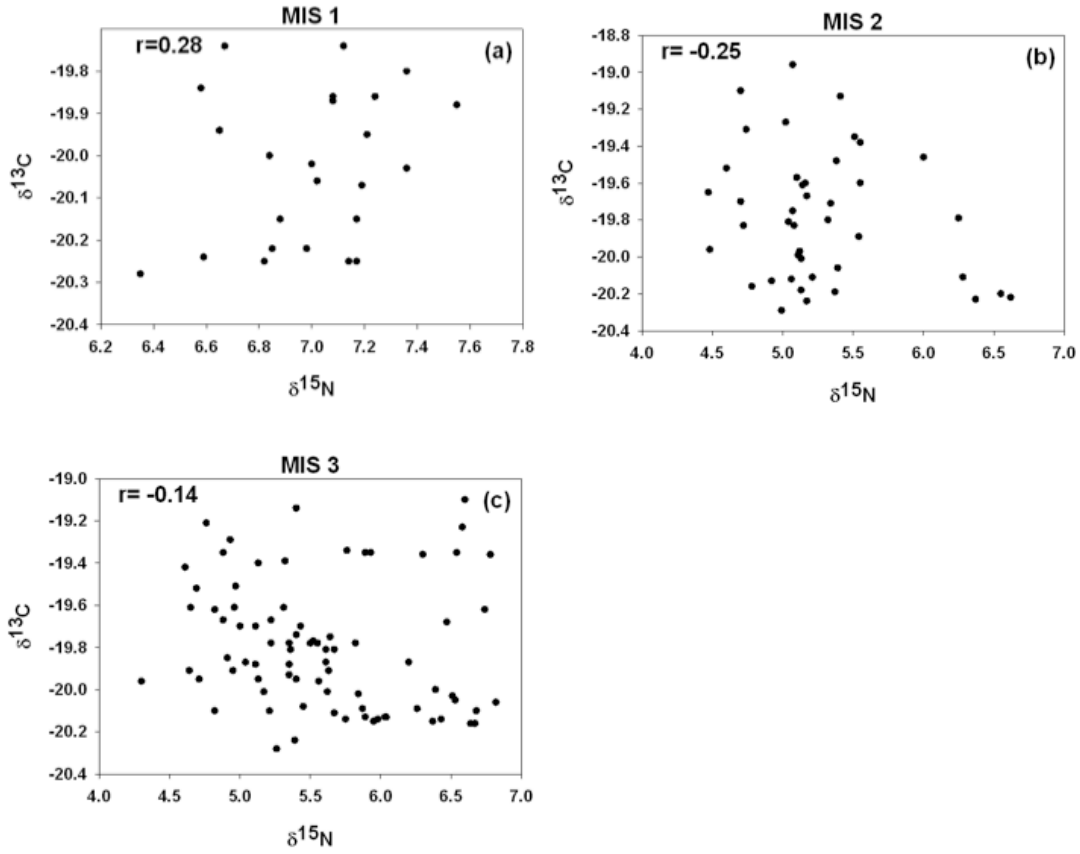

Figure 24. Correlation of $\delta^{13}C$ with $\delta^{15}N$ during MIS 1(a), MIS 2(b), and MIS 3(c). Correlation coefficient is given by r-value.

Further, early diagenetic effects if any, on the $\delta^{15}N$ signal of the present study were examined through relationships among $\delta^{15}N$ and TOC, TN and C/N ratios. Early digenetic degradation of organic matter would increase $\delta^{15}N$, resulting in an anti-covariance trend with TOC and TN contents and covariance with atomic C/N ratios. During MIS 3 and MIS 1 we obtained a very weak positive correlation between $\delta^{15}N$ and TOC (r= 0.06, MIS 3; Fig. 25f and r = 0.13, MIS 1; Fig. 25d) and TN (r= 0.05, MIS 3; Fig. 25i and r = 0.00, MIS 1; Fig. 25g) thereby suggesting no effect of early digenesis during these periods. During MIS 2 a good anti-correlation obtained between $\delta^{15}N$ versus TOC (r= -0.78; Fig. 25e) and TN (r= -0.32; Fig. 25h) suggests the possibility of early digenesis during this time. However, a good anti-correlation

obtained between $\delta^{15}N$ and atomic C/N (r= -0.89; Fig. 27k) suggests that digenesis may not be a significant factor during MIS 2 period, which is a contradictory to the above relation obtained between $\delta^{15}N$ versus TOC and TN during MIS 2. Nevertheless, various studies from different regions of the Arabian Sea have reported little to a significant amount of digenetic alteration of the near surface $\delta^{15}N$ (Altabet and Francois, 1994, Altabet et al., 2002; Gruber and Galloway, 2008). The amount of alteration was attributed to sinking rate of the particulate organic matter and its preservation (Altabet, 1988).

Another possible factor affecting sedimentary $\delta^{15}N$ variation involves changes in the degree of nitrate utilization by phytoplankton. Fractionation of nitrogen isotopes during the assimilative reduction of nitrate promotes the enrichment in ^{15}N of the unused pool. If the nitrate residence time in the euphotic zone is sufficiently long, the degree of consumption of nitrate will generate an isotopic signal that will be attained by the newly formed organic particles and that will eventually reach the sea floor. However, enhanced N fixation has been suggested as an alternative reason for the low $\delta^{15}N$ in glacial sediment intervals from the Arabian Sea (Altabet et al., 1995; Emeis et al., 1995; Suthhof et al., 2001), stimulated by the supply of excess phosphate and iron

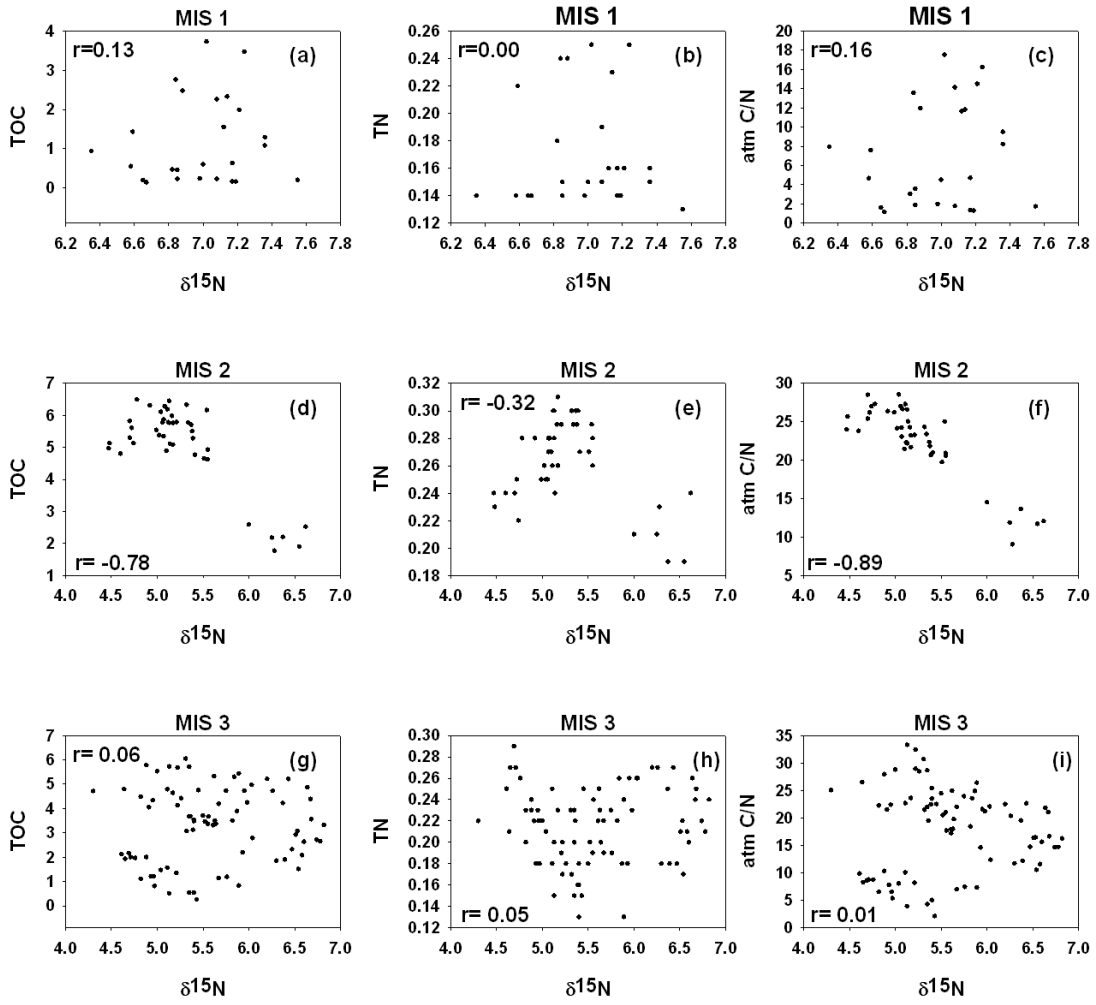

Figure 25. Correlation of TOC with $\delta^{15}N$, TN, and atomic C/N during MIS 1 (a, b, c), MIS 2 (d, e, f) and MIS 3 (g, h, i) respectively. Correlation coefficient is given by r value.

from the more arid continents via dust supply (Prins, 1999; Sirocko et al., 2000). In this case, N fixation in surface waters provided N with low $\delta^{15}N$ that may have masked the high $\delta^{15}N$ signal from denitrification. Nevertheless, the distribution pattern of N∗ (Fig. 26) illustrates that there must be an addition of $^{14}NO_3^-$ into the system to cancel out the isotopic enrichment caused by denitrification. Since the upwelling zones distribute at the very north and the west of the Arabian Sea and the upwelled water travels southward (or outward) on the surface, it is reasonable to see the phenomenon of denitrification induced N_2 fixation to compensate the nitrogen

deficiency. Consistent to this thought, Deutsch et al., (2007) discovered the spatial coupling between denitrification in eastern tropical Pacific (upstream) and N_2 fixation in western equatorial Pacific (downstream). Such a horizontal nitrogen addition process can also be seen clearly in our background information of N∗ (Fig. 26). However, the $\delta^{15}N$ trend observed in the present study is consistent with the synchronous early deglacial abrupt increase in sedimentary $\delta^{15}N$ records of the Arabian Sea, which suggests a common origin for the signal. Similarly, the lower glacial $\delta^{15}N$ values of our core should reflect reduced or even absent denitrification at the core site.

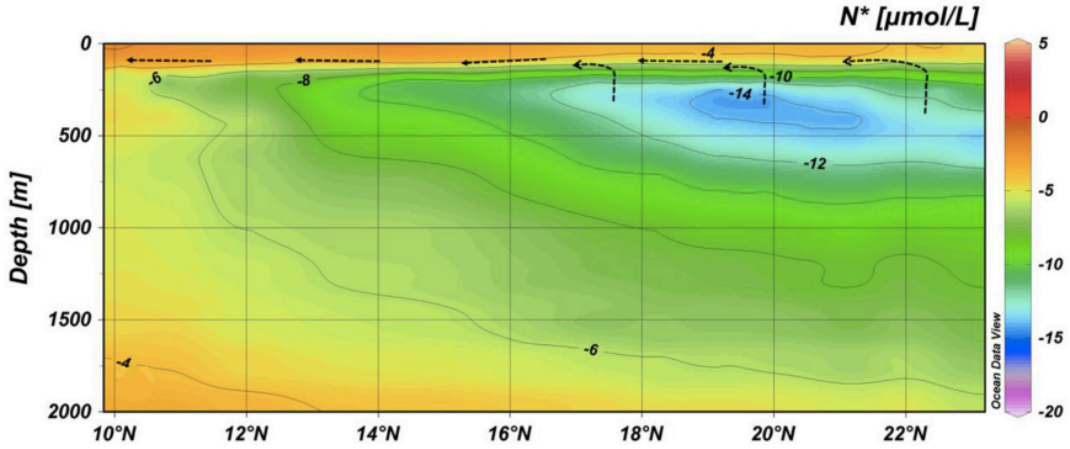

Figure 26. Nitrate deficit transact for the Arabian Sea from 23N to 8S at 0 to 2000 m water depth.

6.9. Normalization of $\delta^{15}N$ values for inter-comparison among different regions

At present, strong upwelling in the western Arabian Sea is responsible for transporting enriched nitrate from 250-300 m water depth into surface waters with $\delta^{15}N$ values up to >20 ‰ (Gaye et al., 2013; Yoshinari et al., 1997). Therefore, coastal sediments from the western Arabian Sea upwelling areas have $\delta^{15}N$ elevated to >10 ‰. The $\delta^{15}N$ values between 7 and 8 ‰, which are identical with the signal of

sub-thermocline nitrate (Gaye et al., 2013a; Gaye et al., 2013b), are obtained for sediments collected at water depths < 1000 m, where the effect of digenesis on the sedimentary $\delta^{15}N$ is small or negligible (Altabet and Francois, 1994; Gaye-Haake et al., 2005). The $\delta^{15}N$ values >11 ‰ in the central part of the basin are a result of lateral advection of ^{15}N enriched nitrate from upwelling areas (Naqvi et al., 2003), as well as early digenetic increase of $\delta^{15}N$ in deep sea sediments (Gaye-Haake et al., 2005; Möbius et al., 2011). Therefore, in order to understand the reasons for such differences in denitrification intensities and its variability in the Arabian Sea OMZ, we calculated the normalized averaged $\delta^{15}N$ values (please refer to Material and Methods for the normalization technique used). This normalization procedure yields an averaged-out, representative trend of denitrification for that particular region. It makes the relative changes in $\delta^{15}N$ comparable among different regions despite differences in the sedimentation rate and sampling resolution.

6.10. Spatial and temporal variability of denitrification in the Arabian Sea

6.10.1. During MIS 3 and MIS 2

The normalized $\delta^{15}N$ records of the last 50 kyrs (Fig. 27) suggest that the denitrification/$\delta^{15}N$ in the Arabian Sea rapidly oscillated between the high values during during MIS 3 and low values during the MIS 2. These changes are accompanied by parallel evidence of water column suboxia from trace metal concentrations (Kienast, et al., 2002; Ivanochko and Pedersen, 2004; Nameroff, et al., 2004; Hendy and Pedersen, 2005; McKay, et al., 2005), benthic foraminiferal assemblages (Ohkushi, et al., 2003) and sediment laminations (Ganeshram, et al., 2000; Suthhof, et al., 2001; van Geen, et al., 2003; Thunell and Kepple, 2004) confirming that intermediate water suboxia expanded during periods with high $\delta^{15}N$.

A possible explanation for the increased (decreased) denitrification during MIS 3 (MIS 2) was a reduced (enhanced) inflow of the Sub Antarctic Mode Water - Antarctic Intermediate Water (SAMW-AAIW) having high dissolved oxygen. The SAMW-AAIW is a dominant southern hemisphere water mass that spreads from its formation region lying north of the Antarctic Circumpolar Current to at least 20°S into all the oceans (Schmidtko and Johnson, 2012). This water mass enters the Arabian Sea as Indian Ocean Central Water (Rixen and Ittekkot, 2005, Pichevin et al., 2007), which could prograde deeper into the northern part of the basin as the lower sea level during MIS 2 severely reduced the inflow of PGW and RSW (Rixen and Ittekkot, 2005, Pichevin et al., 2007). Deep mixing probably added to ventilation of the upper OMZ during stadials (Reichart et al., 2004) so that denitrification was significant only when productivity enhanced and ventilation reduced during interstadial periods (Pichevin et al., 2007). This indicates that denitrification enhanced during the warm interstadial MIS 3 and reduced during the cold stadial MIS 2 in the Arabian Sea.

6.10.2. During MIS 1

The overall pattern of $\delta^{15}N$ variability during MIS 3 and MIS 2 remains almost similar across all the basins except during MIS 1 that differ across the basin. MIS 1 has a distinctively marked increase in denitrification throughout the Arabian Sea with a major strengthening of denitrification observed in its northern part (Fig 27). During the MIS 2, when sea level was 120 m lower compared to today, the Red Sea outflow and Persian Gulf outflow - more depleted in oxygen than the inflowing IOCW - was reduced by 85% (Rohling and Zachariasse, 1996). It reached to 50% at 10 kyr BP and increased progressively thereafter with sea level rise until it reached its present state at

around 6 kyr BP (Rohling and Zachariasse, 1996). Probably this change in the circulation must have obstructed the ingression of IOCW further into the northern and eastern part of the Arabian Sea enabling a continuous build-up of oxygen deficiency (Pichevin et al., 2007) during MIS 1 resulting in increased denitrification. The decline in denitrification in the western Arabian Sea between 9 to 5 kyr BP (Fig 27c) indicate that IOCW was able to ventilate the western part of the Arabian Sea. Benthic foraminifera indicate that oxygen concentrations were high and denitrification was low during this period despite enhanced productivity (Das et al., 2017). Evidently, the enhanced upwelling during the Holocene climatic optimum was fed by inflow of oxygen rich IOCW from the south, thereby ventilating the western Arabian Sea and thus compensated for the enhanced respiration (Rixen et al., 2014). Further, the lower $\delta^{15}N$ values observed during the late Holocene in the western Arabian Sea (Fig 27c) is probably attributed to the reduced advection of ^{15}N enriched nitrate from the adjoining upwelling areas. Pichevin et al. (2007) pointed out that circulation probably changed after the sea level in the Persian Gulf and Red Sea reached its present position at about 6 ka BP and water masses from these two basins prevented the ingression of IOCW to the northeastern part of the Arabian Sea. The reduced OMZ ventilation is the likely reasons for the OMZ and denitrification maximum in the northern and eastern part of the basin during the Holocene.

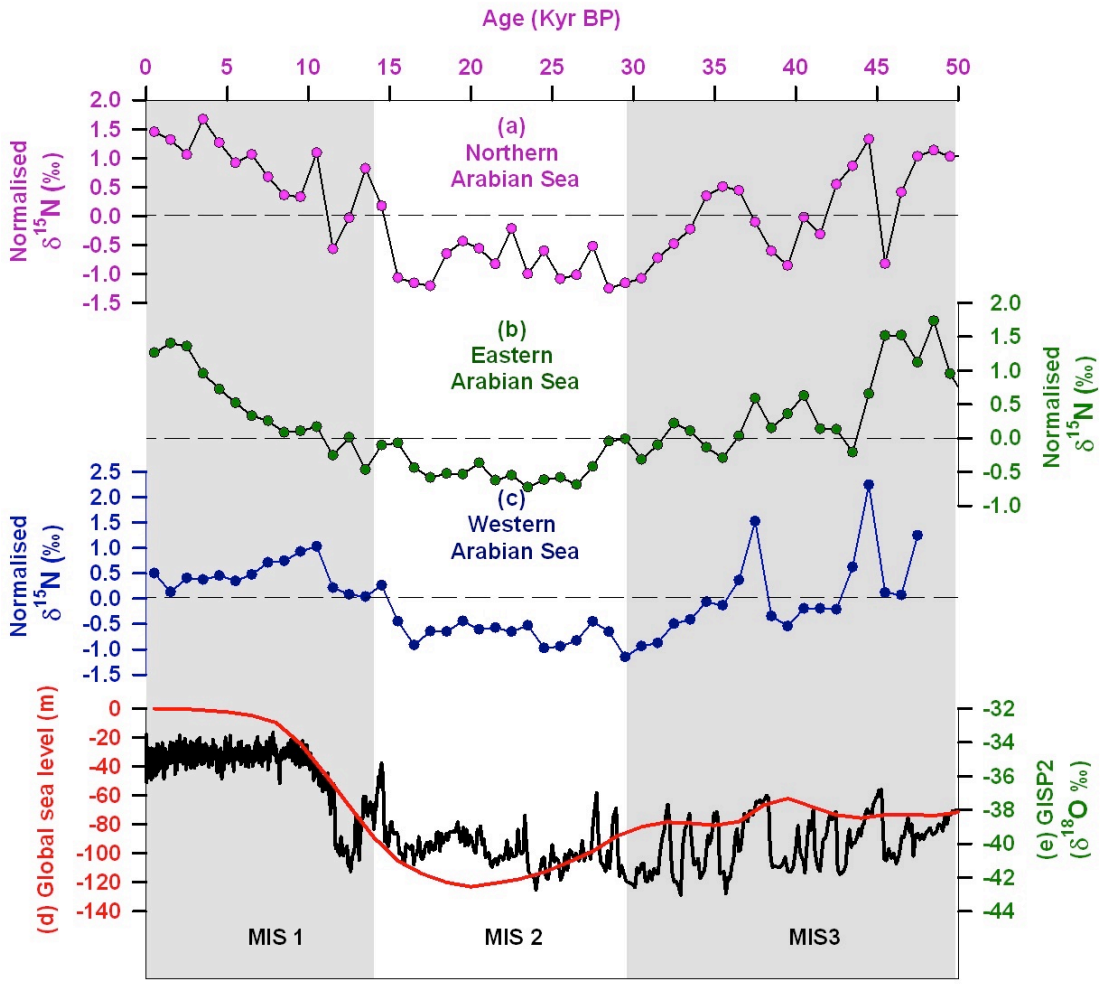

Figure 27. Regional averages of normalized and averaged $\delta^{15}N$ values from the northern (a), eastern (b), and western (c) Arabian Sea, compared with sea level reconstruction from the Red Sea (Siddall et al., 2003) (d), and $\delta^{18}O$ record from the GISP2 ice core (Grootes and Stuiver, 1997) (e).

6.11. Global Denitrification changes: Implications to the atmospheric CO_2 and N_2O variability

The Denitrification process that takes place in the OMZs of the Arabian Sea and the eastern North and South Pacific oceans has the potential of affecting the climate in an indirect fashion, since it partially modulates the total amount of nitrogen available for phytoplankton growth and hence the efficiency of the oceanic carbon sequestration, and directly by the production of the greenhouse gas N_2O. However, the net effect

that an individual OMZ and changes in its denitrification intensity would have on the oceanic NO_3^- budget is a complex calculation. Therefore, we have further attempted to qualitatively constrain the denitrification forcing on oceanic NO_3^- by comparing our normalized $\delta^{15}N$ record with that of atmospheric CO_2. As this comparison would inversely describe the corresponding changes in marine nitrogen inventory due to oscillation in Arabian Sea denitrification related to the biological sequestration of CO_2. This idea was first introduced by Altabet et al., (2002), which was applied only to the Oman margin. We now include, for the first time, the contribution of the entire Arabian Sea along with the $\delta^{15}N$ record from the eastern north pacific and eastern south pacific for obtaining a global picture of the potential effect of denitrification on atmospheric CO_2.

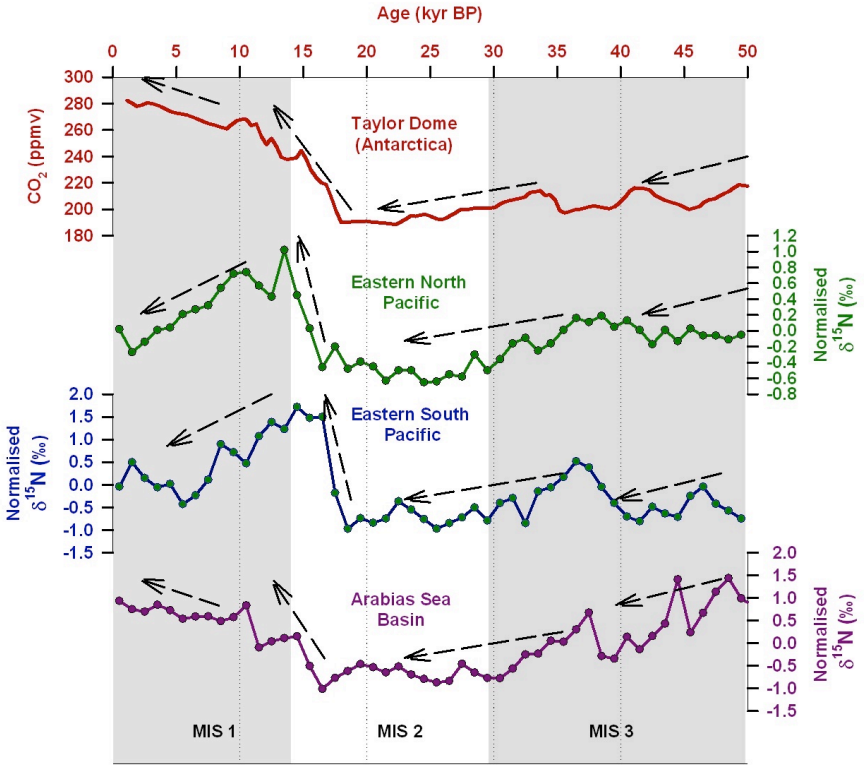

Figure 28. CO_2 concentration in the Antarctic Taylor Dome ice core (Smith et al., 1999) (a) compared with the regional averages of normalized and averaged $\delta^{15}N$ values from the Eastern North Pacific (b), Eastern South Pacific (c), and the Arabian Sea (d). See text for more details.

The normalized $\delta^{15}N$ record exhibits a similar trend to those found in Antarctic ice core atmospheric CO_2 record suggesting a mechanistic linkage (Fig. 28). In Fig. 28, we have marked certain features of these records that resemble the observed variability in the late quaternary evolution of atmospheric CO_2. For example, between 20-50 kyr BP, the CO_2 fall about 30 ppmv (shown by a dashed arrow in Fig. 28a). The decreasing intensity of the CO_2 incursions between 20-50 kyr BP, might be related to a pronounced decreasing denitrification trend in the ETNP and Arabian Sea and a moderate decreasing trend in the ETSP (dashed arrows). The 15 kyr increasing trend in CO_2 is also present in the three OMZs (dotted arrows). However, the increasing trend in CO_2 during the Holocene period is seen only in the OMZ of the Arabian Sea. Thus raising the possibility that the Arabian Sea represents an important feedback on the Holocene climate through sustained increase in N_2O production and marine nitrogen loss. The decline in denitrification in the ETNP and ETSP during the Holocene was a result of the intensification of the equatorial subsurface countercurrents that brought more oxygenated waters to intermediate depths off eastern tropical pacific (Salvatteci et al., 2016; Kienast et al., 2002). This was related to a strengthening of the Walker circulation as a result of an enhanced zonal SST gradient across the tropical Pacific during Early and mid-Holocene (Koutavas et al., 2006).

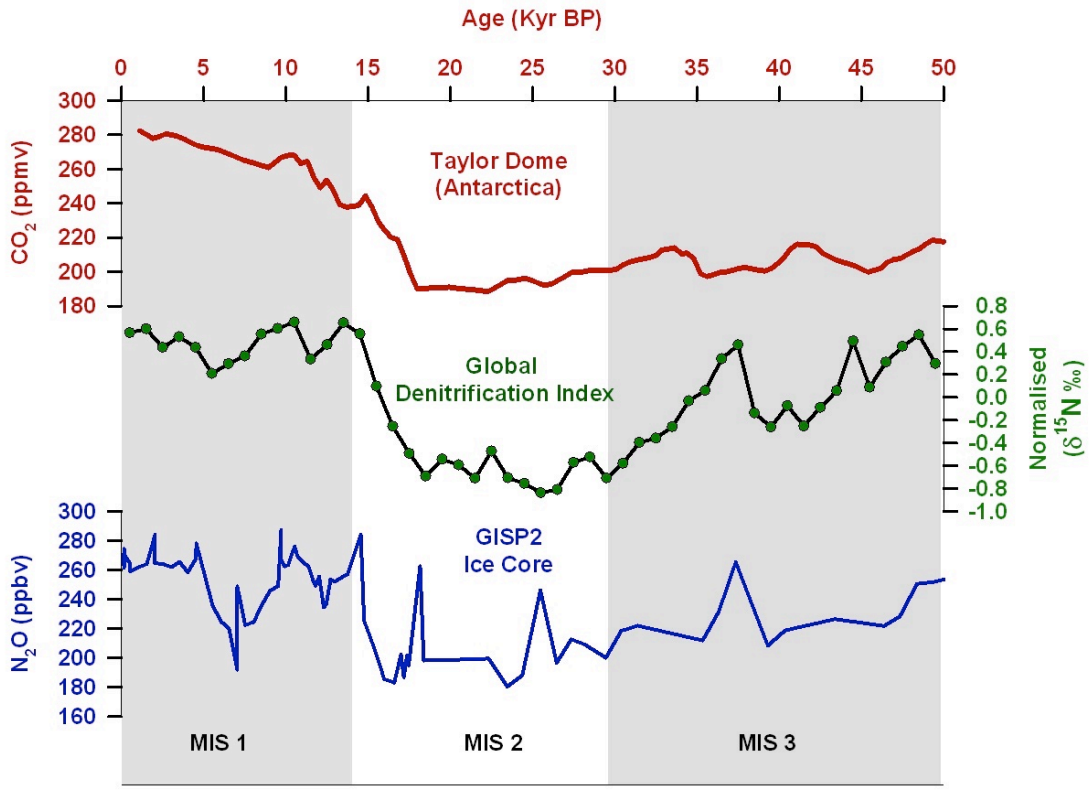

Figure 29. Comparison of the atmospheric CO_2 concentration from the Taylor-Dome ice core (a) and atmospheric N_2O concentration from the GISP2 ice core (c) with the global denitrification index (b) calculated by averaging the individual normalized $\delta^{15}N$ values from the ETNP, ETSP, and the Arabian Sea.

Further, we reconstruct a normalized global marine denitrification forcing index (Fig. 29b) using $\delta^{15}N$ data from the three OMZs using the same normalization technique as described in the Materials and Methods section. It shows a remarkable resemblance to the late Quaternary variability of atmospheric CO_2 (Fig. 29a) in great detail than through the comparison of the Arabian Sea or ETNP or ETSP history alone. For example, between 20-50 kyr BP, the clear decreasing trend that is present in the CO_2 record is now fully featured in the denitrification forcing. Moreover, the deglacial CO_2 rise is matched both in timing and intensity by the denitrification forcing once the three OMZ's are considered. The general consistency of both curves indicates a close coupling between the oceanic N cycle and atmospheric CO_2. A change in

oceanic nutrient inventory is one means for forcing changes in atmospheric CO_2, via alteration of marine productivity (Broecker et al., 1982; Sigman et al., 2000). Increased denitrification would reduce combine nitrogen and thus the strength of the marine biological pump for carbon if sustained sufficiently for long period of time. The widespread diminished denitrification during the last glacial period inferred from global denitrification forcing index of the present study has profound global consequence. Several studies have raised the possibility that the oceanic nitrogen content increased during the last glacial period in several regions. Lowering of sea level to 120 m during LGM converted the continental shelves into coastal land, removing much of the continental shelf denitrification environment as a site of oceanic N loss. Assuming that the decrease in denitrification is proportional to the shelf area, reduction of shelf area by 75%, during the LGM (Hay and Southam, 1977), must have decreased modern shelf denitrification rates from 100 (Devol, 1999) to 25 Tg N yr^{-1}. The declines in water column denitrification in the ETNP, ETSP and the Arabian Sea, which account for almost all of the 100 Tg N yr^{-1} lost to water column denitrification in the present ocean, imply that global denitrification must have been greatly diminished during the last glacial period. On the other hand, the atmospheric iron deposition during the last glacial was substantially larger than it is today. Globally, atmospheric iron deposition on the surface ocean was estimated to be about twice of that today (Mahowald et al., 1999), while the increase over the Southern Ocean and other low iron deposition regions was likely manifold (Martin, 1990). This increase in iron availability not only eased the iron stress of phytoplankton in general, but also enhanced N fixation substantially (Falkowski, 1997; Broecker and Henderson, 1998; Michaels et al., 2001; Karl et al., 2002). This combination of nitrogen supply due to increased nitrogen fixation combined with

reduced nitrogen loss from denitrification, must have led to an increase in the glacial nitrogen inventory during the last glacial period. This stimulated surface production and export of organic carbon in the nitrogen limited regions and finally the drawdown of atmospheric CO_2.

Further, the comparison of the atmospheric N_2O (Fig. 29c) record with our Global marine denitrification index (Fig. 29b) suggest that changes in oceanic denitrification may also have modulated glacial-interglacial climate by influencing atmospheric concentration of N_2O. From this, it is clear that major marine denitrification centers such as ETNP, ETSP and Arabian Sea, release large amount of N_2O into the atmosphere through a combination of biogeochemical/physical processes. Finally, we note that regardless of whether the link between denitrification and atmospheric CO_2 and N_2O is governed by biological and/or physical processes, the agreement between the global denitrification index and the atmospheric CO_2 and N_2O concentrations during the last 50 kyr BP is strong evidence of a tight connection between the N and C cycles during the Late Quaternary.

6.12. Conclusion

Denitrification in the world OMZ's was weaker during MIS 2 compared to MIS 3. The overall pattern of denitrification variability during the MIS 3 and MIS 2 remains almost similar across all the basins (ETNP, ETSP, and Arabian Sea) except during the Holocene. The probable cause of the observed regional differences in denitrification in the world OMZ's is the ventilation changes due to millennial scale variations in oxygen rich southern water masses formation during last glacial period and circulation reorganization following sea level rise during the Holocene period.

Moreover, our new normalized $\delta^{15}N$ record clearly shows intensified denitrification from about 8 kyr BP in the northeastern part of the Arabian Sea whereas denitrification in world's OMZs including the western Arabian Sea generally decreased following the deglacial maximum. We further find that the denitrification in the world OMZs matches almost every millennial-scale feature of the CO_2 and N_2O evolution during the last 50 kyrs. It suggests that marine denitrification variability played an important role in governing the global carbon and nitrogen cycle, and the climate on millennial timescale.

Chapter 7

Conclusions and Recommendation

for Future Research

7.1. Conclusions

This chapter summarizes the major findings of the thesis. It presents the inferred changes in monsoon intensity during the Late Quaternary on centennial to millennia time scales. Conclusions drawn based on the chemical and isotopic proxies in three well-dated sediment cores from the eastern Arabian Sea and their comparison with other records are given below:

1. **South Asian Summer Monsoon quantification and its relation with solar variability spanning the past 5000 years**

   South Asian Summer Monsoon (SASM) shows a weak correlation with solar variability in the 20th century. However, such climatological observations on sunspot activity-monsoon relationship are very short hence uncertain. A few paleomonsoon records also exhibit prominent correspondence with solar activity during early Holocene and beyond. But despite the strong recent solar minima (e.g., Maunder, Spörer, Oort, Wolf), their correlation with monsoon precipitation is weak and inconclusive. The sea surface temperature (SST) and sea surface salinity (SSS) reconstructed in this study using Mg/Ca ratio and oxygen isotope ratios of planktic foraminifera (*G. ruber*) overlaps with that of TSI (Total Solar Irradiance; index of solar variability). This record over the past 5000 years shows that ISM intensity varied in unison with solar variability and suggests a strong solar control on monsoonal climate on multi-centennial time scales. Using this precise reconstruction and spectral analysis (Continuous Wavelet Transform and the Squared Wavelet Coherence), we, for the first time, show that the salinity/SASM precipitation declined statistically significantly during recent periods of major solar minima but lagged by a couple of hundred years beyond

1300 yr BP toward the mid-Holocene. This is confirmed through spectral analysis and also through comparison with earlier marine and terrestrial studies.

2. **Organic carbon as a function of preservation in the slope sediments of the Southeastern Arabian Sea**

Sediments from the Southeastern Arabian Sea are used widely to reconstruct past South Asian Summer Monsoon (SASM) variability. Total organic carbon (TOC) concentration of these sediments is used as a proxy for past productivity related to SASM intensity. But still, there are certain uncertainties and controversies regarding TOC accumulation and its linkage to monsoon and surface productivity particularly in the eastern Arabian Sea. So, it needs to be ascertained whether the TOC is a signal of productivity or preservation in the Southeastern Arabian Sea sediments. The history of the past productivity, redox conditions, and SASM intensity reconstructed in this study using a suite of geochemical proxies, including major and trace elements, suggests that the observed increase in the TOC is a result of the enhanced preservation due to increasingly reducing conditions since mid-Holocene to present in the SEAS. The SASM actually declined during this period as shown by a decline in Ti/Al since mid-Holocene, which matches with the previous studies from this region. Further our comprehensive comparison among the major monsoon systems of the world (South Asian, East Asian, and North African Summer Monsoon) also show that the SASM has been declining since mid-Holocene due to precession forcing as suggested by previous models ensemble studies.

3. Differential response of denitrification during the Holocene and the Last Glacial Maxima

Past denitrification intensity is also used to infer past SASM strength on millennial and longer timescales. Therefore, it is important to understand the mechanisms controlling the denitrification intensity, not only with respect to the modern day settings but also on glacial-interglacial timescales. We studied multiple proxies in a sediment core from the SEAS to understand denitrification variability at high-resolution (centennial scale) and its response to different periods of the earth's climatic history and the underlying mechanisms. Such high-resolution records from this region are not readily available. High *G. bulloides* abundance of the present study, suggesting changes in the surface water productivity for the last 43 kyrs, is not always accompanied by a corresponding increase in $\delta^{15}N$ and TOC especially during LGM and since early- Holocene in the SEAS. Decoupling between *G. bulloides* abundance and TOC as shown in the present study points towards factors other than productivity affecting TOC accumulation in sediments. Whereas, a similar trend observed between the $\delta^{15}N$ and the TOC suggests that accumulation of organic carbon in SEAS is mainly a response to better preservation under enhanced sub-oxic conditions in the OMZ rather than changes in primary productivity. Our high-resolution denitrification record shows that during the last glacial period, both the ventilation of the Sub Antarctic Mode Water – Antarctic Intermediate Water (SAMW-AAIW) into the SEAS and the SASM induced productivity played a crucial role in modulating denitrification. But, during the Holocene and LGM, denitrification increased despite reduced monsoon-induced productivity. This study shows that this increase in denitrification is caused by the enhanced inflow of oxygen-depleted

Red Sea Water and Persian Gulf Water into the intermediate depths of the SEAS due to the rising sea level. During LGM, reduced ventilation of the intermediate waters of the SEAS due to the weakened thermohaline circulation resulted in a differential response of the denitrification. This finding will have major implication towards the interpretation of $\delta^{15}N$ variability in future studies using sediments from the SEAS, which would help to understand past SASM variability more accurately. Further, our comprehensive comparison among the major monsoon systems of the world (Asian, African, and South American) shows millennial scale synchronicity between the denitrification in the SEAS, global monsoon and North Atlantic climate implying a systematic link among them confirmed statistically using wavelet analysis.

4. Marine denitrification and its implications for global carbon and nitrogen cycles

The compilation of available published $\delta^{15}N$ record from the Arabian Sea along with our two new records from the SEAS and from ETNP and ETSP for the past 50 kyrs was done to understand various plausible causes/mechanism (atmospheric and ocean circulations) for spatial and temporal variation in denitrification. Most importantly, this study tries to assess the hypothesis of a global, millennial-scale, pelagic denitrification forcing on nitrogen and carbon cycle. The results of this study suggest that during MIS 3 and MIS 2 denitrification variability remained almost similar across all the three basins. However, during the Holocene, increasing denitrification occurs in the Arabian Sea in contrast to the ETNP and ETSP due to a postglacial reorganization of intermediate water circulation following sea level rise. This study further

suggests that the denitrification in the world OMZs matches almost every millennial-scale feature of the CO_2 and N_2O evolution during the last 50 kyrs. It suggests that marine denitrification variability played an important role in governing the global carbon and nitrogen cycle, and the climate on a millennial timescale

7.2. Recommendation for future research

This research demonstrates the usefulness and significance of applying a multiproxy approach to reconstructing past climate, especially in combining proxies that reflect varying aspects of the climate system at centennial to millennial time-scales. Valuable information will continue to arise from measurements of the isotopic composition of bulk sediments, especially in margin environments. Expanding the network of high-resolution $\delta^{15}N_{bulk}$ records is crucial to map out patterns of changing $\delta^{15}N_{nitrate}$ in space and in time, without which mechanistic hypotheses cannot be tested. However, it is critical that we work to address the ambiguities that affect $\delta^{15}N_{bulk}$ in open ocean records, with the ideal goal of quantifying diagenetic isotope effects so that they can be removed from the bulk records. One promising approach is the isolation and analysis of organic matter that is of known origin and protected from diagenesis, such as microfossil-bound N. The development of compound-specific techniques, such as for chlorophyll and amino acids, also holds promise for the future, as does the coupling of compound-specific techniques with the use of microfossil-bound organic matter (Ingalls, et al., 2003; McCarthy, et al., 2003).

The interpretation of isotopic data needs to become more quantitative and mechanistic. The use of numerical models with realistic circulation, coupled with the

inclusion of other paleoceanographic proxies, will lead to much better-defined pictures of how water column denitrification zones have interacted with physical circulation and oxygen cycling. The inclusion of nitrogen isotope dynamics in biogeochemical models will allow estimates of past rates of denitrification, N_2 fixation, and high latitude nitrate utilization to be drawn from the expanding array of $\delta^{15}N$ records. These advances will illuminate the connections of N cycle processes to other aspects of the climate system and to each other.

This work will necessarily go hand in hand with studies to link N isotopic patterns in the modern ocean to underlying N transformations. Some important processes such as sedimentary denitrification can only be studied indirectly with available paleoceanographic tools. These processes should be considered critical targets for improved understanding through the study of modern environments. Finally, paleoceanographic techniques that, to date, have focused mostly on open-ocean processes, can be brought to bear on the critical environment of the coastal zone. This prospect offers a wealth of unexploited areas of research with implications for preindustrial human impacts on the environment, fisheries, and coastal zone management.

References:

Abram N. J., Gagan M. K., Liu Z., Hantoro W. S., Mc Culloch M. T. and Suwargadi BW (2007). Seasonal characteristics of the Indian Ocean Dipole during the Holocene epoch. *Nature,* 445: 299-302.

Agnihotri, R., K. Dutta, R. Bhushan, and B. L. K. Somayajulu (2002), Evidence for solar forcing on the Indian monsoon during the last millennium, *Earth and Planetary Science Letters, vol. 198*, 521–527.

Agnihotri, R., S. K. Bhattacharya, M. M. Sarin, and B. L. K. Somayajulu (2003), Changes in surface productivity and subsurface denitrification during the Holocene: a multiproxy study from the eastern Arabian Sea, *The Holocene, 13,* 701-713, doi:10.1191/0959683603hl656rp.

Altabet, M. A., and Francois, R., 1994, Sedimentary nitrogen isotopic ratio as a recorder of surface ocean nitrate utilization: Global Biogeochemical Cycles, v. 8, p. 103-116.

Altabet, M. A., Francois, R., Murray, D. W., and Prell, W. L., 1995, Climate related variations in denitrification in the Arabian Sea from sediment $^{15}N/^{14}N$ ratios: Nature, v. 373, p. 506-509.

Altabet, M., 1988, Variations in nitrogen isotopic composition between sinking and suspended particles: Implications for nitrogen cycling and particle transformation in the open ocean: Deep-Sea Research, v. 35, p. 535–554.

Altabet, M. A., Murray, D. W., and Prell, W. L., 1999, Climatically linked oscillations in Arabian Sea denitrification over the past 1 m.y.: Implications for the marine N cycle: Paleoceanography, v. 14, p. 732-743.

Altabet, M. A., Higginson, M. J., and Murray, D. W., 2002, The effect of millennial-scale changes in Arabian Sea denitrification on atmospheric CO_2: Nature, v. 415 (6868), p. 159–162.

Altabet, M. A., and Herbert, T. D., 2006, Influence of marine denitrification on atmospheric N_2O variability during the Holocene: Geophysical Research Letters, v. 33, L13704.

Altabet, M., 2006, Isotopic tracers of the marine nitrogen cycle: Present and past, in: Marine organic matter: biomarkers, isotopes and DNA, edited by: Volkman, J. K., Springer-Verlag Berlin Heidel- berg, p. 251–293.

Anand P, Elderfield H and Conte MH (2003) Calibration of Mg/Ca thermometry in planktonic foraminifera from sediment trap time series. *Paleoceanography* 18(2): 1050. doi:10.1029/2002PA000846.

Anand, P., D. Kroon, A. D. Singh, R. S. Ganeshram, G. Ganssen, H. Elderfield (2008), Coupled sea surface temperature seawater δ18O reconstructions in the Arabian Sea at the millennial scale for the last 35 ka, *Paleoceanography, 23,* 4207. doi:10.1029/2007PA001564.

Anderson, D. M., J. T. Overpeck, and A. K. Gupta (2002), Increase in the Asian SW Monsoon during the past four centuries, *Science, 297*, 596–599.

Avinash, K., B. R., Manjunath, and P. J. Kurian (2015), Glacial-interglacial productivity contrasts along the eastern Arabian Sea: Dominance of convective mixing over upwelling, *Geoscience Frontiers, 6,* 913-925.

Azharuddin, S., P. Govil, A. D. Singh, R. Mishra, S. Agrawal, A. K. Tiwari, K. Kumar (2016), Monsoon-influenced variations in productivity and lithogenic flux along offshore Saurashtra, NE Arabian Sea during the Holocene and Younger Dryas: A multi-proxy approach, *Palaeogeography, Palaeoclimatology, Palaeoecology*, doi: 10.1016/j.palaeo.2016.11.018.

Balaram, V., and T. G. Rao, (2003), Rapid determination of REEs and other trace elements in geological samples by microwave acid digestion and ICP-MS, *At. Spectrosc., 24,* 206–212.

Banse, K. (1987), Seasonality of phytoplankton chlorophyll in the central and northern Arabian Sea. *Deep-Sea Res., 34,* 713-723.

Banse, K., Naqvi, S. W. A., Narvekar, P. V., Postel, J. R., and Jayakumar, D. A., 2014. Oxygen minimum zone of the open Arabian Sea: variability of oxygen and nitrite from daily to decadal timescales. Biogeosciences 11, 2237-2261.

Barker S, Greaves M and Elderfield H (2003) A study of cleaning procedures used for foraminiferal Mg/Ca paleothermometry. *Geochemistry Geophysics Geosystems* 4(9): 8407. doi: 10.1029/2003GC000559.

Bar-Matthews, M., A. Ayalon, M. Gilmour, A. Matthews and C. J. Hawkesworth (2003), Sea–land oxygen isotopic relationships from planktonic foraminifera and speleothems in the Eastern Mediterranean region and their implication for paleorainfall during interglacial intervals, *Geochimica et Cosmochimica Acta, 67,* 3181–3199.

Bassinot, F. C., Marzin, C., Braconnot, P., Marti, O., Mathien-Blard, E., Lombard, F., and Bopp, L., 2011, Holocene evolution of summer winds and marine productivity in the tropical Indian Ocean in response to insolation forcing: data-model comparison: Climate of the Past, v. 7, p. 815–829, doi:10.5194/cp-7-815-2011.

Bemis BE, Spero HJ, Bijma J and Lea DW (1998) Re-evaluation of the oxygen isotopic composition of planktonic foraminifera: Experimental results and revised paleotemperature equations, *Paleoceanography* 13(2): 150-160. doi: 10.1029/98PA00070.

Berger, A., M. F. Loutre (1991), Insolation values for the climate of the last 10 million years, *Quaternary Science Review, 10*, 297–317.

Bhattathiri, P. M. A., Pant, A., Sawant, S., Gauns, M., Matondakar, S. G. P., and Mohanraju, R., 1996. Phytoplankton production and chlorophyll distribution in the eastern and central Arabian Sea in 1994–1995. Curr. Sci. 71, 857–862.

Bhattacharya S and Narasimha R (2005) Possible association between Indian monsoon rainfall and solar activity. *Geophysical Research Letters* 32: L05813. doi: 10.1029/2004GL021044

Bhushan, R., K. Dutta, and B. L. K. Somayajulu (2001), Concentrations and burial fluxes of organic and inorganic carbon on the eastern margins of the Arabian Sea, *Mar. Geol., 178,* 95–113.

Blunier, T., and Brook, E. J., (2001), Timing of millennial-scale climate change in Antarctica and Greenland during the last glacial period. Science 291, 109–112.

Boyer T. P., Antonov J. I., Baranova O. K., Garcia H. E., Johnson D. R., Locarnini R. A., Mishonov A. V., Seidov D., Smolyar I. V. and Zweng M. M. (2009), World Ocean Database 2009. In: Levitus S (eds) *NOAA Atlas NESDIS 66*. Washington D.C: U.S. Gov. Printing Office pp. 216.

Brandes, J. A., Devol, A. H., Yoshinari, T., Jayakumar, D. A., and Naqvi, S.W.A., (1998), Isotopic composition of nitrate in the central Arabian Sea and eastern tropical North Pacific: A tracer for mixing and nitrogen cycles. Limnol. Oceanogr. 43, 1680-1689.

Bristow, L. A., Callbeck, C. M., Larsen, M., Altabet, M. A., Dekaezemacker, J., Forth, M., Gauns, M., Glud, R. N., Kuypers, M. M. M., Lavik, G., Milucka, J., Naqvi, S. W. A., Pratihary, A., Revsbech, N. P., Thamdrup, B., Treusch, A. H., and

Butzin, M., Prange, M., and Lohmann, G., (2005), Radiocarbon simulations for the glacial ocean: The effects of wind stress, Southern Ocean sea ice and Heinrich events: Earth and Planetary Science Letters, v. 235(1–2), p. 45–61.

Brodie, C. R., Casford, J. S. L., Lloyd, J. M., Leng, M. J., Heaton, T. H. E., Kendrick, C. P., and Zong, Y. Q., (2011), Evidence for bias in C/N, δ13C and δ15N values of bulk organic matter, and on environmental interpretation, from a lake sedimentary sequence by pre-analysis acid treatment methods. Quat. Sci. Rev. 30, 3076–3087.

Broecker, W. S., Peteet, D. M., and Rind, D., (1985), Does the ocean-atmosphere system have more than one stable mode of operation?. Nature 315, 21–26.

Brumsack, H. J., (1989), Geochemistry of recent TOC-rich sediments from the Gulf of California and the Black Sea, *Geol. Rundsch. 78*, 851– 882.

Butzin, M., Prange, M., and Lohmann, G., (2005), Radiocarbon simulations for the glacial ocean: The effects of wind stress, Southern Ocean sea ice and Heinrich events. Earth Planet. Sci. Lett. 235(1–2), 45–61.

Cai, Y., H. Zhang, H. Cheng, Z. An, R. L. Edwards, X. Wang, L. Tan, F. Liang, J. Wang, and M. Kelly (2012), The Holocene Indian monsoon variability over the

southern Tibetan Plateau and its teleconnections, *Earth Planetary Science Letters, 335,* 135–144.

Calder, J. A., Parker, P. L., (1968), Stable carbon isotope ratios as indices of petrochemical pollution of aquatic systems. Environ. Sci. Techno. 2, 535–539.

Calvert, S. E., T. F. Pedersen, P. D. Naidu, and U. Stackelberg-Von (1995), On the organic carbon maximum on the continental slope of the Eastern Arabian Sea, *J. Mar. Res., 53,* 269-296.

Calvert, S.E., and T. F. Pedersen (1993), Geochemistry of oxic and anoxic sediments: Implications for the geological record, *Mar. Geol. 113,* 67-88.

Canfield, D. E., (2017), N_2 production rates limited by nitrite availability in the Bay of Bengal oxygen minimum zone: Nature Geoscience, v. 10, p. 24-29, doi:10.1038/ngeo2847.

Cao, L., Fairbanks, R. G., Mortlock, R. A., et al., (2007), Radiocarbon reservoir age of high latitude North Atlantic surface water during the last deglacial. Quat. Sci. Rev. 26(5–6), 732–742.

Capone, D. G., Subramaniam, A., Montoya, J. P., Voss, M., Hum- borg, C., Johansen, A. M., Siefert, R. L., and Carpenter, E. J., (1998), An extensive bloom of the N_2-fixing cyanobacterium Trichodesmium erythraeum in the central Arabian Sea: Marine Ecology Progress, v. 172, p. 281–292.

Charles, C. D., Lynch-Stieglitz, J., Niennemann, U. S., and Fairbanks, R. G., (1996), Climate connections between the two hemispheres revealed by deep-sea sediment core/ice core correlations. Earth Planet. Sci. Lett. 142, 19-27.

Charles, C. D., and Fairbanks, R. G., (1992), Evidence from southern ocean sediments for the effect of North Atlantic deep water flux on climate. Nature 355, 416–419.

Chauhan, O. S., E. Vogelsang, N. Basavaiah, and U. S. A. Kader (2010), Reconstruction of the variability of the southwest monsoon during the past 3 ka, from the continental margin of the southeastern Arabian Sea, *Journal Of Quaternary Science, 25(5),* 798-807.

Chevalier, M., S. Brewer, and M. C. Brian (2017), Qualitative assessment of PMIP3 rainfall simulations across the eastern African monsoon domains during the mid-Holocene and the Last Glacial Maximum, *Quaternary Science Reviews, 156,* 107-120.

Craig, H., L. I. Gordon (1965), Deuterium and oxygen-18 variations in the ocean and marine atmosphere, In: Tongiorgi, E. (Ed.), Stable Isotopes in Oceanographic Studies and Paleotemperatures, *Proc. of the Spoleto Conference. Laboratorio di Geologia Nucleare, Pisa*, 9–130.

Clemens, S., W. L., Prell, D. Murray, G. B. Shimmield, and G. Weedon (1991), Forcing mechanisms of the Indian Ocean monsoon. *Nature, 353,* 720-725.

Clement AC, Seager R and Cane MA (2000), Suppression of El Niño during the mid Holocene by changes in the Earth's orbit. *Paleoceanography* 15(6): 731-737.

Codispoti, L. A., Brandes, J. A., Christensen, J. P., Devol, A. H., Naqvi, S.W.A., Paerl, H.W., and Yoshinari, T., (2001), The oceanic fixed nitrogen and nitrous oxide budgets: Moving targets as we enter the anthropocene?. Sci. Mar. 65, 85-105.

Cullen, J. L., and Prell, W. L., (1984), Planktonic foraminifera of the northern Indian Ocean: distribution and preservation in surface sediments. Mar. Micropaleont. 9, 1–52.

Curry WB, Ostermann DR, Guptha MVS and Ittekkot V (1992), Foraminiferal production and monsoonal upwelling in the Arabian Sea: Evidence from sediment traps, in Upwelling Systems: Evolution since the Early Miocene. vol. 64, edited by C. P. Summerhayes, W. L. Prell, and K. C. Emeis, pp. 93-106, Geological Society Special Publication, London.

Dahl KA, and Oppo DW (2006), Sea surface temperature pattern reconstructions in the Arabian Sea. *Paleoceanography* 21(1): PA1014. doi: 10.1029/2005PA001162.

Dansgaard, W., Johnsen, S. J., Clausen, H. B., Dahl-Jensen, D., Gundestrup, N. S., et al., (1993), Evidence for general instability of past climate from a 250-kyr ice-core record. Nature 364, 218–220.

Demaison, G. J., and G. T. Moore (1980), Anoxic environments and oil source bed genesis, *Amer. Assoc. Petrol. Geol. Bull., 64,* 1179-1209.

deMenocal, P., J. Ortiz, T. Guilderson, and M. Sarnthein (2000), Coherent High and Low-Latitude Climate Variability During the Holocene Warm Period, *Science, 288,* 2198–2202.

Deutsch, C., Sigman, D. M., Thunell, R. C., Meckler, A. N., and Haug, G. H., (2004), Isotopic constraints on glacial/interglacial changes in the oceanic nitrogen budget. Global Biogeochemical Cycles 18, GB4012, doi:4010.1029/2003GB002189.

Deutsch, C., Sarmiento, J. L., Sigman, D. M., Gruber, N., and Dunne, J. P., (2007), Spatial coupling of nitrogen inputs and losses in the ocean: Nature, v. 445, p. 163–167.

De Villiers S., Greaves M. and Elderfield H. (2002), An intensity ratio calibration method for the accurate determination of Mg/Ca and Sr/Ca of marine carbonates by ICP‐AES. *Geochemistry Geophysics Geosystems* 3(1). doi: 10.1029/2001GC000169.

Dow, W. G., (1978), Petroleum source beds on continental slopes and rises, *American Association Petroleum Geology Bulletin, 62,* 1584-1606.

Durand, F., Shankar, D., Boyer de Montegut, C., Shenoi, S. S. C., Blanke, B. and Madec, G., 2007, Modeling the barrier-layer formation in the southeastern Arabian Sea: Journal Climate, v. 20(10), p. 2109–2120.

Dutta, K., Bhushan, R., and Somayajulu, B. L. K., 2001, ΔR correction values in the Northern Indian Ocean: Radiocarbon, v. 43 (2a), p. 483-488.

Emeis, K.-C., Anderson, D. M., Doose, H., Kroon, D., and Schulz-Bull, D., 1995, Sea-Surface Temperatures and the History of Monsoon Upwelling in the Northwest Arabian Sea during the Last 500,000 Years: Quaternary Research, v. 43, p. 355-361.

Erez J, and Luz B (1983) Experimental paleotemperature equation for planktonic foraminifera. *Geochimistry Cosmochimistry Acta* 47(6): 1025-1031.

Eugster, O., Gruber, N., Deutsch, C., Jaccard, S. L., and Payne, M. R., 2013. The dynamics of the marine nitrogen cycle across the last deglaciation. Paleoceanography 28, 14.

Farquhar, G. D., Ehleringer, J. R., and Hubick, K.T., 1989. Carbon isotope discrimination and photosynthesis. Annu. Rev. Plant Physiol. Plant Mol. Biol. 40, 503–537.

Field DB (2004) Variability in vertical distributions of planktonic foraminifera in the California Current: relationships to vertical ocean structure. *Paleoceanography* 19(2): PA2014.

Fleitmann D, Burns SJ, Mudelsee M, Neff U, Kramers J, Mangini A and Matter A (2003) Holocene forcing of the Indian monsoon recorded in a stalagmite from southern Oman. *Science* 300(5626): 1737-1739.

Fontugne, M. R., and J. C. Duplessy (1986), Variations of the monsoon regime during the Upper Quaternary: Evidence from carbon iso-topic record of organic matter in North Indian Ocean sediment cores, *Palaeogeogr. Palaeoclimatol. Palaeoecol. , 56,*69 – 88, doi:10.1016/0031-0182(86)90108-2.

Gagan MK, Hendy EJ, Haberle SG and Hantoro WS (2004) Post-glacial evolution of the Indo-Pacific warm pool and El Niño-Southern Oscillation. *Quaternary International* 118-119: 127-143.

Galbraith, E. D., Kienast, M., Albuquerque, A. L., Altabet, M. A., Batista, F., Bianchi, D., Calvert, S. E., Contreras, S., Crosta, X., De Pol-Holz, R., Dubois, N., Etourneau, J., Francois, R., Hsu, T. C., Ivanochko, T., Jaccard, S. L., Kao, S. J., Kiefer, T., Kienast, S., Lehmann, M. F., Martinez, P., McCarthy, M., Meckler, A. N., Mix, A., Mobius, J., Pedersen, T. F., Pichevin, L., Quan, T. M., Robinson, R. S., Ryabenko, E., Schmittner, A., Schneider, R., Schneider-Mor, A., Shigemitsu, M., Sinclair, D., Somes, C., Studer, A. S., Tesdal, J. E., Thunell, R., Yang, J. Y. T., and Members, N. W. G., 2013. The acceleration of oceanic denitrification during deglacial warming. Nature Geoscience 6, 579-584.

Gallego-Torres, D., F. Martinez-Ruiz, G. J. De Lange, F. J. Jimenez-Espejo, M. Ortega- Huertas (2010), Trace-elemental derived paleoceanographic and

paleoclimatic conditions for Pleistocene Eastern Mediterranean sapropels, *Palaeogeogrphy Palaeoclimatoly Palaeoecology 293*, 76–89.

Ganeshram, R. S., Pedersen, T. F., Calvert, S. E., and Murray, J. W., 1995. Large changes in oceanic nutrient inventories from glacial to interglacial periods. Nature 376, 755-758.

Ganeshram, R. S., Pedersen, T. F., Calvert, S. E., and McNeil, G. W., 2000. Glacial-interglacial variability in denitrification in the world's oceans: Causes and consequences. Paleocenagraphy 15, 361-376.

Gasse F (2000) Hydrological changes in the African tropics since the Last Glacial Maximum. *Quaternary Science Review* 19(1-5): 189-211.

Gasse, F., F. Chalié, A. Vincens, M. A. Williams, and D. Williamson (2008), Climatic patterns in equatorial and southern Africa from 30000 to 10000 years ago reconstructed from terrestrial and near-shore proxy data, *Quaternary Science Review, 27,* 2316–2340.

Gaye-Haake, B., Lahajnar, N., Emeis, K.-C., Unger, D., Rixen, T., Suthhof, A., Ramaswamy, V., Schulz, H., Paropkari, A. L., Guptha, M. V. S., and Ittekkot, V., 2005. Stable nitrogen isotopic ratios of sinking particles and sediments from the northern Indian Ocean. Marine Chemistry, 96, 243-255.

Gaye, B., Nagel, B., Dähnke, K., Rixen, T., and Emeis, K. C., 2013a, Evidence of parallel denitrification and nitrite oxidation in the ODZ of the Arabian Sea from paired stable isotopes of nitrate and nitrite: Global Biogeochemical Cycles, v. 27, doi10.1002/2011GB004115.

Gaye, B., Nagel, B., Dähnke, K., Rixen, T., Lahajnar, N., and Emeis, K. C., 2013b, Amino acid composition and $\delta^{15}N$ of suspended matter in the Arabian Sea: implications for organic matter sources and degradation: Biogeosciences, v. 10, p. 7689-7702.

Gaye, B., Böll, A., Segschneider, J., Burdanowitz, N., Emeis, K. C., Ramaswamy, V., Lahajnar, N., Lückge, A., and Rixen, T., 2017. Glacial-Interglacial changes and Holocene variations in Arabian Sea denitrification. Biogeoscience

Gray LJ, et al. (2010) Solar influences on climate. *Reviews of Geophysics* 48(4): RG4001. doi:10.1029/2009RG000282.

Grinsted A, Moore JC, Jevrejeva S (2004) Application of the cross wavelet transform and wavelet coherence to geophysical time series. *Nonlin Processes Geophysics* 11: 561-566. doi: 10.5194/npg-11-561-2004.

Govil, P., and P. D. Naidu (2010), Evaporation-precipitation changes in the eastern Arabian Sea for the last 68 ka: Implications on monsoon variability, *Paleoceanography, 25,* PA1210, doi:10.1029/2008PA001687.

Govil, P., P. D. Naidu (2011), Variations of Indian monsoon precipitation during the last 32 kyr reflected in the surface hydrography of the Western Bay of Bengal, *Quaternary Science Reviews, 30,* 3871- 3879.

Gruber, N. and Galloway, J. N., 2008, An earth-system perspective of the global nitrogen cycle: Nature, v. 451, p. 293-296.

Gupta, A. K., Anderson, D. M., and Overpeck, J. T., 2003. Abrupt changes in the Holocene Asian southwest monsoon and their links to the north Atlantic Ocean. Nature 421, 354–357.

Gupta, A. K., M. Das, D. M. Anderson (2005), Solar influence on the Indian summer monsoon during the Holocene, *Geophysical Research Letters, 32,* L17703, doi:10.1029/2005GL022685.

Gupta AK, Mohan K, Das M and Singh RK (2013) Solar forcing of the Indian summer monsoon variability during the Ållerød period. *Science Reports* 3 (2753). doi: 10.1038/srep02753.

Haigh JD (1994) The role of stratospheric ozone in modulating the solar radiative forcing of climate. *Nature* 370: 544-546.

Haigh JD (1999) Modelling the impact of solar variability on climate. *Journal of Atmospheric & Solar Terrestrial Physics* 61(1-2): 63-72.

Hallberg R. O. (1976), A geochemical method for investigation of paleoredox conditions in sediments, *AmBio Special Report*, 139–147.

Haug, G. H., Pedersen, T. F., Sigman, D. M., Calvert, S. E., Nielsen, B., and Peterson, L. C., 1998, Glacial/interglacial variations in production and nitrogen fixation in the Cariaco Basin during the last 580 kyr: Paleoceanography, v. 13, p. 427–432, doi:10.1029/98PA01976.

Heggie, D., T. Lewis (1984), Cobalt in pore waters of marine sediments, *Nature 311*, 453–455.

Helly, J. J., and L. A. Levin (2004), Global distribution of naturally occurring marine hypoxia on continental margins, *Deep-Sea Res., I, 51,* 1159–1168.

Hiremath KM and Mandi PI (2004) Influence of the solar activity on the Indian monsoon rainfall. *New Astronomy* 9: 651-662. doi: 10.1016/S1364-6826(98)00117-5.

Hiremath KM, Manjunath H and Soon W (2015) Indian summer monsoon rainfall: Dancing with the tunes of the sun. *New Astronomy* 35: 8-19.

Holmes, M. E., Schneider, R. R., Müller, P. J., Segl, M., and Wefer, G., 1997, Reconstruction of past nutrient utilization in the eastern Angola Basin based on sedimentary 15N/ 14N ratios: Paleoceanography, v. 12, p. 604–614.

Howell, E. A., Doney, S. C., Fine, R. A., and Olson, D. B., 1997. Geochemical estimates of denitrification in the Arabian Sea and the Bay of Bengal during WOCE. Geophys. Res. Lett. 24, 2549–2552.

Hu, J., Peng, P., Jia, G., Mai, B., Zhang, G., 2006. Distribution and sources of organic carbon, nitrogen and their isotopes in sediments of the subtropical Pearl River estuary and adjacent shelf, Southern China. Mar. Chem. 98, 274–285.

Hu, C., G. M. Henderson, J. Huang, S. Xie, Y. Sun, K. R. Johnson, (2008), Quantification of Holocene Asian monsoon rainfall from spatially separated cave records, *Earth and Planetary Science Letters, 266,* 221–232.

Ivanochko TS, Ganeshram RS, Brummer GJA, Ganssen G, Jung SJA, Moreton SG and Kroon D (2005) Variations in tropical convection as an amplifier of global climate change at the millennial scale. *Earth & Planetary Science Letters* 235**:** 302-314.

Jiang, D., X. Lang, Z. Tian, and L. Ju (2013), Mid-Holocene East Asian summer monsoon strengthening: Insights from Paleoclimate Modeling Intercomparison Project (PMIP) simulations, *Palaeogeography, Palaeoclimatology, Palaeoecology, 369*, 422-429.

Jones, B., D. A. Manning (1994), Comparison of geochemical indices used for the interpretation of palaeoredox conditions in ancient mudstones, *Chemical Geology, 111*,111-129.

Joussaume, S. et. al (1999) Monsoons changes for 6000 years ago: Results of 18 simulation from the Paleoclimate Modeling Intercomparison Project (PMIP), *Geophysical Research Letters, 26 (7),* 859-862.

Joos, F., Plattner, G., Stocker, T., Körtzinger, A., and Wallace, D., 2003. Trends in Marine Dissolved Oxygen: Implications for Ocean Circulation Changes and the Carbon Budget. EOS, Transaction, AGU 84 (21), 197–204.

Jung, S., Kroon, D., Ganssen, G., and Peeters, F., 2009. Enhanced Arabian Sea intermediate water flow during glacial North Atlantic cold phases. Earth Planet. Sci. Lett. 280, 220–228.

Kao, S.J., and Liu, K.K., 2000, Stable carbon and nitrogen isotope systematics in human disturbed watershed (Lanyang-His) in Taiwan and the estimation of biogenic particulate organic carbon and nitrogen fluxes: Global Biogeochemical Cycles, v. 14, p. 189–98.

Karl, D., Michaels, A., Bergman, B., Capone, D., Carpenter, E., Letelier, R., Lipschultz, F., Paerl, H., Sigman, D. and Stal, L., 2002. Dinitrogen fixation in the world's oceans. Biogeochemistry, 57/58, 47–98.

Kessarkar, P. M., Rao, V. P., Naqvi, S. W. A., Chivas, A. R., and Saino, T., 2000, Fluctuations in productivity and denitrification in the southeastern Arabian Sea during the Late Quaternary: Current Science, v. 99, p. 485-491.

Kessarkar, P.M., and V.P. Rao (2007), Organic carbon in sediments of the southwestern margin of India: influence of productivity and monsoon variability during the Late Quaternary, *Journal of Geological Society of India, 69,* 42–52.

Kessarkar, P. M., V. P. Rao, S. W. A. Naqvi, A. R. Chivas, and T. Saino (2010), Fluctuations in productivity and denitrification in the southeastern Arabian Sea during the Late Quaternary, *Current Science, 99,* 485–491.

Kessarkar PM, Purnachadra Rao SW, Naqvi A and Karapurkar SG (2013) Variation in the Indian summer monsoon intensity during the Bølling-Ållerød and Holocene. *Paleoceanography* 28(3):413-425. doi: 10.1002/palo.20040.

Kodera K (2004) Solar influence on the Indian Ocean monsoon through dynamical processes. *Geophysical Research Letters* 31(24): L24209.

Kuhnt, W., Holbourn, A. E., Hall, R., Zuleva, M., and Kase, R., 2004. Cenozoic history of the Indonesian Throughflow, in Clift, p., et.al., eds., Continent-Ocean Interactions in the East Asian Marginal Seas: Geophysical Monograph Series, American Geophysical Union, Washington, D. C., 149, 287 – 308.

Kutzbach JE and Otto-Bliesner BL (1982) The sensitivity of the African-Asian monsoonal climate to orbital parameter changes for 9000 years BP in a low resolution general circulation model. *Journal of Atmospheric Science* 39(6): 1177-1188.

Kutzbach JE and Street-Perrott FA (1985) Milankovitch forcing of fluctuations in the level of tropical lakes from 18 to 0 kyr BP. *Nature* 317: 130-134.

Labitzke K and van Loon H (1995) Connections between the troposphere and stratosphere on a decadal scale. *Tellus* 47: 275-286. doi:10.1034/j.1600-0870.1995.t01-1-00008.x.

Lekshmy PR, Midhun M, Ramesh R and Jani RA (2014) ^{18}O depletion in monsoon rain relates to large scale organized convection rather than the amount of rainfall. *Science Reports* 4: 5661. doi: 10.1038/srep05661.

Laskar A.H., M.G. Yadava, R. Ramesh et al. (2013), A 4 kyr stalagmite oxygen isotopic record of the past Indian Summer Monsoon in the Andaman Islands. *Geochemistry Geophysics Geosystems 14(9)*, 3555–3566.

Levitus, S., and T. Boyer (1994), *World Ocean Atlas 1994*, vol. 4, *Temperature, NOAA Atlas NESDIS,* vol. 4, U.S. department of Commerce, Washington, D.C.

Levy, M., Shankar, D., Andre, J. M., Shenoi, S. S. C., Durand, F., DeBoyer Montegut, C., 2007, Basin-wide seasonal evolution of the Indian Ocean's phytoplankton blooms: Journal of Geophysical Research, v. 112, p. C12014, doi:10.1029/2007JC004090.

Liu Z, Harrison SP, Kutzbach J and Otto-Bliesner B (2004) Global monsoons in the mid-Holocene and oceanic feedback. *Climate Dynamics* 22(2-3): 157-182.

Lückge, A., H. D. Rolinski, A. A. Khan, H. Schulz, and U. von Rad (2001), Monsoonal variability in the northeastern Arabian Sea during the past 5000 years: geochemical evidence from laminated sediments, *Palaeogeology Palaeoclimatology Palaeoecology, 167,* 273-286.

Madhupratap, M., Prasanna Kumar, M. S., Bhattathiri, P. M. A., Dileep Kumar, M., Raghukumar, S., Nair, K. K. C., and Ramaiah, N., 1996. Mechanism of the biological response to winter cooling in the northeastern Arabian Sea. Nature 384, 549–552.

Mahesh, B. S., Banakar, V. K., 2014. Change in the intensity of low-salinity water inflow from the bay of Bengal into the eastern Arabian Sea from the last glacial maximum to the Holocene: implications for monsoon variations. Palaeogeography Palaeoclimatology Palaeoecology 397, 31–37.

McIntyre, A., and B. Molfino (1996), Forcing of Atlantic equatorial and subpolar millennial cycles by precession, *Science, 274*, 1867–1870.

Meehl GA and Arblaster JM (2002) GCM sensitivity experiments for the Indian monsoon and tropospheric biennial oscillation transition conditions. *Journal of Climate* 15: 923-944.

Mehta VM and Lau KM (1997) Influence of solar irradiance on the Indian monsoon-ENSO relationship at decadal-multidecadal time scales. *Geophysical Research Letters* 24(2): 159-162.

Meissner, K. J., Galbraith, E. D., and Volker, C., 2005. Denitrification under glacial and interglacial conditions: A physical approach. Paleoceanography 20, 3001, doi:10.1029/2004PA001083.

Meyers, P. A., 1994. Preservation of elemental and isotopic source identification of sedimentary organic matter. Chem. Geol. 114, 289– 302.

Möbius, J., Gaye, B., Lahajnar, N., Bahlmann, E., and Emeis, K.-C., 2011, Influence of diagenesis on sedimentary $\delta^{15}N$ in the Arabian Sea over the last 130 kyr: Marine Geology, v. 284, p. 127-138, doi: 110.1016/j.margeo.2011.1003.1013.

Molfino, B. and A. McIntyre (1990), Precessional forcing of nutricline dynamics in the Equatorial Atlantic, *Science (Washington), 249*, 766–769.

Morford, J. L., and S. Emerson (1999), The geochemistry of redox-sensitive trace metals in sediments, *Geochimica Cosmochimca Acta. 63*, 1735-1750.

Muller, P. J., and E. Suess (1979), Productivity, sedimentation rate and sedimentary organic carbon in the ocean-Organic carbon preservation, *Deep-Sea Research, 26,* 1347-1362.

Nagoji, S. S., and Tiwari, M., 2017. Organic carbon preservation in Southeastern Arabian Sea sediments since mid-Holocene: Implications to South Asian Summer Monsoon variability. Geochem. Geophys. Geosyst. 18, doi:10.1002/2017GC006804.

Naidu PD and Malmgren BA (1996) A high-resolution record of late Quaternary upwelling along the Oman margin, Arabian Sea based on planktonic foraminifera. *Paleoceanography* 11(1): 129-140.

Naidu, P. D., Singh, A. D., Ganeshram, R., Bharti, S. K., 2014. Abrupt climate-induced changes in carbonate burial in the Arabian Sea: causes and consequences. Geochemistry Geophysics Geosystems 15, 1398–1406.

Naik, D. K., Saraswat, R., Lea, D. W., Kurtarkar, S. R., and Mackensen A., 2017. Last glacial-interglacial productivity and associated changes in the eastern Arabian Sea. Palaeogeogr. Palaeoclimatol. Palaeoecol. 483, 147–156 doi: 10.1016/j.palaeo.2016.07.014.

Naik, S. S., S. P. Godad, P.D. Naidu, M. Tiwari, A. L. Paropkari (2014), Early-to late-Holocene contrast in productivity, OMZ intensity and calcite dissolution in the eastern Arabian Sea, *Holocene 24,* 749–755.

Nair, R. R., V. Ittekkot, S. J. Manganini, V. Ramaswamy, B. Haake, E. T. Degens, B. N. Desai, and S. Honjo (1989), Increased particle flux to the deep ocean related to monsoons, *Nature, 338,* 749-751.

Narayana, A. C., P. D. Naidu, N. Shinu, P. Nagabhushanam, and B.S. Sukhija (2009), Carbonate and organic carbon content changes over last 20 ka in the southeastern Arabian Sea: Paleoceanographic implications, *Quaternary International, 206,* 72–77.

Naqvi, S. W. A. (1987), Some aspects of the oxygen-deficient conditions and denitrification in the Arabian Sea, *J. Mar. Res., 45,* 1049–1072.

Naqvi SWA and Noronha RJ (1991) Nitrous oxide in the Arabian Sea. *Deep Sea Research* 38: 871-890.

Naqvi, S. W. A., 1994. Denitrification processes in the Arabian Sea, in Proceedings of the Indian Academy of Sciences. Earth Planet. Sci. 103, 279-300.

Naqvi, S. W. A., Yoshinari, T., Jayakumar, D. A., Altabet, M. A., Narvekar, P. V., Devol, A. H., Brandes, J. A., and Codispoti, L. A., et al., 1998. Budgetary and biogeochemical implications of N_2O isotope signatures in the Arabian Sea. Nature, 394, 462-464.

Naqvi, S. W. A., Jayakumar, D. A., Narvekar, P. V., Naik, H., Sarma, V. S., D'Souza, W., Joseph, T., and George, M. D., 2000. Increased marine production of N2O due to intensifying anoxia on the Indian continental shelf. Nature 408, 346–349.

Naqvi, S. W. A., Naik, H., and Narvekar, P. V., 2003, The Arabian Sea. In: Biogeochemistry in Marine Systems, Black, K. and Shimmield, G. (Eds.), Academic Press, Sheffield.

Naqvi, S. W. A., H. Naik, D. A. Jayakumar, D. A., M. S. Shailaja, and P. V. Narvekar, (2006), Seasonal oxygen deficiency over the western continental shelf of India, In *Past and Present water column anoxia*, edited by Neretin, *Springer*, 195-224.

Neff U, Burns SJ, Mangini A, Mudelsee M, Fleitmann D and Matter A (2001) Strong coherence between solar variability and the monsoon in Oman between 9 and 6 kyr ago. *Nature* 411: 290-293.

O'Leary, M. H., 1988. Carbon isotopes in photosynthesis. Biosci. 38, 328-336.

Olson, D. B., Hitchcock, G. L., Fine, R. A., and Bruce, A. W., 1993. Maintenance of low oxygen layer in the central Arabian Sea. Deep-Sea Res. II (40) 673–685.

Pahnke, K., and Zahn, R., 2005. Southern Hemisphere water mass conversion linked with North Atlantic climate variability. Science 307 (5716), 1741 – 1746.

Parab, S. G. and Matondkar, S., 2012, Primary productivity and nitrogen fixation by Trichodesmium spp. in the Arabian Sea: Journal of Marine Systems, v. 105, p. 82–95.

Paropkari, A. L., S. D. Iyer, O. S. Chauhan, and C. B. Prakash, (1991), Depositional environments inferred from variations of calcium carbonate, organic carbon and sulfide sulfur: A core from the southeastern Arabian Sea, *Geo-Marine Letters, 11,* 96-102.

Pattan, J. N., and N. J. G. Pearce (2009), Bottom water oxygenation history in southeastern Arabian Sea during the past 140 ka: results from redox-sensitive elements, *Palaeogeography, Palaeoclimatology, Palaeoecology, 280 (3–4),* 396–405.

Pattan, J. N., P. D. Toshiyuki Masuzawab, G. P. Naidu, and M. Yamamoto (2003), Productivity fluctuations in the southeastern Arabian Sea during the last 140 ka, *Palaeogeography Palaeoclimatology Palaeoecology, 193,* 575–590.

Pattan, J. N., T. Masuzawa, and M. Yamamoto (2005), Variations in terrigenous sediment discharge in a sediment core from southeastern Arabian Sea during the last 140 ka, *Current Science, 89,* 1421-1425.

Pedersen, T. F., G. B. Shimmield, and N. B. Price (1992), Lack of enhanced preservation of organic matter in sediments under the oxygen minimum on the Oman Margin, *Geochimica et Cosmochimica Acta, 56*, 545–551.

Peltier WR and Fairbanks RG (2006) Global glacial ice volume and Last Glacial Maximum duration from an extended Barbados sea level record. *Quaternary Science Reviews* 25: 3322-3337.

Peters, K. E., Sweeney, R. E., and Kaplan, I. R., 1978. Correlation of carbon and nitrogen stable isotope ratios in sedimentary organic matter. Limnol. Oceanogr. 23, 598-604.

Peterson L. C., W. L. Prell (1985), Carbonate dissolution in the recent sediments of eastern equatorial Indian Ocean: preservation patterns and carbonate loss above the lysocline, *Marine Geology, 64*, 259 - 290.

Pichevin, L., Bard, E., Martinez, P., and Billy, I., 2007. Evidence of ventilation changes in the Arabian Sea during the Late Quaternary: Implications for denitrification and nitrous oxide emission. Global Biogeochem. Cy. 21, GB4008, doi:10.1029/2006GB002852.

Pokras, E. M. and A. C. Mix (1987), Earth's precession cycle and Quaternary climatic change in tropical Africa, *Nature, 326*, 486–487.

Prasad S, Anoop A, Riedel N, Sarkar S, Menzel P, Basavaiah N, Krishnan R, Fuller D, Plessen B, Gaye B, Röhl U, Wilkes H, Sachse D, Sawant R, Wiesner MG and Stebich M (2014) Prolonged monsoon droughts and links to Indo-Pacific warm pool: A Holocene record from Lonar Lake, central India. *Earth & Planetary Science Letters* 391: 171-182.

Prasanna Kumar, S., and Prasad, T. G., 1999. Formation and spreading of Arabian Sea high salinity water mass. Joumal of Geophysical Research 104, 1455-1464.

Premuzic, E. T., Benkovitz, C. M., Gaffney, J. S., Walsh, J. J., 1982. The nature and distribution of organic matter in the surface sediments of the world oceans and seas. Org. Chem. 4, 63–77.

Qasim, S. Z. (1977), Biological productivity of the Indian Ocean, *Indian Journal of Marine Science, 6,* 122–137.

Radhakrishna, K., (1969), Primary productivity studies in the shelf waters off Alleppey, south-west India, during the post-monsoon, 1967, *Marine Biology, 4,* 174-181.

Ramesh, R., S. K. Bhattacharya, K. Gopalan (1985), Dendroclimatological implications of isotope coherence in trees from Kashmir Valley, India, *Nature, 317*, 802-804.

Reichart, G. J., M. den Dulk, H. J. Visser, C. H. van der Weijden, and W. J. Zachariasse (1997), A 225 kyr record of dust supply, paleoproductivity and the oxygen minimum zone from the Murray Ridge (northern Arabian Sea), *Palaeogeography Palaeoclimatology Palaeoecology, 134(1–4),* 149–169, doi:10.1016/S0031-0182(97)00071-0.

Reichart, G. J., Lourens, L. J., and Zachariasse, W. J., 1998. Temporal variability in the northern Arabian Sea Oxygen Minimum Zone (OMZ) during the last 225,000 years. Paleoceanography 3, 607-621.

Reichart, G. J., Brinkhuis, H., Huiskamp, F., and Zachariasse, W. J., 2004, Hyper stratification following glacial overturning events in the northern Arabian Sea: Paleoceanography, v. 19, p. 8.

Reimer, P. J., et al., 2009. Intcal09 and Marine09 radiocarbon age calibration curves, 0-50,000 years cal BP. Radiocarbon 51, 1111–1150.

Ren, H. J., Sigman, D. M., Chen, M. T., and Kao, S. J., 2012. Elevated foraminifera-bound N isotopic composition during the last ice age in the South China Sea and its global and regional implications. Global Biogeochemical Cycles 26, 13.

Rein B, Lückge A, Reinhardt L, Sirocko F, Wolf A, Dullo WC (2005) El Niño variability off Peru during the last 20,000 years. *Paleoceanography* 20: PA4003. doi:10.1029/2004PA001099.

Riquier, L., N. Tribovillard, O, Averbuch, X. Devleeschouwer, A. Riboulleau (2006), The Late Frasnian Kellwasser horizons of the Harz Mountains (Germany): two oxygen-deficient periods resulting from different mechanisms, *Chemical Geology, 233*, 137–155.

Rixen, T. and Ittekkot, V., 2005, Nitrogen deficits in the Arabian Sea, implications from a three component mixing analysis: Deep-Sea Research Part II-Topical Studies in Oceanography, v. 52, p. 1879-1891.

Rixen, T., Baum, A., Gaye, B., and Nagel, B., 2014. Seasonal and interannual variations in the nitrogen cycle in the Arabian Sea. Biogeosciences 11, 5733-5747.

Robinson, R. S., Brunelle, B. G., and Sigman, D. M., 2004, Revisiting nutrient utilization in the glacial Antarctic: Evidence from a new method for diatom-bound N isotopic analysis: Paleoceanography, v. 19, p. 3001, doi:10.1029/2003PA000996.

Rohling, E. J., and Zachariasse, W. J., 1996, Red Sea out flow during the Last Glacial Maximum: Quaternary International, v. 31, p. 77–83.

Russell, J.M., T.C. Johnsan and M. R. Talbot (2003), A 725 yr cycle in the climate of central Africa during the late Holocene, *Geology, 31(8),* 677-680.

Saenko O. A., Weaver, A. J., and Schmittner, A., 2003. Atlantic deep circulation controlled by freshening in the Southern Ocean. Geophys. Res. Lett. 30 (14), 1754, doi:10.1029/2003GL017681.

Saraswat, R., R. Nigam, S. Weldeab, A. Mackensen, P. D. Naidu (2005), A first look at past sea surface temperatures in the equatorial Indian Ocean from Mg/Ca in foraminifera, *Geophysical Research Letters, 32,* doi:10.1029/2005GL024093.

Saraswat, R., R. Nigam, A. Mackensen, S. Weldeab (2012), Linkage between seasonal insolation gradient in the tropical northern hemisphere and the sea surface salinity of the equatorial Indian Ocean during the last glacial period, *Acta Geologica Sinica, 86*, 1265-1275.

Saraswat, R., D.W. Lea, R. Nigam, A. Mackensen, D. K. Naik (2013), Deglaciation in the tropical Indian Ocean driven by interplay between the regional monsoon and global teleconnections, *Earth and Planetary Science Letters, 375*, 166-175.

Saraswat, R., Naik, D. K., Nigam, R., and Gaur, A. S., 2016. Timing, cause and consequences of mid-Holocene climate transition in the Arabian Sea. Quat. Res. 86, 162-169.

Sarma, V. V. S. S., 2002. An evaluation of physical and biogeochemical processes regulating perennial suboxic conditions in the water column of the Arabian Sea: Global Biogeochemical Cycles, v. 16 (4), p. 1082, doi:10.1029/2001GB001461.

Sarkar, A., R. Ramesh, B. L. K. Somayajulu, R. Agnihotri, A. J. T. Jull, and G. S. Burr (2000), High-resolution Holocene monsoon record from the eastern Arabian Sea, *Earth and Planetary Science Letters, 177*, 209–218.

Sarkar, S., S. K. Bhattacharya, and M. M. Sarin (1993), Geochemical evidence for anoxic deep water in the Arabian Sea during the last glaciation, *Geochimica et Cosmochimica Acta., 57*, 1009-1016.

Schäfer, P. and Ittekkot, V., 1993. Seasonal variability of $\delta^{15}N$ in settling particles in the Arabian Sea and its palaeogeochemical significance. Naturwissenschaften 80, 511–513.

Schmittner, A., Galbraith, E. D., Hostetler, S. W., Pedersen, T. F., and Zhang, R., 2007, Large fluctuations of dissolved oxygen in the Indian and Pacific oceans during Dansgaard-Oeschger oscillations caused by variations of North Atlantic Deep Water Subduction: Paleoceanography, v. 22, p. 3207, doi:10.1029/2006PA001384.

Schulte, S., F. Rostek, E. Bard, J. Rullkötter, and O. Marchal (1999), Variations of oxygen-minimum and primary productivity recorded in sediments of the Arabian Sea, *Earth and Planetary Science Letters, 173,* 205-221, doi:10.1016/S0012-821X(99)00232-0.

Schott, F., McCreary, J. P., 2001, The monsoon circulation of the Indian Ocean: Progress in Oceanography, v. 51, p. 1-123.

Schott, F. A., S. P. Xie, and J. P. McCreary Jr. (2009), Indian Ocean circulation and climate variability, *Reviews of Geophysics, 47*, RG1002, doi:10.1029/2007RG000245.

Schulte, S., Rostek, F., Bard, E., Rullkötter, J., and Marchal, O., 1999, Variations of oxygen-minimum and primary productivity recorded in sediments of the Arabian Sea: Earth and Planetary Science Letters, v. 173, p. 205-221, doi:10.1016/S0012-821X(99)00232-0.

Schulz, H., U. von Rad, and H. Erlenkeuser (1998), Correlation between Arabian Sea and Greenland climate oscillations of the past 110,000 years, *Nature, 393,* 54-57.

Shackleton, N. J., 2000. The 100,000-year ice-age cycle identified and found to lag temperature, carbon dioxide, and orbital eccentricity. Science 289, 1897–1902.

Shapiro, G. I., Meschanov, S. L., 1991. Distribution and spreading of Red SeaWater and salt lens formation in the northwest Indian Ocean. Deep-Sea Research 38, 21–34.

Sharma, G. S., 1978, Upwelling off the southwest coast of India: Indian Journal of Marine Science, v. 7, p. 209-218.

Shenoi S. S. C., Shankar, D., Shetye, S. R., 2004. Remote forcing annihilates barrier layer in southeastern Arabian Sea. Geophysical Research Letters 31, L05307.

Shetye, S. R., Gouveia, A. D., Shenoi, S. S. C., Sunder, D., Michael, G., S., Almeida, A. M., and Santanam, K., 1990, Hydrography and circulation of the west coast of India during the southwest monsoon 1987: Journal of Marine Research, v. 48, p. 359–378.

Shetye, S. R., Gouveia, A. D., Shenoi, S. S. C., 1994. Circulation and water masses of the Arabian Sea. Proc. Indian Acad. Sci. Earth Planet. Sci. 103, 107-123.

Shetye, S. R., and Gouveia, A. D., 1998. Coastal circulation in the North Indian Ocean, in Robinson, A. R., and Brink, K. H., eds., The Sea: Coastal segment (14, S-W), John Wiley & Sons, New York, 11, 523- 556.

Shukla J and Misra BM (1977) Relationships between sea surface temperature and wind speed over the central Arabian Sea and monsoon rainfall over India. *Monthly Weather Review* 105: 998-1002.

Sigman, D. M., Altabet, M. A., Michener, R., McCorkle, D. C., Fry, B., and Holmes, R. M., 1997. Natural abundance-level measurement of the nitrogen isotopic

composition of oceanic nitrate: An adaptation of the ammonia diffusion method, Marine Chemistry, 57, 3–4.

Singh, A. D., Kroon, D., Ganeshram, R., 2006. Millennial scale variations in productivity and OMZ intensity in the eastern Arabian Sea. J. Geol. Soc. India 68, 369–377.

Singh A, Jani RA and Ramesh R (2010) Spatiotemporal variations of the $\delta^{18}O$–salinity relation in the northern Indian Ocean. *Deep-Sea Research Part I* 57: 1422-1431.

Singh, A. D., S. J. A. Jung, K. Darling, R. Ganeshram, T. Ivanochko, and D. Kroon (2011), Productivity collapses in the Arabian Sea during glacial cold phases, *Paleoceanography, 26,* PA3210, doi:10.1029/2009PA001923.

Sinha, A., K. G. Cannariato, L. D. Stott, H.C. Li, C.F. You, H. Cheng, R. L. Edwards, and I. B. Singh (2005), Variability of southwest Indian summer monsoon precipitation during the Bølling-Allerød, *Geology, 33,* 813–816.

Sirocko, F. and H. Lange (1991), Clay-mineral accumulation rates in the Arabian Sea during the late Quaternary, *Marine Geology, 97,* 105-119.

Sirocko F, Sarnthein M, Erlenkreuser H, Lange H, Arnold M and Duplessy JC (1993) Century scale events in monsoon climate over the past 24,000 years. *Nature* 364: 322-324.

Smith CR, Levin LA, Hoover DJ, McMurtry G and Gage JD (2000) Variations in bioturbation across the oxygen minimum zone in the northwest Arabian Sea. *Deep-Sea Research Part II* 47: 227-257.

Somayajulu, B. L. K., R. Bhushan, A. Sarkar, G. S. Burr, and A. J. T. Jull (1999), Sediment deposition rates on the Continental margins of eastern Arabian Sea using 210-Pb, 137-Cs and 14-C, *Science of Total Environment, 237-238,* 429-439.

Southon, J., Kashgarian, M., Fontugne, M., Metivier, B., and Yim, W. W. S., 2002, Marine reservoir corrections for the Indian Ocean and southeast Asia: Radiocarbon, v. 44 (1), p. 167-180.

Stramma, L., Johnson, G. C., Sprintall, J., and Mohrholz, V., 2008. Expanding oxygen minimum zones in the tropical oceans. Science 320, 655–658.

Staubwasser M, Sirocko F, Grootes PM and Segl M (2003) Climate change at the 4.2 ka BP termination of the Indus valley civilization and Holocene south Asian monsoon variability. *Geophysical Research Letters* 30: 1425. doi:10.1029/2002GL016822.

Steinhilber F, Abreu JA, Beer J, Brunner I, Christl M, Fischer H, Heikkilä U, Kubik PW, Mann M, McCracken KG, Miller H, Miyahara H, Oerter H and Wilhelms F (2012) 9,400 years of cosmic radiation and solar activity from ice cores and tree rings. *Proceedings of National Academy of Science* 109: 5967-5971.

Stuiver, M., and T. F. Braziunas (1993), Modeling atmospheric ^{14}C influences and ^{14}C ages of marine samples to 10,000 BC, *Radiocarbon, 35(1),* 137–89.

Suthhof, A., Ittekkot, V., and Haake, B. G., 2001, Millennial scale oscillation of denitrification intensity in the Arabian Sea during the late Quaternary and its potential influence on atmospheric N_2O and global climate: Global Biogeochemical Cycles, v. 15, p. 637-649.

Swallow, J. C., (1984), Some aspects of the physical oceanography of the Indian Ocean, *Deep Sea Research, 31,* 693-650.

Sweeney, R. E., and Kaplan, I. R., 1980. Natural abundance of 15N as source indicator of near- shore marine sedimentary and dissolved nitrogen. Mar. Chem. 9, 81-94.

Thamban, M., V. P. Rao and S. V. Raju (1997), Controls on organic carbon distribution in sediments from the eastern Arabian Sea Margin, *Geo-Marine Letters, 17,* 220-227.

Thamban, M., V. P. Rao, R. R. Schneider, and P. M. Grootes (2001), Glacial to Holocene fluctuations in hydrography and productivity along the southwestern continental margin of India, *Palaeogeography Palaeoclimatology Palaeoecology, 165,* 113–127, doi:10.1016/S0031-0182 (00)00156.

Thamban, M., H. Kawahata and V. P. Rao (2007), Indian summer monsoon variability during the Holocene as recorded in sediments of the Arabian Sea: timing and implications, *Journal of Oceanography, 63*,1009-1020.

Thunell, R. C., Sigman, D. M., Muller-Karger, F., Astor, Y., and Varela, R., 2004, Nitrogen isotope dynamics of the Cariaco Basin, Venezuela: Global Biogeochemical Cycles, v. 18, p. GB3001, doi:10.1029/2003GB002185.

Tiwari, M., R. Ramesh, B. L. K. Somayajulu, A. J. T. Jull, G. S. Burr (2006), Paleomonsoon precipitation deduced from a sediment core from the equatorial Indian Ocean, *Geo-Marine Letters, 26*, 23–30.

Tiwari, M., R. Ramesh, R. Bhushan, M. S. Sheshshayee, B. L. K. Somayajulu, A. J. T. Jull, and G. S. Burr (2010), Did the Indo-Asian summer monsoon decrease during the Holocene following insolation?, *Journal of Quaternary Science, 25,* doi:10.1002/jqs.1398.

Tiwari, M., S. S. Nagoji, and R. Ganeshram (2015a), Multi-centennial scale SST and Indian summer monsoon precipitation variability since mid-Holocene and its nonlinear response to solar activity, *Holocene, 25,* 1-10, DOI: 10.1177/0959683615585840.

Tiwari, M., A. K. Singh, D. K. Sinha (2015b), Stable Isotopes: Tools for Understanding Past Climatic Conditions and Their Applications in Chemostratigraphy, *Chemostratigraphy,* 65-92.

Torrence, C., and Compo, G. P., 1998. A practical guide to wavelet analysis. Bull. Am. Meteorol. Soc. 79, 61–78.

Tribovillard, N. P., J. P. Caulet, C. V. Grazzini, N. Moureau, P. Tremblay (1996), Lack of organic matter accumulation on the upwelling influence Somalia margin in a glacial-interglacial transition, *Marine Geology, 133*, 157-182.

Tribovillard, N., T. J. Algeo, T. Lyons, and A. Ribaulleau (2006), Trace metals as paleoredox and paleoproductivity proxies: An update, *Chemical Geology, 232,* 12-32.

Vidal, L., Labeyrie, L., Cortijo, E., Arnold, M., Duplessy, J. C., Michel, E., Becque, S., and van Weering, T. C. E., 1997. Evidence for changes in the North Atlantic Deep Water linked to melt water surges during Heinrich events. Earth Planet. Sci. Lett. 146 (1–2), 13–27.

Von Rad, U., H. Schulz, V. Reich, M. Den Dulk, U. Berner, and F. Sirocko (1999), Multiple monsoon-controlled breakdown of oxygen-minimum conditions during the past 30,000 years documented in laminated sediments off Pakistan, *Palaeogeogr. Palaeoclim. Palaeoecol*., *152*, 129-161.

Von Rad, U., M. Schaaf, K. H. Michels, H. Schulz, W. H. Berger, and F. Sirocko (1999), A 5000-yr record of climate change in varved sediments from the oxygen minimum zone off Pakistan, Northeastern Arabian sea, *Quaternary Research, vol. 51*, 39–53.

Von Rad, U., A. Luckge, W. H. Berger, and H. D. Rolinski (2006), Annual to millennial monsoonal cyclicity recorded in Holocene varved sediments from the NE Arabian sea, *Journal of the Geological Society of India, vol. 68*, 353–368.

von Stackelberg, U. (1972), Faziesverteilung in Sedimenten des indisch.-pakistanischen Kontinentalrandes (Arabisches Meer), *Meteor-Forsch.Ergeb. C9*, l-73.

Wang, Y., H. Cheng, R. L. Edwards, Y. He, X. Kong, Z. An, J. Wu, M. J. Kelly, C. A. Dykoski, X. Li (2005), The Holocene Asian monsoon: links to solar changes and North Atlantic climate, *Science, 308*, 854-857.

Webster, P. J (1987), The variable and interactive monsoon, *in: Monsoons, Wiley, New York,* 269-330.

Wedepohl, K. H., (1971), Environmental influences on chemical composition of shales and clays, Physics and Chemistry of the Earth, *Pergamon, Oxford, 8,* 307-331.

Weldeab, S., D. W. Lea, R. R. Schneider, and N. Andersen (2007), 155 000 years of West African monsoon and ocean thermal evolution, *Science, 316*, 1303–1307.

Wyrtki, K. (1971), Oceanographic Atlas of the International Indian Ocean Expedition*, National Science Foundation, Washington DC*, 531.

Wyrtki, K., 1973. Physical oceanography of the Indian Ocean, In: Zeitzschel, B., eds., The Biology of the Indian Ocean. Ecological Studies, Springer- Verlag, Berlin, 3, 18–36.

Yadav, R. R., (2013), Tree ring-based seven-century drought records for the Western Himalaya, India, *Journal of Geophysical Research: Atmosphere 118*, doi:10.1002/jgrd.50265.

Yadava, M. G., and R. Ramesh (2005), Monsoon reconstruction from radiocarbon dated tropical Indian speleothems, *Holocene, 15*, 48–59.

Yoshinari, T., Altabet, M. A., Naqvi, S. W. A., Codispoti, L., Jayakumar, A., Kuhland, M., and Devol, A., 1997, Nitrogen and oxygen isotopic composition of N_2O from suboxic waters of the eastern tropical North Pacific and the Arabian Sea - measurement by continuous- flow isotope-ratio monitoring: Marine Chemistry, v. 56, p. 253-264.

You, Y. Z., 1998. Intermediate water circulation and ventilation of the Indian Ocean derived from water-mass contributions. J. Mar. Res. 56, 1029 – 1067.

Zahn, R., T. F. Pedersen (1991), A Pleistocene evolution of surface and mid-depth hydrography at the Oman Margin: planktic and benthic isotope records at site 724, In: Prell, W. L., N. Niitsuma, et al. (Eds.), *Proceedings of Ocean Drilling Program, Scientific Results, 117*, 291–303.

Ziegler, M., E. Tuenter and L. J. Lourens (2010), The precession phase of the boreal summer monsoon as viewed from the eastern Mediterranean (ODP Site 968), *Quaternary Science Review, 29,* 1481–1490.